ENDF-230

Vol. I

BENCHMARK TESTING OF ENDF/B-IV

March 1976

BNL-NCS-21118
(ENDF-230) Vol. I
Limited Distribution

ENDF-230
Vol. I

BENCHMARK TESTING OF ENDF/B-IV

March 1976

INFORMATION ANALYSIS CENTER REPORT

NATIONAL NEUTRON CROSS SECTION CENTER

BROOKHAVEN NATIONAL LABORATORY
ASSOCIATED UNIVERSITIES, INC.
UPTON, NEW YORK 11973

UNDER CONTRACT NO. E(30-1)-16 WITH THE
UNITED STATES ENERGY RESEARCH AND DEVELOPMENT ADMINISTRATION

April 1976 300 copies

ENDF-230, Vol. I

BENCHMARK TESTING OF ENDF/B-IV

Edited by: E. M. Bohn (ANL)
R. Maerker (ORNL)
B. A. Magurno (BNL
F. J. McCrosson (SRL)
R. E. Schenter (HEDL)

PARTICIPANTS

Many personnel at several laboratories participated in the Benchmark Testing of ENDF/B-IV. The following list identifies the testers, laboratories and areas of participation.

Thermal Reactors

Aerojet Nuclear Co. (ANC)
- F. J. Wheeler

Bettis Atomic Power Laboratory (BAPL)
- J. Hardy, Jr.

Brookhaven National Laboratory (BNL)
- W. Rothenstein

Chalk River Nuclear Laboratories (CRNL)
- D. S. Craig

Electric Power Research Institute (EPRI)
- O. Ozer

General Atomic Company (GA)
- D. Mathews

Savannah River Laboratory (SRL)
- F. J. McCrosson, Data Testing Coordinator
- D. R. Finch

Fast Reactors

Argonne National Laboratory (ANL)
- E. M. Bohn, Data Testing Coordinator
- H. Henryson, II
- E. M. Pennington

Brookhaven National Laboratory (BNL)
- P. Rose

General Atomic Co. (GAC)
- A. Hess

General Electric Co. (GE)
- C. Cowan
- E. Kujawski

Hanford Engineering Development Laboratory (HEDL)
R. W. Hardie
R. E. Schenter

Los Alamos Scientific Laboratory (LASL)
R. Kidman
R. LaBauve

Oak Ridge National Laboratory (ORNL)
C. R. Weisbin
J. E. White
R. Q. Wright

Westinghouse (W)
A. Bortz
N. C. Paik

Shielding

Oak Ridge National Laboratory (ORNL)
R. Maerker, Data Testing Coordinator

Dosimetry

Aerojet Nuclear Co. (ANC)
Y. Harker

Brookhaven National Laboratory (BNL)
B. A. Magurno, Data Testing Coordinator

Centre d'Etude de l'Energie Nucleaire (Belgium)
A. Fabry

Hanford Engineering Development Laboratory (HEDL)
W. N. McElroy

Oak Ridge National Laboratory (ORNL)
F. B. K. Kam

Fission Products

Bettis Atomic Power Laboratory (BAPL)
S. B. Gunst

Chalk River Nuclear Laboratories (CRNL)
W. H. Walker

Hanford Engineering Development Laboratory (HEDL)
R. E. Schenter, Data Testing Coordinator
F. Schmittroth

Los Alamos Scientific Laboratory (LASL)
T. R. England

Oak Ridge National Laboratory (ORNL)
J. K. Dickens
G. W. Morrison
C. R. Weisbin

Westinghouse (W)
J. C. Connor, Data Testing Coordinator

FOREWARD

The purpose of this report is fourfold:

1. To present the results of the benchmark testing of ENDF/B-IV in a clear and consistent fashion and to provide documentation of the testing results at this point in time.
2. To qualify the testing results recognizing that, in addition to the evolution in the evaluated data, the computational methods are also evolving.
3. To indicate those areas of basic nuclear data that require additional evaluations.
4. To indicate deficiencies in current benchmark tests.

Benchmark models for data testing have been identified by CSWEG for five areas of application: thermal reactors, fast reactors, shielding, dosimetry and fission products. The testing results for each of these areas are presented in Volume I, Sections II through VI. Each of these sections was prepared as a stand-alone report, i.e., page numbers, table and figure numbers sequence independently in each section. A brief summary of all testing results is given in Section I.

The testing results compiled in this report were computed over a period roughly defined by calendar year 1975. The results, especially those for thermal and fast reactors, are thus representative of the computational capabilities during this time. In Sections II and III, the computational methods used by the testers are briefly described.

Volume II of ENDF-203 is comprised of two appendices. Appendix A contains a more complete description of the reactor computational methods used in the thermal reactor data testing and detailed comparisons of broad group cross sections and reaction rates for the TRX-1 benchmark. Appendix B contains a description of the computational methods used by each tester and the results of fast reactor benchmark tests. Most of the important information contained in Volume II is summarized in Volume I. For this reason, and since Volume II is rather voluminous, Volume II will be available only on a very limited basis.

SUMMARY

I. SUMMARY

A. Thermal Reactor Benchmark Testing

Use of ENDF/B-IV yields a significant improvement in the prediction of the measured integral parameters in uranium benchmarks. Criticality is well predicted for the bare spheres of uranyl (93 wt% ^{235}U) nitrate solution and this test indicates no major deficiencies in the H_2O and ^{235}U cross sections for thermal systems. Calculations of the criticality of H_2O-moderated lattices of slightly enriched uranium rods and D_2O-moderated lattices of natural uranium rods yield an underprediction of k_{eff} by $\sim$1%. This underprediction of k_{eff} appears to be caused at least in part, to an overprediction of the ratio of epithermal-to-thermal ^{238}U capture (ρ^{28}) in these lattices. Overall, the use of ENDF/B-IV demonstrates better agreement than ENDF/B-III for these uranium benchmark lattices: the prediction of k_{eff} is almost 1% higher and ρ^{28} is reduced nearly 5%. These improvements are due primarily to revisions of the ^{235}U thermal data and the ^{238}U resonance capture cross sections. Calculations of the bare spheres of plutonium nitrate solutions yield values of k_{eff} 1-2% above experiment with the overprediction increasing as the thermal neutron spectrum hardens.

For ENDF/B-V, it is recommended that the ^{238}U capture data be carefully evaluated and recent high precision differential data be cast into resonance parameter form. The shapes of the thermal cross sections for the fissile nuclides, ^{233}U, ^{235}U, ^{239}Pu and ^{241}Pu, and σ_{2200} values should be reevaluated with particular attention paid to ^{239}Pu. Evaluations of heavier actinides should also be included to support studies of actinide production and recycle.

CSEWG thermal benchmark testing should be extended to include more tests of plutonium cross sections, uranium oxide and mixed oxide lattices, and thorium oxide lattices.

B. Fast Reactor Benchmark Testing

Computing the fast reactor benchmarks with ENDF/B-IV data gave results very similar to those obtained previously with ENDF/B-III. Criticality is generally predicted within ~1% with k_{eff} of the Pu fueled benchmarks underpredicted relative to the U-fueled assemblies and the criticality of large, dilute assemblies underpredicted relative to smaller, harder-spectrum benchmarks. Tests of reaction rate ratios indicate that the fission rate in ^{239}Pu relative to ^{235}U fission is generally underpredicted and the capture rate in ^{238}U relative to the fuel fission rate is overpredicted in the large, dilute assemblies. For the first time, evaluated delayed neutron data were included in ENDF/B-IV and tests of small sample central reactivity worths were compiled on a consistent basis. Fissile sample worths are significantly overpredicted, low energy absorber samples appear to be well predicted, and, all sample worths are overpredicted more in Pu fueled assemblies than in U-fueled assemblies.

These testing results indicate that the $^{239}Pu(n,f)$ cross section relative to $^{235}U(n,f)$, $^{239}\nu$ relative to $^{235}\nu$, and the prompt fission neutron spectra should be carefully reevaluated for ENDF/B-V. The ^{238}U inelastic and capture cross sections impact importantly on the neutron balance and neutron spectra in large, fast assemblies, these cross sections are apparently uncertain and must be reevaluated. Reactivity worths in Pu-fueled assemblies are significantly impacted by the ^{238}U delayed neutron yield and these data must be examined carefully for ENDF/B-V.

Data not tested in the fast reactor benchmarks but of interest to fast reactor design and in need of evaluation includes the cross sections of actinide isotopes and thorium capture and fission cross sections.

Several deficiencies in the current benchmark testing procedure were cited. Specifications of benchmark models, application of certain corrections (geometry, transport, heterogeneity factors) applied to calculations, and use of certain unreliable integral measurements are factors that limit the usefulness of benchmark tests for fast reactors and they must be carefully examined before ENDF/B-V testing.

C. Shielding Benchmark Testing

Total neutron cross sections in the range 1-10 MeV were tested with the "broomstick" transmission benchmarks and ENDF/B-IV was found to be deficient in the following areas:

Iron, σ_T appears to be about 5% too high below 5 Mev.

Oxygen, σ_T is $\sim$4% too high in the range 4-6 MeV.

Nitrogen, σ_T is a 5-10% too low in the range 1-4 MeV and $\sim$7% too high in the range 4.2-4.6 MeV.

Sodium, σ_T is 8-10% too low in the regions 1-1.5 MeV and 3.2-3.7 MeV. Everywhere else, σ_T is too low by $\sim$5%.

Broomstick measurements for nickel and chromium not yet incorporated into the shielding benchmark series indicate discrepancies ranging from 4-20% below 5 MeV when tested with ENDF/B-IV.

Benchmark tests of capture gamma-ray production indicates relatively good agreement with ENDF/B-IV for iron, stainless steel, nitrogen and sodium. Gamma-ray production cross sections for nickel are about 7% too high in the gamma energy range 1.5-9 MeV.

Benchmark tests of gamma-ray production cross sections averaged over a fast neutron spectrum indicate that the sodium production cross section in ENDF/B-IV needs to be reevaluated.

Pulsed sphere-spectrum transmission benchmark measurements indicate generally poor agreement in the spectrum range 2-12 MeV, especially for magnesium, titanium, tungsten and lead.

Tests of neutron transmission through thick slabs of sodium indicate that the total cross sections in the MeV range are a few percent too low.

D. Dosimetry Benchmark Testing

For most of the dosimetry tests, the general order of disagreement between measured reaction rates and reaction rates computed with ENDF/B-IV data is a few percent or more and is outside the range of uncertainty reported for the measurements. Of the integral spectrum indices, only ^{115}In shows some degree of agreement. $^{238}U(n,\gamma)$ is overpredicted by $\sim$13% in both the $\Sigma\Sigma$ and CFRMF spectra and $^{197}Au(n,\gamma)$ is underpredicted by $\sim$30% in $\Sigma\Sigma$. $^{235}U(n,f)$ is computed $\sim$4% low in CFRMF while $^{239}Pu(n,f)$ is consistently computed a few percent low in all spectra. The threshold fission reactions, $^{232}Th(n,f)$, $^{238}U(n,f)$ and $^{237}Np(n,f)$ are consistently calculated too low. $^{10}B(n,\alpha)$ and $^{6}Li(n,\alpha)$ disagree by 5% and 10% respectively with measurements in CFRMF. It is noted that the results of these dosimetry tests are qualitatively consistent with similar tests in the fast reactor benchmarks; i.e., $^{239}Pu(n,f)$ is calculated lower than $^{235}U(n,f)$ and $^{238}U(n,\gamma)$ is calculated too high.

From the wide range of disagreement between calculations and measurements, it appears that not only are some of the cross sections in the dosimetry file in error, but the benchmark spectra are not well enough known. In addition, measured

reaction rates must be carefully evaluated for possible heterogeneity effects and consistent calculational procedures must be implemented in the testing process.

E. Fission Product Benchmark Testing

Benchmark testing of the ENDF/B-IV fission product data files involved four areas: decay heat, β and γ spectra production, fission product absorption, and delayed and prompt neutron yields. Most of the comparisons between calculations with ENDF/B-IV data and integral experiments were for decay heat following both "burst" and long-time exposure fission. Results of several recent measurements in this area have been published and comparisons using the ENDF/B-IV data in summation calculations show good agreement, generally well within the quoted experimental uncertainties and the calculational uncertainties (in basic data for yields and energies). Total uncertainties range from ~5% for decay heat results to 10% or greater for fission product absorption and β and γ spectra.

Thermal Reactors

II. THERMAL REACTORS

INTRODUCTION AND SUMMARY

The scope of thermal data testing has advanced with each new version of ENDF/B. Although only a few laboratories participated in small-scale testing programs for the initial two ENDF/B versions, five laboratories participated in varying degrees in testing the thermal data for ENDF/B-III, and seven laboratories participated in the ENDF/B-IV program, which is the most ambitious to date. The seven laboratories are: Aerojet Nuclear Company (ANC), Bettis Atomic Power Laboratory (BAPL), Brookhaven National Laboratory (BNL), Chalk River Nuclear Laboratories (CRNL), Electric Power Research Institute (EPRI), General Atomic Company (GA), and Savannah River Laboratory (SRL).

Seventeen thermal benchmark experiments have been analyzed:

- Five unreflected spheres of uranyl nitrate (93 wt % ^{235}U) solution were analyzed to test the H_2O and ^{235}U cross sections. For four experiments, the radius of the spheres was 34.6 cm; for the fifth experiment, the radius was 61.0 cm. The ENDF/B-IV calculations for the spheres yielded values of k_{eff} about 0.1% below experiment for the smaller spheres and about 0.3% below experiment for the large sphere.

- Four H_2O-moderated lattices of slightly enriched uranium rods and three D_2O-moderated lattices of natural uranium rods were analyzed to test the ^{238}U thermal and resonance region capture cross sections in addition to the ^{235}U and moderator cross sections.

  The most rigorous calculations for the H_2O-moderated lattices yielded reasonably good predictions of criticality and the measured activation parameters, viz.,

  ρ^{28} = ratio of epithermal-to-thermal ^{238}U captures

  δ^{25} = ratio of epithermal-to-thermal ^{235}U fissions

  δ^{28} = ratio of ^{238}U fissions to ^{235}U fissions

The information contained in this article was developed during the course of work under Contract No. AT(07-2)-1 with the U. S. Energy Research and Development Administration.

Typically, however, k_{eff} is somewhat underpredicted, and ρ^{28} is overpredicted. The D_2O-moderated lattices are not as well predicted; on an average, k_{eff} is about 1% low, although ρ^{28} is well-predicted. There are significant differences in the values reported by the laboratories for both the H_2O- and D_2O-moderated lattices.

- Five unreflected spheres of plutonium nitrate solutions were analyzed to test the ^{239}Pu cross sections. The calculated values for k_{eff} are typically 1-2% above experiment. Differences between ENDF/B-III and ENDF/B-IV are small.

The specifications for the seventeen CSEWG thermal benchmarks are given in Reference 1. The calculated results for k_{eff} and the activation parameters ρ^{28}, δ^{25}, and δ^{28} are given in Tables 1-4. The experimental values for the activation parameters have been revised in these tables to be consistent with the recent preliminary corrections reported by Sher et al.[2] These experimental values may be adjusted further based on additional work by Sher et al. at Stanford University and by Hardy at BAPL.

Comparisons of intermediate results, viz., the processed multigroup libraries and calculated fewgroup reaction rates for individual nuclides of the H_2O lattice benchmark TRX-1, have been made in order to better isolate the effects that data and calculational methods have on calculated integral parameters. Appendix A contains descriptions of the calculational methods, tabulations of the multigroup libraries for the fast and thermal energy regions, and fewgroup reaction rates and slowing down sources for benchmark TRX-1. There has not been sufficient time to permit the laboratories to make corrections to obvious errors. Hopefully, future iterations will bring into better agreement not only the intermediate calculational results, but also the prediction of the measured integral parameters.

DISCUSSION

Calculational Methods

Details concerning the calculations are given in Appendix A. Brief descriptions of the methods are given here to provide the minimum framework needed to present the calculated results in the next section.

ANC - The homogeneous spheres and TRX lattices were calculated using S_N theory and the RABBLE resonance treatment.

BAPL - The calculations for the homogeneous spheres were P_3 epithermally and double P_1 thermally with Marshak boundary conditions. The lattice calculations were fully Monte Carlo for the infinite lattice with subsequent leakage corrections based on B_1 calculations.

BNL - The lattices were calculated using the HAMMER integral transport theory code, but with the standard Nordheim treatment replaced by a Monte Carlo resonance treatment.

CRNL - The lattices were calculated using HAMMER with the Nordheim resonance treatment.

EPRI - Benchmark TRX-1 was calculated using HAMMER with the Nordheim resonance treatment replaced by RABBLE.

GA - The homogeneous spheres and TRX and MIT lattices were calculated using S_N theory with resonance region cross sections obtained from GAND3 and MICROX calculations with one (spheres) or two (lattices) space regions.

SRL - The TRX and MIT lattices were calculated using integral transport theory with the Nordheim resonance treatment. The zero leakage integral transport results were leakage-corrected by subsequent B_1 calculations. The homogeneous spheres were analyzed using S_N theory.

SRL* - The lattices were calculated using the same methods described just above except the Nordheim treatment was replaced by a more accurate method developed by D. R. Finch.

Results

a. Measured Integral Parameters

Unreflected Spheres of Uranyl Nitrate Solution

The good prediction of criticality for the uranyl (93 wt % ^{235}U) nitrate solutions in Table 1 implies there are no major deficiencies in the H_2O and ^{235}U cross sections for thermal systems. ENDF/B-IV predictions of criticality for these spheres are about 0.2% higher than ENDF/B-III (in closer agreement with the measurements). The closer agreement can be attributed to the ENDF/B-IV revisions to the ^{235}U cross sections based on the least-squares analysis reported by J. R. Stehn.[3]

Uranium Lattices

The ENDF/B-IV predictions of criticality for the H_2O-moderated lattices of slightly enriched uranium rods and the D_2O-moderated lattices of natural uranium rods vary appreciably from one laboratory to another. Taken collectively, however, they indicate k_{eff} is underpredicted by approximately 1%; the underprediction is about 0.5% for the more moderated lattices and increases to about 1.5% as the moderator-to-fuel ratio decreases.

When the results of all the laboratories are averaged, ρ^{28} is 3-5% too high for the H_2O lattices and less than 2% above the measurements for the D_2O lattices. Thus, the observed underprediction of k_{eff} is traceable, at least in part, to an overprediction of epithermal ^{238}U capture. Background on this problem is documented in the proceedings of the March 18-20, 1975 *Seminar on ^{238}U Resonance Capture*, held at BNL, during which the accuracy of the ρ^{28} measurements, ^{238}U differential cross sections measurements, and calculational methods were reviewed.[4]

From Tables 1 and 2, it becomes obvious that although there may be residual deficiencies in the ^{238}U resonance region cross sections, the most pressing need is to establish the "correct" calculational method. For example, BAPL yields values of k_{eff} that are about 0.7% higher than the average for the H_2O-moderated lattices, whereas ANC and CRNL yield values about 0.5% lower than the average. The BNL calculations of ρ^{28} for the four H_2O-moderated lattices are in general agreement with measurements (even though predictions of criticality are about 1% low). The BAPL and SRL* calculations of ρ^{28} are generally within two standard deviations of the measured ρ^{28} values, and k_{eff} is predicted reasonably close to unity.

When the results from the various laboratories are averaged, the calculated δ^{25} for the TRX lattices are in good agreement with measurement (Table 3). There are, however, significant differences in the reported values of the individual laboratories: CRNL is about 10% higher than experiment, whereas SRL* is about 6% below experiment. For the MIT lattices, averaging the calculated δ^{25} of the various laboratories yields severe overpredictions: 6% for MIT-1 and approximately 20% for MIT-2 and -3. These overpredictions primarily follow from the CRNL and SRL calculations that do not properly include the effects of shielding of the ^{235}U resonances. The BNL, GA, and SRL* calculations that accurately account for this effect are not far outside the precision of the measurements.

In Table 4, δ^{28} is well-predicted for the H_2O-moderated lattices if the results from the various laboratories are averaged, and is underpredicted significantly for the D_2O-moderated lattices (about 5% for MIT-1, 10% for MIT-2, and 14% for MIT-3). The ENDF/B-IV calculations for δ^{28} are 4-5% higher than ENDF/B-III because of the decrease in the ^{238}U inelastic scattering cross section between 1 and 5 MeV.

Overall, the ENDF/B-IV results for the benchmark lattices are in better agreement with experiment than ENDF/B-III: prediction of k_{eff} is almost 1% higher than ENDF/B-III, and ρ^{28} is reduced nearly 5%.

Unreflected Spheres of Plutonium Nitrate Solutions

The calculated values of k_{eff} for the plutonium nitrate solutions are 1-2% above experiment. The ANC and GA calculations are in excellent agreement with each other, whereas the SRL results tend to be higher. The explanation for the large difference between the ANC/GA result and the SRL result for PNL-2 is being sought. ENDF/B-II calculations reported by L. E. Hansen and E. D. Clayton yielded higher values of k_{eff} for PNL-2 than for PNL-1, consistent with the ENDF/B-IV SRL results.[5] The overprediction of k_{eff} increases as the thermal neutron spectrum hardens. The ENDF/B-IV criticality predictions are somewhat higher than for ENDF/B-III (and ENDF/B-II) due to revisions to the thermal cross sections based on the least-squares analysis reported in Reference 3.

b. Comparison of Fewgroup Reaction Rates and Multigroup Libraries

Appendix A contains a detailed comparison of 4-group (and 2-group) capture and fission reaction rates by nuclide for benchmark TRX-1. The fewgroup slowing down sources for TRX-1 are also given. The upper energy boundaries of the 4-group structure are 10 MeV, 67.379 keV, 3.355 keV, and 0.625 eV. The first three groups are collapsed to one group in the 2-group structure. Edits of the multigroup cross sections for the energy bands of the first and fourth groups of the 4-group structure are supplied. The fast multigroup structure (fewgroup 1) consists of the first 20 MUFT groups (E_{max} = 10 MeV, 0.25 lethargy intervals); the thermal multigroup structure (fewgroup 4) consists of the familiar 30-group THERMOS structure.

Examination of the fewgroup and multigroup edits yielded several sizeable discrepancies; these have been noted in Appendix A in many cases by enclosing the discrepant number(s) within a rectangular box. Some observations are given below:

Fewgroup 1 (MUFT groups 1-20)

1. The SRL elastic scattering cross sections for H, D, and ^{27}Al are too low by a few percent. This is probably due to the flat weighting spectrum used in the SRL cross section processing. Other laboratories used a more realistic spectrum weighting which consisted of the fission spectrum coupled to the 1/E energy dependence in the slowing down region.

2. The CRNL elastic scattering cross section for D is 25% too large in MUFT group 1 and 14% too large in group 2. The CRNL value for $\bar{\mu}$ is underestimated.

3. Fast reaction rates for CRNL are consistently higher than others. Fast fission rates among other laboratories are reasonably consistent. Fast capture rates for moderators are in good agreement.

4. The ^{16}O multigroup cross sections contain several sizeable discrepancies designated by ruled rectangular boxes in Section IV of Appendix A. The values for $\bar{\mu}$ are especially discrepant, particularly those for CRNL. The discrepancies in the capture cross sections for ^{16}O are apparently due to differences in spectrum weighting of the cross sections in the vicinity of the (n,α) threshold.

5. SRL fast capture for ^{27}Al is 8% higher than BAPL. This is also reflected in the multigroup edits where SRL cross sections are probably low because of flat weighting in the vicinity of the (n,p), (n,d), and (n,α) thresholds. The SRL and ANC data for $\bar{\mu}$ of ^{27}Al are in significant disagreement with BAPL, BNL and CRNL between groups 1 and 8.

6. The ^{235}U and ^{238}U $\bar{\mu}$ data for BAPL and BNL differ by up to 60% from the data of SRL, ANC, and CRNL.

7. Differences in the SRL, ANC, and CRNL values for the ^{238}U fission spectrum of secondary neutrons are probably due to the assumed spectrum of the incident neutrons. The SRL χ-vector corresponds to fissions occurring in MUFT group 7.

Fewgroups 2 and 3

1. BAPL and BNL captures in the cladding and moderator are significantly higher than SRL and SRL*: for H, 7% higher in group 2, 17% higher in group 3; for ^{27}Al, 11% higher in group 2 and 20% higher in group 3.

2. Rates in group 2 for ANC, BAPL, BNL, and EPRI are higher than SRL by 5% for ^{235}U fission, 4% for ^{235}U capture and 6-13% for ^{238}U capture. The discrepancies may arise from the use of different values for the nuclear radius in calculating penetrabilities for p-wave capture. SRL used the expression

$$\text{Channel radius} = 1.23\, y^{1/3} + 0.8 \qquad \text{(fermi)}$$

which is given in the procedures manual.[6] The parameter y denotes the atomic weight of the nuclide relative to that of a neutron.

3. Group 2 ^{235}U fissions and captures for CRNL differ greatly from other laboratories.

4. Group 3 ^{235}U fission rates for BAPL and BNL are 2-1/2% lower than SRL; EPRI is 5% lower. Group 3 is made up of ^{235}U resolved and unresolved regions (82 eV breakpoint). Since the trend was opposite for the group 2 ^{235}U unresolved region, BAPL, BNL, and EPRI are presumably lower than SRL by even greater margins in the ^{235}U resolved region. The SRL calculations for resonance self-shielding for a given nuclide do not include shielding effects accruing from other nuclides.

5. ^{238}U resolved resonance capture differences from SRL:

ANC	1-1/2% lower
BAPL	6% lower
BNL	4% lower
CRNL	1-1/2% higher
EPRI	6% lower
SRL*	4-1/2% lower

Fewgroup 4 (THERMOS groups 1-30)

1. The THERMOS multigroup cross sections are in generally good agreement.

2. The SRL and BNL capture cross sections for D differ by 10-30%, agreement worsening as energy increases. The SRL 2200 m/sec capture cross section is 0.52 mb.

3. The BAPL and BNL elastic scattering cross sections for ^{16}O below 0.02 eV differ significantly from SRL. There are also significant differences in $\bar{\mu}$.

CONCLUSIONS AND RECOMMENDATIONS

ENDF/B-IV predictions of the measured integral parameters are significantly improved over those of ENDF/B-III for the uranium systems. These improvements are due primarily to the revisions of the ^{235}U thermal data (Reference 3), which raised predictions of k_{eff} for the uranyl nitrate spheres by 0.2%, and the revisions of the ^{238}U resonance capture cross sections (Reference 4, p 122), which raised k_{eff} for the lattices by about 1% and reduced ρ^{28} nearly 5%. Limited testing of the plutonium cross sections has yielded values of k_{eff} that are 1 to 2% high (similar to the ENDF/B-III results).

The ENDF/B-IV predictions of the uranium benchmark experiments are sufficiently close that effects of uncertainties in the unnormalized calculational methods and in the integral parameter measurements (e.g., ρ^{28}, δ^{25}, and δ^{28}) are becoming at least as large as those in the cross sections themselves. To ensure continued meaningful testing of the differential data for succeeding ENDF/B versions,

- The Thermal Data Testing Group of CSEWG should determine the most accurate available calculational method, establish its expected uncertainties in predicting integral parameters, and use this calculation in reporting the results and recommendations of ENDF/B data testing. Processed cross section libraries and intermediate results of the calculations should be checked by the members of the Thermal Data Testing Group as a safeguard against errors in processing. Results of more approximate calculations should also be included in the data testing report to provide a measure of sensitivity to calculational methods.

- Work, such as that by the groups at Stanford University and BAPL, to better define the measurements of the lattice benchmark experiments should continue.

In planning for Version V, it is recommended that every effort be made to factor in the results of the ^{238}U self-indication transmission measurements in progress at ORNL and RPI. All currently available differential cross section measurements correspond to the infinitely dilute case, not to the heavily self-shielded cases encountered in the integral benchmark experiments. The measurements therefore pertain primarily to the peaks of the cross sections and not to the wings of the resonances where a significant number of the ^{238}U reactions occur. The self-indication transmission measurements would supply differential information for heavily self-shielded cases.

The ENDF/B-V ^{238}U evaluation should avoid the negative scattering cross sections that occur in certain interference valleys of ENDF/B-IV through the use of bound levels, e.g., the picket fence model.[7]

To permit full utilization of the G. de Saussure et al. ^{238}U capture data,[8] it is recommended that this high precision differential data be cast into resonance parameter form. The required neutron widths could be taken from the Columbia transmission measurements[9] or from new transmission experiments that could be performed at the ORELA.

The shapes of the thermal cross sections for the fissile nuclides $^{233,235}U$, $^{239-241}Pu$ should be re-evaluated for Version V, in addition to σ_{2200} values. The least-squares analysis for the Version IV thermal parameters assumed the same g-factors as the 1969 IAEA review.[3] The need to reanalyze the cross section shapes is indicated especially in the ENDF/B integral data tests for thermal plutonium systems where k is typically overpredicted by 1-2%.

In addition to re-evaluations of the cross sections for the Big 3 + 2 ($^{235,238}U$, ^{239}Pu plus $^{240,241}Pu$), Version V should include re-evaluations for $^{234,236}U$, ^{242}Pu, $^{241,243}Am$, and ^{244}Cm. The SRL cross section evaluations for the heavier actinides extending up to ^{253}Cf should also be added to ENDF/B-V to support studies concerned with actinide production and recycle.[10]

The range of CSEWG thermal benchmark experiments should be extended for ENDF/B-V to include

- More experiments for testing plutonium cross sections
- Uranium oxide and mixed oxide (uranium-plutonium) lattices in H_2O
- Thorium oxide lattices in H_2O, D_2O, and graphite.

REFERENCES

1. *Cross Section Evaluation Working Group Benchmark Specifications*, ENDF-202 (November 1974).

2. R. Sher, S. Fiarman, and J. Pedersen, *Progress Report*, EPRI-RP-247-0-0 (July 7, 1975).

3. J. R. Stehn, "Thermal Data for Fissile Nuclei in ENDF/B-IV," *Trans. Am. Nucl. Soc., 18*, 351 (1974).

4. S. Pearlstein (Ed.), *Seminar on ^{238}U Resonance Capture*, ENDF-217 (March 1975).

5. L. E. Hansen and E. D. Clayton, "Theory-Experiment Tests Using ENDF/B Version II Cross-Section Data," *Trans. Am. Nucl. Soc., 15*, 309 (1972).

6. M. K. Drake (Ed.), *Data Formats and Procedures for the ENDF Neutron Cross Section Library*, ENDF-102, Vol 1 (October 1970).

7. B. R. Leonard, Jr., "Energy-Dependent Cross Sections in the Thermal Region," *National Topical Meeting on New Developments in Reactor Physics and Shielding, Kiamesha Lake, N.Y.* CONF-720901, Book 1, p 81 (1972).

8. G. de Saussure, E. G. Silver, R. B. Perez, R. Ingle, and H. Weaver, *Measurement of the ^{238}U Capture Cross Section for Incident Neutron Energies up to 100 keV*, ORNL-TM-4059 (1973).

9. F. Rahn, H. S. Camarda, G. Hacken, W. W. Havens, Jr., H. I. Liou, J. Rainwater, M. Slagowitz, and S. Wynchank, "Neutron Resonance Spectroscopy.X. ^{232}Th and ^{238}U," *Phys. Rev., C6*, 1854 (1972).

10. R. W. Benjamin, F. J. McCrosson, T. C. Gorrell, and V. D. Vandervelde, *A Consistent Set of Heavy Actinide Multigroup Cross Sections*, DP-1394 (1975).

TABLE 1

CRITICALITY (ENDF/B-IV)

BENCHMARK	DESCRIPTION	k-eff							
		ANC	BAPL	BNL	CRNL	EPRI	GA	SRL	SRL*
ORNL	Spheres of uranyl nitrate								
-1	H/U-235=1378; R=34.595 cm	1.0025	0.9983				1.0012	0.9996	
-2	H/U-235=1177; R=34.595 cm	1.0018	0.9980				1.0007		
-3	H/U-235=1033; R=34.595 cm	0.9984	0.9949				0.9978		
-4	H/U-235= 971; R=34.595 cm	0.9998	0.9963				0.9989	0.9976	
-10	H/U-235=1835; R=61.011 cm	0.9988	0.9957				0.9982	0.9951	
TRX	H_2O moderated U lattices								
-1	Mod/Fuel - 2.35	0.9827	0.9954	0.9880	0.9824	0.9903	0.9855	0.9871	0.9921
-2	Mod/Fuel = 4.02	0.9893	0.9996	0.9921	0.9898		0.9961	0.9924	0.9967
-3	Mod-Fuel = 1.00		0.9965	0.9935					
-4	Mod/Fuel = 8.11		0.9962	0.9974					
MIT	D_2O moderated U lattices								
-1	Mod/Fuel = 20.74			0.9825	0.9829		0.9972	0.9851	0.9912
-2	Mod/Fuel = 25.88			0.9807	0.9829		1.0006	0.9856	0.9902
-3	Mod/Fuel = 34.59			0.9820	0.9850		1.0076	0.9879	
PNL	Spheres of Pu nitrate								
-1	H/Pu-239 = 698; R=19.509 cm	1.0232					1.0225	1.0289	
-2	H/Pu-239 = 124; R=19.509 cm	1.0196					1.0201	1.0354	
-3	H/Pu-239 = 1204; R=22.70 cm	1.0028					1.0021	1.0029	
-4	H/Pu-239 = 911; R=22.70 cm	1.0105					1.0102	1.0123	
-5	H/Pu-239 = 578; R=20.1265 cm	1.0160					1.0159	1.0227	

TABLE 2

RATIO OF EPITHERMAL-TO-THERMAL ^{238}U CAPTURES (ENDF/B-IV)[a]

BENCH-MARK	ρ^{28} EXP	ANC	BAPL	BNL	CRNL	EPRI	GA	SRL	SRL*
TRX-1	1.324 ±0.020	1.426	1.362	1.367	1.433	1.344	1.407	1.402	1.365
TRX-2	0.842 ±0.015	0.8903	0.859	0.846	0.882		0.881	0.858	0.839
TRX-3	3.027 ±0.05		3.19	3.07					
TRX-4	0.485 ±0.01		0.500	0.491					
MIT-1	0.523 ±0.008			0.502	0.528		0.529	0.541	0.515
MIT-2	0.419 ±0.002			0.413	0.433		0.431	0.443	0.422
MIT-3	0.330 ±0.004			0.318	0.337		0.331	0.344	

(a) Thermal cutoff energy = 0.625 eV

TABLE 3

RATIO OF EPITHERMAL-TO-THERMAL ^{235}U FISSIONS (ENDF/B-IV)[a]

BENCH-MARK	δ^{25}								
	EXP	ANC	BAPL	BNL	CRNL	EPRI	GA	SRL	SRL*
TRX-1	0.0995 ±0.001	0.1005	0.0992	0.0993	0.111	0.0966	0.0982	0.1014	0.0946
TRX-2	0.0622 ±0.0007	0.0615	0.0610	0.0611	0.067		0.0606	0.0617	0.0577
TRX-3	0.232 ±0.003		0.244						
TRX-4	0.0365 ±0.0004		0.0353						
MIT-1	0.0465 ±0.0019			0.0466	0.0520		0.0469	0.0534	0.0475
MIT-2	0.0328 ±0.003			0.0380	0.0424		0.0382	0.0436	0.0390
MIT-3	0.0266 ±0.0010			0.0297	0.0327		0.0293	0.0336	

(a) Thermal cutoff energy = 0.625 eV

TABLE 4

RATIO OF ^{238}U FISSIONS TO ^{235}U FISSIONS
(ENDF/B-IV)

δ^{28}

BENCH-MARK	EXP	ANC	BAPL	BNL	CRNL	EPRI	GA	SRL	SRL*
TRX-1	0.0934 ±0.0020	0.0957	0.0948	0.0939	0.0937	0.0940	0.0965	0.0959	0.0935
TRX-2	0.0687 ±0.002	0.0691	0.0678	0.0663	0.0661		0.0700	0.0680	0.0645
TRX-3	0.165 ±0.004		0.177						
TRX-4	0.0472 ±0.0007		0.0477						
MIT-1	0.0617 ±0.0020			0.0570	0.0554		0.0607	0.0591	0.0618
MIT-2	0.0630 ±0.0017			0.0554	0.0539		0.0585	0.0570	0.0600
MIT-3	0.0631 ±0.0012			0.0539	0.0527		0.0559	0.0552	

FAST REACTORS

III. FAST REACTORS

A. Introduction

The fast reactor benchmarks used to test ENDF/B-IV are described in the ENDF-202 report and are listed in Table I. There are nine plutonium fueled assemblies (Jezebel, VERA-11A, ZEBRA-3, SNEAK-7A, -7B, ZPR3-48, -56B, ZPR6-7, and ZPPR2) and seven uranium fueled assemblies (Godiva, ZPR3-6F, -11, -12, VERA-1B, ZEBRA-2, and ZPR6-6A). Jezebel and Godiva are small, bare metal spheres; ZEBRA-3, ZPR3-6F, -11 are small, reflected, cylindrical metal assemblies; VERA-1B, 11A, ZPR3-48, 12 and ZEBRA-2 are small carbide assemblies; ZPR6-6A is a large, dilute oxide assembly; ZPR3-56B, ZPR6-7, ZPPR-2, SNEAK-7A, -7B are mixed oxide fueled assemblies ranging in size from the relatively small SNEAK reactors to the large, dilute ZPR6-7 and ZPPR-2 assemblies. This set of benchmarks covers a diverse range of compositions and geometries and affords the testing of nuclear data over a range of neutron spectra important for fast reactor design.

The metal spheres provide integral tests of nuclear data in a fission spectrum ($\sim$100 keV to 10 MeV) while the larger, more dilute assemblies provide tests in a relatively softer spectrum ($\sim$1 keV to 10 MeV). The most important nuclear data tested in these benchmarks include the fission properties and capture cross sections of plutonium and uranium, the moderating properties of uranium, oxygen, carbon, sodium and the stainless steel isotopes, and, the capture cross sections of sodium and stainless steel.

The measurements in these benchmark experiments that are most often used to test nuclear data are criticality, reaction rate ratios and reactivity coefficients. The measurements are integral in nature, i.e., the results reflect an integral weighting of the measured quantity by the neutron spectrum in the assembly. The

typical imprecision (2σ) in these measurements is ±0.1-0.3% for criticality (k_{eff}), ±2% for reaction rate ratios, and ±5% for reactivity coefficients. These estimates of imprecision do not include possible systematic errors.

Eight testers participated in ENDF/B-IV fast reactor data testing; five national laboratories (Argonne National Laboratory (ANL), Brookhaven National Laboratory (BNL), Hanford Engineering Development Laboratory (HEDL), Los Alamos Scientific Laboratory (LASL), Oak Ridge National Laboratory (ORNL)) and three industrial reactor designers (General Atomic Corp. (GAC), General Electric Co. (GE), and Westinghouse (W)). The benchmark experiments computed by each tester are summarized in Table I. Appendix B contains a detailed presentation of calculations by each tester plus certain ancillary information useful for comparing calculations (e.g., fission neutron spectra, real and adjoint central spectra, and a discussion of some details of the calculations). The results presented in the following sections of this report are a summary of the information in Appendix B.

TABLE I. Benchmarks Calculated by Fast Reactor Testers

Benchmark	ANL	BNL	GAC	GE	HEDL	LASL	ORNL	W
1. JEZEBEL		X		X		X	X	X
2. VERA 11A	X				X	X		
3. ZPR3-48	X	X	X	X	X			
4. ZEBRA-3	X				X			X
5. GODIVA		X				X	X	
6. VERA-1B		X			X			
7. ZPR3-6F		X			X			
8. ZPR3-11	X				X	X	X	
9. ZPR3-12					X			
10. ZEBRA-2	X				X			
11. ZPPR-2	X		X	X	X			X
12. ZPR6-7	X	X	X	X	X	X	X	X
13. ZPR3-56B				X	X		X	
14. SEFOR								
15. ZPR6-6A	X		X		X	X	X	X
16. SNEAK-7A				X	X			
17. SNEAK-7B				X	X			

B. Computational Methods

The calculations required in performing the benchmark studies include (1) preprocessing of ENDF/B data tapes; (2) calculation of assembly dependent multigroup cross sections; (3) neutronics and perturbation calculations. Appendix B includes a detailed discussion of the code systems used by each of the data testers. In addition several testers have reported on the differences and similarities of the various processing methods. This section will therefore attempt only to outline some of the important points of commonality and difference among the data testers.

In the neutronics and perturbation calculations standard computational tools were used. Attempts have been made to report the nature of the calculation, e.g., discrete ordinates, diffusion theory, but such details as the discrete ordinate quadratures were neither reported nor standardized on the assumption that differences of this nature had little impact on reported results. All of the data testers calculated the one-dimensional homogeneous benchmarks defined in ENDF-202. In addition HEDL and ANL calculated the two-dimensional diffusion theory models. ANL also calculated heterogeneous one-dimensional models to provide a check on the heterogeneity corrections reported for the homogeneous models.

The processing of ENDF/B data tapes and the subsequent multigroup cross section calculation was performed by each of the data testers using their production code systems. A large degree of commonality existed among the data testers in their code and/or library use. For example, a 50 group library of cross sections and self-shielding factors was generated by LASL using the MINX code and used for subsequent multigroup calculations by LASL, GE, ORNL and Westinghouse. ORNL also used the MINX code to generate a 171 group library.

HEDL generated a 42 group library using the ETOX code and this library was used by BNL in their multigroup calculations. Thus intercomparisons among data testers using common libraries provide tests of the collapsing codes, and the transportability of common libraries but do not provide an independent test of the data libraries or the ENDF/B processing codes.

The codes used by the data testers are listed in Table II. Among the different codes there are many points of similarity and difference. For example all of the code systems except ANL and GA use the self-shielding factor formulation to treat resonance cross sections. However, such a characterization of the code systems is far too simplistic since the calculation of the self-shielding factors in the resolved resonance regions differ significantly between the codes MINX and ETOX. Similarly the treatment of elastic removal differs among the self-shielding factor codes TDOWN, 1DX and SPHINX. The ANL calculations include a 2000-group spectrum calculation which differs from all the other codes which assume a weighting function in the generation of fine group libraries. Although a detailed discussion of the treatment of each of the ENDF/B reaction types is beyond the scope of this section, some discussion of particular formats is required for an understanding of later sections of this report. The general method for treating the statistical integrations required for the unresolved resonance calculations is identical for all the codes in Table II except the VIM Monte Carlo code. The specifics of these calculations however, differ both in the numerics and physics of the calculation. The numeric differences are found to account for a large part of the difference among the various codes in the reactivity calculations. Similarly it was found that differences in the treatment of the fission spectrum distribution accounted for reactivity differences. All of the methods except those

TABLE II. Methods Used by Testers

ANL	1. MC^2-II/1-D Diffusion or 1-D Transport for all Calculations of Homogeneous Models. 2. MC^2-II/SDX/2-D Diffusion, Homogeneous and Heterogeneous Calculations for ZPR6-7, ZPR6-6A, ZPR3-48. 3. VIM Monte Carlo for ZPR6-7.
BNL	ETOX/1DX or ANISN (Used HEDL 42 gp Library - Collapsed to 26 gps.)
GA	GAM/GAR/GGC5/1-D and 2-D Diffusion, 1-D Transport.
GE	MINX/T DOWN-II (Used LASL 50 gp Library.)
HEDL	ETOX/1DX.
LASL	MINX/1DX or DTF.
ORNL	MINX/SPHINX or XSDRNPM (Used 171 gp Library and 50 gp LASL Library.) Results of 171 gp Calculations are Reported in Tables.
W	MINX/SPHINX (Used LASL 50 gp Library.)

reported by ANL allowed only one fission spectrum temperature for the neutronics calculation. The ANL MC^2-2 calculations allowed isotope dependent spectra. Neither prescription is faithful to the ENDF/B specifications which provide isotope and incident energy dependent fission spectra. The VIM Monte Carlo code does treat the ENDF/B specifications in detail.

Such differences among the code systems were identifiable and were quantified. No attempt was made by the data testers to perform a complete methods sensitivity analysis and it should not be inferred from this discussion or the results presented below that any one of the methods used by the data testers is better than or indeed equivalent to any other method. Rather, the purpose in the discussion below is to present a carefully compiled list of data testing results, qualified where necessary, so that at this point in time and methods availability, a positive statement of fact may be made concerning the use of ENDF/B-IV as applied to fast reactor benchmark calculations.

C. Results of Benchmark Calculations

CRITICALITY

Calculations of k_{eff} are summarized in Tables III, III.a, and IV. These tables present the values of k_{eff} calculated for the 1-D homogeneous models specified in ENDF-202 without correction factors applied (Table III), a listing of the heterogeneity and transport correction factors that are to be applied to the calculations of the 1-D homogeneous models (Table III.a), and, the values of k_{eff} for the 1-D benchmark models after all corrections have been applied (Table IV). The presentation of k_{eff} calculations in this series of three tables serves two purposes; it demonstrates clearly and unambiguously the manner in which the final corrected values of k_{eff} in Table IV were derived, and, it assures a consistent, common basis for comparison of calculated k_{eff} values among all testers and all benchmarks.

The k_{eff} values in Table III were obtained primarily from diffusion calculations except, as noted, for some of the small benchmark assemblies where transport theory was applied. These k_{eff} values were corrected for heterogeneity effects and adjusted to correspond to higher order transport calculations with the factors listed in Table III.a. Three sets of transport adjustment factors are given; those currently specified in ENDF-202, diffusion theory-to-S_8 factors computed by HEDL, and, recently calculated factors for Jezebel and Godiva by LASL. (The HEDL and LASL transport adjustment factors are presented in Appendix B.) These correction factors are themselves not completely independent of the nuclear data and methods used to compute them, and, hence, may be subject to change with time.* The factors listed in Table III.a represent the best available information.

*Heterogeneity corrections factors for ZPR6-7, ZPR6-6A and ZPR3-48 were recently computed at ANL with ENDF/B-IV and latest methods. They were found to agree closely with those listed in Table III.a. Similarly, results recently obtained at ORNL validate the transport correction factors specified in ENDF-202 for some assemblies.

TABLE III. k_{eff} for 1-D Homogeneous Models (No Corrections Applied)[a]

Benchmark	ANL	BNL	GAC	GE	HEDL	LASL	ORNL	W
Pu Fueled:[b]								
JEZEBEL		0.9973[e]		0.9998[e]		1.0009[e]	0.9947[e,i]	0.9920[e]
VERA-11A	0.9877[d]				0.9437	0.9931[e]		
ZEBRA-3	0.9957[d]				0.9884			1.005[d]
SNEAK-7A				0.9900	0.9886			
SNEAK-7B				0.9900	0.9899			
ZPR3-48	0.9706	0.9764	0.9804	0.9757	0.9777			
ZPR3-56B				0.9903	0.9881		0.9829[g]	
ZPR6-7	0.9666[f]	0.9731	0.9810	0.9725	0.9754	0.9726	0.9701[g]	0.9686
ZPPR-2	0.9677		0.9855	0.9736	0.9774			0.9697
U Fueled:[b]								
GODIVA		1.0095[e]				1.0120[e]	1.0069[e,i]	
ZPR3-6F		1.0157[c]			0.9948			
VERA-1B		0.9997[d]			0.9746			
ZPR3-12					0.9965			
ZPR3-11	1.0036[c]				1.0046	1.0149[e]	1.0013[g]	
ZEBRA-2	0.9882[c]				0.9844[h]			
ZPR6-6A	0.9760		0.9876		0.9894	0.9873	0.9900[g]	0.9873

TABLE III. (Contd.)

[a]All calculations are diffusion theory unless otherwise noted.

[b]Arranged in order of spectrum hardness (i.e., by measured $\sigma_f^{28}/\sigma_f^{25}$).

[c]Transport calculation, S4.

[d]Transport calculation, S8.

[e]Transport calculation, S16.

[f]Monte Carlo (VIM) calculation gives 0.9680 ± 0.0019 for 120,000 histories.

[g]171 energy groups used in calculation (compared to 50 gps or less by other testers).

[h]Hydrogen not included.

[i]126 energy groups collapsed from 171 gp library.

TABLE III.a. Corrections to k_{eff} for Heterogeneity and Transport Effects

Benchmark	ENDF-202 Specified Calculation	ENDF-202 Heterogeneity Correction[a]	ENDF-202 Transport Correction	HEDL Transport (Diffusion → S_8)[b]	LASL Transport Corrections[b]
Pu Fueled					
JEZEBEL	S_{16}		$S_{16} \rightarrow S_\infty = -0.0008$ based on GODIVA		$S_{16} \rightarrow S_\infty = -0.0021$ P_∞ Correction = -0.0032
VERA-11A	S_8		$S_8 \rightarrow S_\infty = -0.0024$	+0.0472	
ZEBRA-3	S_8		$S_8 \rightarrow S_\infty = -0.001$	+0.0126	
SNEAK-7A	Diffusion	c	Not given	+0.0120	
SNEAK-7B	Diffusion	c	Not given	+0.0047	
ZPR-3-48	Diffusion	+0.0183	Transport Correction = +0.0072	+0.0064	
ZPR-3-56B	S_4	+0.0102	Diffusion → Transport = +0.0075	+0.0065	
ZPR-6-7	Diffusion	+0.0166	Diffusion → S_8 = +0.0018	+0.0016	
ZPPR-2	Diffusion	+0.0175	Not given	+0.0024	

TABLE III.a. (Contd.)

Benchmark	ENDF-202 Specified Calculation	ENDF-202 Heterogeneity Correction[a]	ENDF-202 Transport Correction	HEDL Transport (Diffusion → S_8)[b]	LASL Transport Corrections[b]
U Fueled					
GODIVA	S_{16}		ANL-7416 gives -0.0007		$S_{16} \rightarrow S_\infty$ = -0.0017 P_∞ Correction = -0.0030
ZPR-3-6F	S_4		$S_4 \rightarrow S_\infty$ = -0.0038 Diff. → S_4 = +0.023	-0.0192	
VERA-1B	S_8		$S_8 \rightarrow S_\infty$ = -0.001	+0.0237	
ZPR-3-12	S_4		$S_4 \rightarrow S_\infty$ = -0.0018	+0.0099	
ZPR-3-11	S_4		$S_4 \rightarrow S_\infty$ = -0.0013 Diff. → S_4 = +0.008	+0.0060	
ZEBRA-2	S_4		$S_4 \rightarrow S_\infty$ = -0.0005	+0.0033	
ZPR6-6A	Diffusion	+0.0073	Diffusion → S_∞ < +0.0018	+0.0013	

[a] These heterogeneity correction factors account for the spatial dependence of the neutron flux within unit-cell platelet loadings. They do not include any anisotropic neutron streaming effects.

[b] See Appendix B. The P_∞ correction is for $P_{1/2} \rightarrow P_\infty$.

[c] Heterogeneity correction already included in specifications of 1-D model.

TABLE IV. k_{eff} for 1-D Models after all Corrections Applied to Calculations in Table III[a]

Benchmark	ANL	BNL	GAC	GE	HEDL	LASL	ORNL	W
Pu Fueled:[b]								
JEZEBEL[c]		0.9920		0.9945		0.9956	0.9926[o]	0.9867
VERA-11A	0.9853				0.9885[h]	0.9911[i]		
ZEBRA-3	0.9947			1.0160[j]	1.0000[j]			1.0040
SNEAK-7A[d]				1.0020	1.0006			
SNEAK-7B[d]				0.9947	0.9946			
ZPR3-48	0.9961	1.0019	1.0059	1.0012	1.0032			
ZPR3-56B[e]				0.9923	0.9901		0.9849	
ZPR6-7	0.9850	0.9915	0.9994	0.9909	0.9938	0.9910	0.9885	0.9870
ZPPR-2[f]	0.9876		1.0054	0.9935	0.9973			0.9896
U Fueled:[b]								
GODIVA[c]		1.0048				1.0073	1.0052[o]	
ZPR3-6F		1.0119			1.0140			
VERA-1B		0.9987			0.9973[k]			
ZPR3-12					1.0064[l]			
ZPR3-11	1.0023				1.0113	1.0149[m]	1.0080	
ZEBRA-2	0.9877				0.9971[n]			
ZPR6-6A[g]	0.9846		0.9962		0.9980	0.9959	0.9986	0.9959

TABLE IV. (Contd.)

[a] Correction factors include heterogeneity and transport corrections from ENDF-202 or Table III.a with exceptions as given by following notes.

[b] Arranged in order of spectrum hardness (i.e., by measured $\sigma_f^{28}/\sigma_f^{25}$).

[c] For JEZEBEL and GODIVA the $S_{16} \rightarrow S_\infty$ transport corrections specified by LASL are used rather than the ENDF-202 values. Also the LASL corrections for P_∞ anisotropic neutron scattering were included. See Appendix for LASL calculations.

[d] No heterogeneity corrections were made for SNEAK-7A and SNEAK-7B. The interpretation of the specifications in ENDF-202 is somewhat ambiguous for these assemblies, but the 1-D model appears to include heterogeneity corrections as it is specified. The HEDL diffusion $\rightarrow S_8$ factor from Table III.a has been included here.

[e] For ZPR-3-56B the 1D $\rightarrow$ 2D correction of -0.0157 was included since the 1-D model is not an equivalent k - 1.0 model (see ENDF-202).

[f] HEDL transport correction of +0.0024 was included for ZPPR-2.

[g] HEDL transport correction of +0.0013 was included for ZPR-6-6A.

[h] HEDL diffusion $\rightarrow S_8$ correction of +0.0472 was included.

[i] An assumed $S_{16} \rightarrow S_8$ correction factor of -0.0020 was used instead of the $S_8 \rightarrow S_\infty$ correction factor of -0.0024.

[j] For ZEBRA-3 the diffusion $\rightarrow S_8$ correction of +0.0126 was included for GE and HEDL.

[k] HEDL diffusion $\rightarrow S_8$ correction of +0.0237 was included.

[l] HEDL diffusion $\rightarrow S_8$ correction of +0.0099 was the only transport correction made.

[m] No transport correction was made to the LASL result.

[n] The HEDL diffusion $\rightarrow S_8$ correction of +0.0033 was the only transport correction made. A correction of +0.0094 was included, as specified by HEDL, to allow for the absence of hydrogen in the uncorrected problem.

[o] P_3 calculation (no P_∞ correction applied), includes $S_{16} \rightarrow S_\infty$.

The final corrected values of k_{eff} for the 1-D benchmark models are given in Table IV along with a detailed accounting of all correction factors applied. The calculated k_{eff}'s range from 0.985 to 1.015 and 75% lie between 0.99 and 1.01. There is no apparent bias according to spectrum hardness but the large dilute benchmarks (both U and Pu fueled) are underpredicted a few tenths of a percent compared to the smaller assemblies. The average k_{eff} calculated by a data tester for the uranium fueled benchmarks is very close to unity and is a few tenths of a percent higher than the average for plutonium fueled benchmarks. The most direct comparisons between uranium and plutonium fueled benchmarks is afforded by the two metal sphere assemblies (Godiva and Jezebel) and by the two large, dilute oxide assemblies, ZPR6-6A and ZPR6-7. (In fact, ZPR6-6A and ZPR6-7 are identical in composition and unit-cell loading pattern with the exception of uranium metal fuel plates in ZPR6-6A replaced with plutonium-uranium metal fuel plates in ZPR6-7.) For the cases where these pairs of assemblies were computed by the same tester (i.e., same computational methods used for each assembly), the k_{eff} for Jezebel is calculated over 1% lower than Godiva and ZPR6-7 is calculated, on the average, about 0.4% lower than ZPR6-6A.* Thus, there does appear to be a bias according to fuel type; the k_{eff} for plutonium fueled assemblies is computed lower than for uranium fueled assemblies. The bias does not appear to be associated with the computational methods or particular characteristics of the benchmark model.

The trends in the calculated k_{eff} values of Table IV were identified in the foregoing discussion by comparing calculations obtained by a given data tester for the range of benchmarks computed. However, there is a wide dispersion among data testers in the calculated k_{eff} value for each benchmark, even among testers using similar calculational methods. For example, for ZPR6-7, the calculated k_{eff}

*In the case of ZPR6-6A and ZPR6-7, a bias in the comparison is not as clearly evident as in the case of the spheres. Four of the six testers compute ZPR6-6A significantly higher; two testers do not.

values range 1.4%. Thus, it becomes difficult to unequivocally identify trends or bias factors of a few tenths of a percent in k_{eff}. In order to investigate this variance, each data tester was requested to compute ZPR6-7. In Table IV.a*, the calculated k_{eff} value reported by each tester is listed along with a number of factors that have been identified as accounting for some of the variation in the calculations. The most important factor is the use of an improved Porter-Thomas quadrature scheme in the calculation of the unresolved resonance region.** The improved scheme is incorporated in the MC^2-2 calculations performed at ANL. Use of this improved scheme in the ETOX and MINX codes would reduce the eigenvalue in ZPR6-7 by 0.43%, a result verfied by several testers. Its impact on the GAC methods has been estimated to be 0.14%. The calculation of the eigenvalue was also found to be sensitive to the fission source spectrum employed. Most calculations assumed a single temperature parameter to describe the Chi distribution for all fissile isotopes in an assembly; ANL used isotope and (spectrum dependent) Chi distributions. In order to compare calculated eigenvalues on a common basis, a single temperature for the Chi distribution was assumed and the resulting adjustments (up to 0.17%) to the eigenvalues are listed. The remaining factors listed in Table IV.a include adjustments due to updates in the ENDF/B-IV files, an update in the 1DX f factor interpolation scheme in the BNL code, and an adjustment in the ORNL results to account for differences between calculations based on different MINX generated fine-group libraries. After all adjustments are applied the final

*Table IV.a is an updated version of a similar table compiled by R. Kidman and included in the LASL portion of Appendix B.

**The use of the improved scheme and its effects on reactor calculations is the result of work by R. N. Hwang and H. Henryson II, "Critical Examination of Low-Order Quadratures for Statistical Integrations," Trans. Am. Nucl. Soc., San Francisco, 1975.

TABLE IV.a. Accounting for the Variation in the Calculation of k_{eff} for ZPR6-7

Tester	k_{eff} from Table IV	Correction to ANL Porter-Thomas Scheme	Correction to 1.41 MeV Chi[a]	Correction to Latest IDX Scheme[b]	To 50-Group Latest ENDF Same Convergence[c]	ORNL 171 Groups to 50 Groups[d]	Final k_{eff}
ANL	0.9850		+0.0017				0.9867
BNL	0.9915	-0.0043	+0.0017	+0.0010	-0.0012		0.9887
GAC	0.9994	-0.0014[e]	+0.0010				0.9990
GE	0.9909	-0.0043					0.9866
HEDL	0.9938	-0.0043			-0.0012		0.9883
LASL	0.9910	-0.0043					0.9867
ORNL	0.9885	-0.0043	+0.0013			+0.0010	0.9865
W	0.9870	-0.0043	+0.0013		+0.0023		0.9863

[a] It is not implied that 1.41 MeV is the best temperature to use for Chi, but it provides a basis for comparison.

[b] BNL version of 1DX, when modified to include latest f - factor interpolation scheme, yields this correction factor. (Letter P. Rose to E. Bohn, July 28 and Aug1 11, 1975; Ref. R. B. Kidman, "An Improved F-Factor Interpolation Scheme for 1DX," TANS 18, 156 (1974)). See Appendix B.

[c] During the process of ENDF/B-IV data testing, several corrections to the ENDF/B tapes were issued and errors in earlier MINX generated cross sections (at LASL) used by some testers were uncovered. The factors listed here account for these differences so that all testers' results should correspond to latest available data.

[d] ORNL calculations (Appendix B) show the following differences between use of 171 gps and 50 gps:

	$k_{171} - k_{50}$
ZPR6-7	-0.001
ZPR6-6A	+0.003
ZPR3-11	-0.0015
ZPR3-56B	-0.001

[e] Preliminary estimate by GAC (see Appendix B).

eigenvalues are in much better agreement. After adjusting to these methods differences, the spread in eigenvalues calculated for ZPR6-7 is only 0.25% if the high (GAC) value is dropped. The GAC result is about 1% higher than the MC^2-2, ETOX and MINX calculations.

It is concluded that the greatest portion of the variance in eigenvalue calculations among data testers (excepting GAC) can be accounted for in the case of ZPR6-7. In addition, adjustment for the use of the ANL Porter-Thomas quadrature scheme reduces the calculated eigenvalue for ZPR6-7 and other large, dilute assemblies* with a significant fraction of the neutron inventory in the lower energy ranges. The eigenvalue for these assemblies is underpredicted by 1-1.5%. The trend or bias in calculated eigenvalues for large, dilute assemblies is thus accentuated.

Whether this bias is a result of the analytical methods used to compute the spectrum in these assemblies or a result of errors in the basic nuclear data, the cause of the bias cannot be determined simply from the data in Table IV. For the most part, the analytical methods forming the basis for the various computational schemes employed are not independent. However, the Monte Carlo calculation of ZPR6-7 with the continuous-energy (i.e., no cross section averaging) code VIM yields an eigenvalue of 0.9846 ± 0.0019** for the 1-D homogeneous model. To the extent that this result forms an independent check of the analytical methods, it suggests

*For ZPR6-6A, LASL reports that the new Porter Thomas quadrature scheme reduces k_{eff} by about 0.46% in the ETOX and MINX based codes, and ANL computes a 0.12% reduction in k_{eff} using SDX (see Appendix B).

**120,000 histories; eigenvalue includes +0.0166 correction for heterogeneity. The heterogeneity correction has also been verified by the Monte Carlo code for the ZPR6-7 unit-cell (see D. C. Wade, "Validation Results for the SDX Cell Homogenization Code," Trans. Am. Nucl. Soc. Vol. 22, Nov. 1975).

that the nuclear data are the primary source of the underprediction of the eigenvalues in the large, dilute assemblies.

REACTION RATE RATIOS

Calculations of reaction rate ratio measurements in the benchmark assemblies are summarized in Tables V-VII.a. Included in the summary are calculated-to-experimental (C/E) ratios for $^{239}Pu(n,f)$, $^{238}U(n,f)$ and $^{238}U(n,\gamma)$ relative to $^{235}U(n,f)$ and $^{238}U(n,\gamma)$ relative to $^{239}Pu(n,f)$.

The fission ratio $^{49}f/^{25}f$ (Table V) is generally predicted 2-5% low. (The results for the two VERA assemblies appear obtrusively high and are the exception.) For a given benchmark, the ratio is consistently computed by the testers and this is a result of the relative insensitivity of this ratio to the computed spectrum.

The $^{28}f/^{25}f$ ratio, Table VI, is a high energy spectrum index. The calculated results range from a few percent overprediction to a few percent underprediction. (The results for the two VERA assemblies again appear exceptionally high.) For a given benchmark, the ratio is consistently over or under predicted by the testers, but, the range among testers is 1-5% and is indicative of differences in the calculated high energy spectrum.

The ^{238}U capture ratios, $^{28}c/^{25}f$ in Table VII and $^{28}c/^{49}f$ in Table VII.a, are indicative of the low energy portion of the spectrum. The calculated results range from a few percent underprediction to a few percent overprediction, and, from the sparse data available, there does appear to be a correlation with the spectrum in these benchmark assemblies; the ratio is overpredicted for the larger, more dilute assemblies. For a given benchmark, the C/E ratios generally agree within 1-2% among testers.

TABLE V. Calculated-to-Experimental (C/E) Ratios for $^{239}Pu(n,f)/^{235}U(n,f)$

Benchmark	ANL	BNL	GAC[b]	GE	HEDL	LASL	ORNL	W
Pu Fueled:[c]								
JEZEBEL		0.934		0.935		0.936		
VERA-11A	1.079				1.073	1.085		
ZEBRA-3	0.990				0.988			0.990
SNEAK-7A				0.962	0.960			
SNEAK-7B				0.989	0.985			
ZPR3-48								
ZPR3-56B				0.951	0.944		0.944	
ZPR6-7	0.962[a]	0.960	0.965	0.967	0.961	0.968	0.960	0.960
ZPPR-2	0.980		0.966	0.985	0.981			0.982
U Fueled:[c]								
GODIVA		0.971				0.970		
ZPR3-6F		1.020			1.020			
VERA-1B					1.062			
ZPR3-12					0.996			
ZPR3-11	0.984				0.987	0.985		
ZEBRA-2	1.001				1.007			
ZPR6-6A								

[a] Monte Carlo (VIM) result is 0.962.

[b] 27-29 gp GAZE calculations repored here.

[c] Arranged in order of spectrum hardness (i.e., by measured $\sigma_f^{28}/\sigma_f^{25}$).

TABLE VI. Calculated-to-Experimental (C/E) Ratios for $^{238}U(n,f)/^{235}U(n,f)$

Benchmark	ANL	BNL	GAC	GE	HEDL	LASL	ORNL	W
Pu Fueled:[b]								
JEZEBEL		0.935		0.944		0.949		
VERA-11A	1.107				1.090	1.153		
ZEBRA-3	0.960				1.001			1.015
SNEAK-7A				0.931	0.911			
SNEAK-7B				0.979	0.967			
ZPR3-48	1.003	1.009	1.008	1.040	1.026			
ZPR3-56B				0.965	0.940		0.950	
ZPR6-7	0.918[a]	0.905	0.914	0.945	0.914	0.939	0.920	0.927
ZPPR-2	1.053		1.035	1.081	1.053			1.065
U Fueled:[b]								
GODIVA		1.064				1.068		
ZPR3-6F		0.995			1.000			
VERA-1B		1.185			1.180			
ZPR3-12					1.060			
ZPR3-11	1.012				1.064	1.054	1.015	
ZEBRA-2	1.013				1.048			
ZPR6-6A	0.926		0.923		0.926	0.935	0.918	0.908

[a] Monte Carlo (VIM) result is 0.915.

[b] Arranged in order of spectrum hardness (i.e., by measured $\sigma_f^{28}/\sigma_f^{25}$).

TABLE VII. Calculated-to-Experimental (C/E) Ratios for $^{238}U(n,\gamma)/^{235}U(n,f)$

Benchmark	ANL	BNL	GAC	GE	HEDL	LASL	ORNL	W
Pu Fueled:[b]								
JEZEBEL								
VERA-11A								
ZEBRA-3								
SNEAK-7A				0.990	0.979			
SNEAK-7B				1.033	1.025			
ZPR3-48	0.976		0.983	0.971	0.963			
ZPR3-56B								
ZPR6-7	1.052[a]		1.048	1.044	1.044	1.041	1.030	1.042
ZPPR-2								
U Fueled:[b]								
GODIVA						1.001		
ZPR3-6F					0.919			
VERA-1B					0.927			
ZPR3-12					0.954			
ZPR3-11	0.969				0.949	0.968	0.959	
ZEBRA-2	0.966				0.968			
ZPR6-6A	1.030		1.036		1.017	1.021		1.021

[a] Monte Carlo (VIM) result is 1.063.

[b] Arranged in order of spectrum hardness (i.e., by measured $\sigma_f^{28}/\sigma_f^{25}$).

TABLE VII.a. Calculated-to-Experimental (C/E) Ratios for $^{238}U(n,\gamma)/^{239}Pu(n,f)$

Benchmark	ANL	BNL	GAC	GE	HEDL	LASL	ORNL	W
Pu Fueled:[b]								
JEZEBEL								
VERA-11A								
ZEBRA-3								
SNEAK-7A				1.029	1.026			
SNEAK-7B				1.044	1.046			
ZPR3-48								
ZPR3-56B								
ZPR6-7	1.093[a]		1.086	1.080	1.086	1.075	1.074	1.085
ZPPR-2								
U Fueled:[b]								
GODIVA						1.032		
ZPR3-6F					0.901			
VERA-1B					0.873			
ZPR3-12					0.958			
ZPR3-11	0.985				0.962	0.983		
ZEBRA-2	0.966				0.961			
ZPR6-6A								

[a] Monte Carlo (VIM) result is 1.105.

[b] Arranged in order of spectrum hardness (i.e., by measured $\sigma_f^{28}/\sigma_f^{25}$).

The results of these reaction rate tests may be directly correlated with the criticality testing results. The underprediction of k_{eff} for Pu vs. U fueled assemblies is consistent with the underprediction of the $^{49}f/^{25}f$ ratio, and, the underprediction of k_{eff} for the large, dilute assemblies is consistent with the overprediction of the $^{28}c/^{25}f$ or $^{28}c/^{49}f$ ratios in these assemblies. For the specific case of ZPR6-7, approximately one-third of all neutron captures occur in ^{238}U in the core and a few percent overprediction of the $^{28}c/^{49}f$ ratio translates directly into a 2-3% underprediction of k_{eff}.

Regarding computational methods, it was determined that the improved Porter-Thomas quadrature scheme for the unresolved resonance region generally raised the reaction rate C/E ratios a few tenths of a percent (see LASL contribution to Appendix B). The Monte Carlo code VIM gave results that were in general agreement with the analytical methods for ZPR6-7 but with the capture rate in ^{238}U calculated about 1% higher.

SMALL SAMPLE CENTRAL REACTIVITY WORTHS

In order to remove inconsistencies and inaccuracies in the testing of small sample reactivity worths, a single set of reactivity conversion factors computed from ENDF/B-IV absolute delayed neutron yields and delayed neutron spectra have been used to convert measured sample reactivities reported in inhours or dollars to absolute reactivities ($\Delta k/k$). These conversion factors are listed in Table VIII along with other sets of conversion factors that had been used by some testers. The difference between the ENDF/B-IV conversion factors and the factors specified in ENDF-202 reflects primarily the difference between the absolute delayed neutron yields measured by Keepin and the newer, evaluated ENDF/B-IV yields. For Pu fueled assemblies, the difference is significant and most of the difference is due to the

TABLE VIII. Reactivity Conversion Factors

Benchmark	ENDF/202[a]		ENDF/B-IV[c]		Other[d]	
	β_e	Ih/%	β_e	Ih/%	β_e	Ih/%
Pu Fueled:						
JEZEBEL	0.0019					
VERA-11A			0.00304	993	0.00331	926
ZEBRA-3		860	0.00442	823	0.00440	838
SNEAK-7A	0.00359				0.00361	912
SNEAK-7B	0.00400				0.00411	844
ZPR3-48		981	0.00359	920	0.00359	933
ZPR3-56B		1130[b]			0.00326	976
ZPR6-7		1007	0.00340	944	0.00337	973
ZPPR-2		1016	0.00336	947	0.00337	963
U Fueled:						
GODIVA	0.0066					
ZPR3-6F		430			0.00782	407
VERA-1B		416			0.00806	377
ZPR3-12		427			0.00773	428
ZPR3-11		470	0.00731	474	0.00745	463
ZEBRA-2		480	0.00743	449	0.00752	442
ZPR6-6A		449	0.00725	436	0.00732	432

[a] Mostly Keepin delayed data.

[b] Used Master's delayed yields.

[c] Calculations from ANL only; 1-D homogeneous reactor models.

[d] Calculations from HEDL only; ENDF/B-IV delayed data, except delayed spectra, were used in a 2-D calculation of the reactor where the reactor fluxes were computed with ENDF/B-III cross sections.

larger ^{238}U and Pu delayed neutron yields in ENDF/B-IV. The small sample central worth C/E ratios in those assemblies for which ENDF/B-IV conversion ratios were available are reported in Tables IX-XIII.

The fissile sample (^{239}Pu and ^{235}U) worth C/E ratios are presented in Tables IX and X. For a given benchmark the C/E ratios are very consistent and this is a result of the relative insensitivity of the fissile sample worth to details of the calculated spectrum. Also, with the exception of ZPPR2, the C/E ratios for fissile samples in Pu and U fueled assemblies is remarkably consistent. There is a very definite bias according to fuel type. The C/E ratios are about 1.17 in Pu fueled assemblies and 1.05 to 1.10 in U fueled assemblies.

The C/E ratios for ^{238}U and ^{10}B small sample reactivity worths are given in Tables XI and XII. These reactivity worths are sensitive to the calculation of the low energy real and adjoint spectra. For a given benchmark, the calculated worths range a few percent with the GAC calculations consistently higher by a few percent. The C/E ratios for ^{238}U range from 5% underprediction to more than 10% overprediction and average slightly greater than 1.0. The C/E ratios for ^{10}B are closer to unity and average less than 1.0. There is no clear difference in the prediction of these reactivity worths in U fueled assemblies vs. Pu fueled assemblies.

The sodium central worth C/E ratios are given in Table XIII. The scatter in calculated sodium worths, both among testers for a given benchmark and among all the benchmarks, is evident. As a test of a specific set of nuclear data the sodium worth is not especially useful but the prediction of the sodium worth is important in liquid metal cooled fast reactors. The sodium reactivity worth is particularly sensitive to the calculation of the shape or slope of the adjoint spectrum and as

TABLE IX. ^{239}Pu Central Worth C/E Ratios in the 1-D Homogeneous Reactor Models[a]

Benchmark	ANL	BNL	GAC	GE	HEDL[b]	LASL	ORNL	W
Pu Fueled:								
ZEBRA-3	1.17				1.16			
ZPR3-48	1.17	1.18	1.18	1.16	1.17			
ZPR6-7	1.18	1.17	1.18	1.18	1.18		1.17	1.18
ZPPR-2	1.09		1.14[c]	1.15	1.11			
U Fueled:								
ZPR3-11	1.03				1.05			
ZEBRA-2	1.07				1.12			
ZPR6-6A	1.05		1.07		1.05			

[a] Reactivity conversion factors calculated by ANL have been applied to all results reported here. The calculated reactivity worths have been taken as $\delta k/k$ (i.e., not $\delta k/k^2$).

[b] For HEDL results, the following conversion was used:

$$(\text{HEDL C/E}) \times \frac{(\text{Ih}/\%)\text{ANL}}{(\text{Ih}/\%)\text{HEDL}} \ .$$

[c] 2-D, 10 gp. calculation for real and adjoint flux at center of ZPPR2.

TABLE X. ^{235}U Central Worth C/E Ratios in the 1-D Homogeneous Reactor Models[a]

Benchmark	ANL	BNL	GAC	GE	HEDL[b]	LASL	ORNL	W
Pu Fueled:								
ZEBRA-3	1.17				1.17			
ZPR3-48	1.18	1.19	1.17	1.17	1.18			
ZPR6-7	1.16	1.16	1.14	1.16	1.16			1.17
ZPPR-2	1.20		1.26[c]	1.26	1.23			
U Fueled:								
ZPR3-11	1.08				1.10			
ZEBRA-2	1.10				1.14			
ZPR6-6A	1.10		1.10		1.09			

[a] Ibid Table IX.

[b] Ibid Table IX.

[c] Ibid Table IX.

TABLE XI. ^{238}U Central Worth C/E Ratios in the 1-D Homogeneous Reactor Models[a]

Benchmark	ANL	BNL	GAC	GE	HEDL[b]	LASL	ORNL	W
Pu Fueled:								
ZEBRA-3	1.09				1.01			
ZPR3-48	1.03	1.06	1.10	0.99	1.02			
ZPR6-7	0.97	0.99	1.04	0.95	0.99			0.97
ZPPR-2								
U Fueled:								
ZPR3-11	1.02				0.99			
ZEBRA-2	1.04				1.02			
ZPR6-6A	1.11		1.17		1.13			

[a] Ibid Table IX.

[b] Ibid Table IX.

TABLE XII. ^{10}B Central Worth C/E Ratios in the 1-D Homogeneous Reactor Models[a]

Benchmark	ANL	BNL	GAC	GE	HEDL[b]	LASL	ORNL	W
Pu Fueled:								
ZEBRA-3	1.01				1.01			
ZPR3-48	0.95	0.96	1.00	0.91	0.95			
ZPR6-7	1.04	1.05	1.11	1.02	1.06			
ZPPR-2			1.02[c]		0.98			
U Fueled:								
ZPR3-11	0.95				0.96			
ZEBRA-2	0.86				0.79			
ZPR6-6A	0.89		0.93		0.91			

[a]Ibid Table IX.

[b]Ibid Table IX.

[c]Ibid Table IX.

TABLE XIII. Sodium Central Worth C/E Ratios in the 1-D Homogeneous Reactor Models[a]

Benchmark	ANL	BNL	GAC	GE	HEDL[b]	LASL	ORNL	W
Pu Fueled:								
ZEBRA-3					1.16			
ZPR3-48	2.14	2.05	1.76	2.39	2.05			
ZPR6-7	1.25	1.13	1.07	1.29	1.11			1.18
ZPPR-2	1.17		1.05[c]	1.11	1.06			
U Fueled:								
ZPR3-11					1.77			
ZEBRA-2					-0.38			
ZPR6-6A[d]	-2.15		-2.49		0.17			

[a] Ibid Table IX.

[b] Ibid Table IX.

[c] Ibid Table IX.

[d] The measured sodium worth is very small and close to zero in ZPR6-6A, hence the large variance in C/E values.

such it provides only a general integral test of the calculations. Clearly, however, the sodium worth does indicate that a problem exists with the calculation of the spectra and/or the data used in the calculations.

All data testing results so far presented have been based upon 1-D homogeneous models of the benchmark assemblies. These models, with their specified correction factors, are appropriate for tests of k_{eff} and central reaction rate ratios but they are not completely appropriate for central reactivity calculations. The reactivity worth includes a calculation of a normalization factor (perturbation denominator) and this factor is geometry dependent. The small sample central worths are sensitive to heterogeneity effects and corrections for heterogeneity are not specified. For illustration, central worth C/E ratios computed for 2-D heterogeneous models are given in Table XIV for ZPR6-6A, ZPR6-7 and ZPR3-48. The fissile sample worth C/E's have increased 1-2% compared with the 1-D homogeneous models and this is due to the 1-2% increase in the calculated 2-D reactivity conversion factors (see footnote b in Table XIV). The ^{238}U and ^{10}B C/E ratios have increased 4-9% and this is due to the enhancement of the low energy spectrum when heterogeneity effects are included. Thus, if geometry and heterogeneity corrections were included in the small sample reactivity tests, the C/E ratios for fissile samples would be slightly higher and the difference between fissile and non-fissile sample C/E ratios would be less accentuated.

The trends noted in the testing of small sample central worths may be related to the trends noted above for criticality and reaction rate tests. The overprediction of sample worths in plutonium fueled assemblies compared to uranium fueled assemblies would be consistent with a difference in the calculated normalization factors (perturbation denominators) and/or calculated reactivity conversion factors in the

TABLE XIV. Central Worth C/E Ratios for 2-D Heterogeneous Models[a]

Benchmark[b]	^{239}Pu	^{235}U	^{238}U	^{10}B	Sodium
ZPR6-6A	1.08	1.12	1.13	0.93	-5.7[c]
ZPR6-7	1.19	1.17	1.04	1.12	1.43
ZPR3-48	1.17	1.17	1.12	1.03	2.17

[a] All calculations performed at ANL. (R. D. McKnight, "Benchmark Testing Using Versions 3 and 4," submitted to Nucl. Sci. Eng.)

[b] Reactivity conversion factors computed for 2-D heterogeneous model:

	β_{eff}	Ih/%
ZPR6-6A	0.00708	444
ZPR6-7	0.00334	959
ZPR3-48	0.00352	934

[c] The measured sodium worth in ZPR6-6A is very small and close to zero, hence the large negative C/E value.

two types of assemblies. The normalization factor is the total neutron production rate in the assembly and, hence, an underprediction of $^{49}f/^{25}f$ is consistent with an overprediction of reactivity worths in plutonium assemblies compared to uranium assemblies. The reactivity conversion factor is primarily a function of the production weighted absolute delayed neutron yields. Since the absolute delayed neutron yield in the fission of ^{239}Pu is less than half that in ^{235}U fission, the impact of recent, higher ^{238}U absolute delayed neutron yields on the reactivity conversion factor in Pu fueled assemblies is greater.

While they probably do contribute to some of the small sample reactivity worth discrepancies, simple differences in the calculated normalization and reactivity conversion factors cannot account for the entire set of observed testing results in Tables IX-XIII. Fissile sample worths are overpredicted consistently but ^{10}B and ^{238}U reactivity worths do not exhibit this same behavior. The calculated reactivity worth is a complex function of a large set of nuclear data. It is a bilinear weighting of the sample cross sections where both the real and adjoint spectra are themselves integrally related to the cross sections of all materials in the assemblies. Thus, the information pertaining to data testing obtained from small sample reactivity worths is not as directly interpretable as criticality and reaction rate tests, but, the calculation of a set of reactivity worths does provide a sensitive indication of the state of evaluated nuclear data.

D. Conclusions and Recommendations

The testing of the fast reactor benchmarks summarized in Section C above demonstrates the current status of ENDF/B with respect to calculations of basic fast reactor parameters. While some trends have been recognized from the benchmark tests, these results are limited both in scope and by the nature of the benchmark models themselves. The tests are integral in nature. In a large fast reactor, the important energy range spans four decades; several heavy and light materials make up the compositions and many reaction types influence the neutron inventory. Thus, very specific recommendations concerning nuclear data evaluations will not be forthcoming, rather, general conclusions will be discussed.

The most important features or trends identified as a result of the foregoing compilation are the following:

1. For benchmark assemblies similar in configuration and non-fuel composition, the k_{eff} of the Pu fueled assemblies is underpredicted relative to the U fueled assemblies.

2. The k_{eff} of large, dilute assemblies is underpredicted relative to smaller, harder-spectrum assemblies.

3. The fission rate in ^{239}Pu relative to ^{235}U fission is generally underpredicted.

4. The capture rate in ^{238}U relative to fission is overpredicted in the large, dilute assemblies.

5. Small sample central reactivity worths for fissile samples are overpredicted more than for the low-energy absorber samples (^{238}U and ^{10}B), and, are overpredicted more in Pu fueled assemblies than in U fueled assemblies.

To the extent that these discrepancies can be attributed to errors or deficiencies in ENDF/B-IV, several nuclear data may be cited for further review. The standard or absolute fission cross section of ^{235}U, $^{239}Pu(n,f)$ relative to $^{235}U(n,f)$, the prompt fission neutron spectrum, and $^{239}\nu$ relative to $^{235}\nu$ impact on items 1, 3, and 5 above. The ^{238}U inelastic scattering cross section is apparently uncertain and it, along with the elastic scattering cross sections of sodium, oxygen and stainless steel, is important in the calculation of the spectra in large, dilute assemblies and, hence impacts on items 2, 4, and 5 above. The ^{238}U capture cross section is a very important part of the neutron balance in a fast reactor; it influences the calculation of the spectrum and impacts on items 2, 4, and 5 above. The absolute delayed neutron yield for ^{238}U fission and the delayed neutron spectra associated with the fission of all isotopes are important for item 5.

There are certain limitations inherent in the benchmark testing procedure as it now stands. The use of 1-D homogeneous composition models facilitates computations, but, except for the two small metal sphere benchmarks, these models do introduce a degree of uncertainty in the testing results. The experimental critical mass or k_{eff} for a benchmark is usually specified with an imprecision on k_{eff} of ±0.001 or ±0.002 which includes uncertainties due to excess reactivity, temperature and boundary smoothing corrections and uncertainties in material compositions. But the specification of the 1-D homogeneous model introduces the following factors that affect the calculation of k_{eff}:

1. 2D-to-1D Geometry Specifications.

The benchmark assemblies usually possess 2-D symmetry and can be well described with a 2-D model. The specification to a 1-D equivalent geometry may be made by applying a computed shape factor, as in the case of some of the older

benchmarks, or by specifying the boundary of the 1-D model to give the same calculated k_{eff} as obtained for the 2-D model. Ideally these 2D-to-1D specifications are invariant for different cross section sets and methods and may be specified once and for all. But recent calculations using ENDF/B-IV showed a difference in k_{eff} of 0.0005 between 2-D and 1-D benchmark models that were originally specified to have the same k_{eff} with calculations using ENDF/B-III.* Also, the difference in k_{eff} between 2-D and 1-D models varies (up to 0.15%) with the computational methods used.**

2. Transport Corrections.

Most benchmark calculations are performed with diffusion theory. Transport (S_n) calculations are considered more exact and calculated correction factors (diffusion-to-S_n and/or S_n-to-S_∞) as listed in Table III.a are applied to the diffusion calculations. From time to time, as methods improve, these factors are recomputed and are found to vary a few tenths of a percent in k_{eff}.

3. Heterogeneity Corrections.

Corrections for heterogeneity effects in plate loaded assemblies are calculated, and, as methods improve, these factors have varied 0.1% or less in k_{eff}. However, anisotropic streaming effects which have only recently been computed as methods became available, indicate that corrections of the order of -0.1% to 0.4% in k_{eff} must be applied to some of the homogeneous models.*

---

*R. D. McKnight, "Benchmark Testing Using ENDF/B Versions 3 and 4," submitted to Nucl. Sci. Eng.).

**For example, compare ENDF/B-III calculation of 2D-to-1D correction factors obtained by HEDL (Appendix B) with calculations by ANL (R. D. McKnight* or ENDF-202 specifications for ZPR6-7, 6A and ZPR3-48).

4. Calculation Specifications.

Certain specifications for the calculations may be varied to yield differences in the calculated k_{eff} for the benchmark models. These specifications include mesh size, number of broad energy groups, and the representation of the prompt neutron spectrum. The net effect of all these factors is estimated to be a few tenths of a percent in k_{eff}.

Considering these factors and the reported imprecision in the measured k_{eff}, the true uncertainty in the 1-D homogeneous benchmark models is estimated to be ±0.5% - ±1% for k_{eff}. Thus, for data testing purposes, a computed k_{eff} within 1% of unity may yield little information. However, since these correction factors are correlated and the specifications are uniform among the benchmark models, a relative comparison of data tests for the set of models (as was done above) does yield useful information.

Regarding reaction rate ratio tests, the major consideration is the correction from the actual measured ratio to an equivalent homogeneous calculation. (This correction is most important for capture rate measurements.) Some measurements were made with fission chambers, some with foil irradiations in the benchmark assemblies. Documentation is generally sparse on the nature of corrections applied, especially in the case of older experiments. (Note the large C/E ratios for reaction rates in the VERA assemblies.) It is recommended that data tests of reaction rates employ only the more recent, well-documented benchmarks.

For small sample reactivity worths, the 1-D homogeneous models are not sufficient tests. Heterogeneity effects were shown to affect the low energy absorber worths a few percent. The reactivity conversion factor is geometry dependent and conversion factors derived from 1-D models may be in error. The current ENDF-202

specifications do not include corrections to be applied to reactivity worth calculations for these factors, and, hence, tests of reactivity worths are limited to identification of only gross trends.

SHEILDING

IV. SHIELDING

A. Introduction

The benchmarks used to test ENDF-IV data, as well as earlier ENDF-III data, are the following: SDT1-5, the "broomstick" series which test the neutron total cross section in the range 1 - 10 MeV for iron, oxygen, nitrogen, sodium, and stainless steel; SDT6, which tests the gamma-ray-production cross sections arising from thermal-neutron capture in iron, stainless steel, nitrogen, and sodium; SDT7, which tests the gamma-ray-production cross sections averaged over a known fast-neutron spectrum in the range 1 - 15 MeV for iron, stainless steel, oxygen, and sodium; SDT10, which tests the neutron cross sections between 2 and 14 MeV by measuring time-of-flight spectra through several mean free paths of a large number of materials; and SDT12, which tests the neutron cross sections between 1 eV and 15 MeV for sodium by measuring neutron spectral fluxes and weighted integrals of these fluxes behind various thicknesses of sodium up to and including 15 ft. These benchmarks are described in ENDF 166, 167, 168, 169, and 170 for SDT1-5 respectively, in ENDF 176 and 177 for SDT6-7, in UCID 16372 for SDT10, and in ENDF 189 for SDT12. The participants in this data testing include BNL and ORNL for SDT1-5, LASL and ORNL for SDT6-7, LLL for SDT10, and ORNL for SDT12.

B. Computational Methods

The methods used to calculate the benchmarks are those recommended in the descriptive reports. SDT1-5 were calculated by BNL using a special code distributed through RSIC, and by ORNL using an updated version of this code. SDT6-7 were calculated by LASL using LAPHANO, and by ORNL using LAPHFOR for ENDF-III and AMPX for ENDF-IV. SDT10 was calculated by LLL using the Monte Carlo TART code, and SDT12 was calculated by ORNL using both the DOT discrete ordinates code (S_8,P_3) and the MORSE Monte Carlo code. Details of the SDT12 calculations can be found in ORNL 4880.

C. Testing Results

The comparisons of calculated and measured results are shown in the accompanying tables and figures. SDT1-5 comparisons are shown in Figs. SDT1-5. Significant and consistent discrepancies between ENDF-IV (circles) and the

measurements (shaded area) are seen to occur for iron in the regions 1.3 - 1.6 MeV, 2.5 - 3 MeV, and 4 - 5 MeV. ENDF-IV represents a considerable improvement over ENDF-III in the region 1 - 2.5 MeV, however. For oxygen, significant discrepancies between ENDF-IV and the measurement occur in the regions 4.3 - 4.7 MeV and 5.5 - 5.9 MeV. ENDF-IV represents some improvement over ENDF-III, but the improvement is minimal. For nitrogen, significant discrepancies between ENDF-IV and the measurement occur in the regions 0.8 - 1.2 MeV, 1.6 - 1.9 MeV, and 3.2 - 4.6 MeV. For sodium, the calculated curve lies slightly above the measured curve everywhere, with more significant discrepancies in the regions 1 - 1.5 MeV and 3.2 - 3.7 MeV. For stainless steel, ENDF-IV represents a considerable improvement over ENDF-III, with no significant discrepancy occurring in the region 1 - 5 MeV.

Comparisons between the calculations and measurements for SDT6 are shown in Tables SDT6-1 through SDT6-4. At unpredictable times it is to be noted that the three processing codes do not yield the same calculated answers, although the discrepancy is never large. Reasons for this are not known at the present time. For iron, significant discrepancies between ENDF-IV and measurement occur in the gamma-ray energy regions 2 - 3.5 MeV and 4 - 5.5 MeV, but ENDF-IV still represents an improvement over ENDF-III. For stainless steel, ENDF-IV disagrees with the measurement only in the regions 1.0 - 1.5 MeV and 2 - 3 MeV. For nitrogen, there is no significant discrepancy. For sodium, there are significant discrepancies in the regions 1.5 - 2 MeV and 4 - 5.5 MeV. In none of the four materials, however, is there a significant discrepancy between the calculated and measured integrals over gamma-ray energy above 1 MeV.

Comparisons between the calculations and measurements for SDT7 are shown in Tables SDT7-1 through SDT7-4. Again, differences in the processing codes occur, but they are slight and not as worrisome as occur for SDT6. For iron, there is only one significant disagreement between ENDF-IV and measurement, in the gamma-ray energy region 6.5 - 7 MeV, and the significance in this interval is even questionable. Again, ENDF-IV considerably improves the agreement with measurement over ENDF-III. For stainless steel and oxygen, there is no significant discrepancy between ENDF-IV and measurement. For

sodium, there is relatively poor agreement between ENDF-IV and measurement, and even the integral over gamma-ray energy is poorly described.

Comparisons between calculations using ENDF-IV and measurement for SDT10 are summarized in Table SDT10-1. The elastic peak comparisons indicate adequate agreement in the ~12 - 14 MeV range for all materials investigated except for magnesium, lead, and ^{239}Pu. In the region 1.9 - ~12 MeV, there is in general poorer agreement, with particularly significant discrepancies in magnesium, titanium, tungsten, and lead.

Comparisons between calculations using ENDF-III sodium (identical to ENDF-IV except for an extension from 15 to 20 MeV) and measurements for SDT12 are summarized in Tables SDT12-1 through SDT12-3 and the figures labelled SDT12. In Table SDT12-1 the Bonner ball counting rates are compared behind 10, 12.5 and 15 ft of sodium. Uncertainties in the response functions for the 10- and 12-in. balls render comparisons with these balls less significant than with the remaining balls. The overall comparisons with the remaining balls indicate that the flux in the region 1 eV - 10 keV is underestimated using ENDF-III sodium by about 10% behind 10 and 12.5 ft of sodium, and by about 25% behind 15 ft of sodium. On the other hand, the flux above ~50 keV is overestimated using ENDF-III by about 30% behind 10, 12.5, and 15 ft of sodium. From Table SDT12-2, comparisons of the flux above 1 MeV indicate that the use of ENDF-III sodium overpredicts this flux by about 20% behind 5 ft of sodium and by about 30% behind 10 ft of sodium. From Table SDT12-3, comparisons of the flux in the region 74 keV - 1.35 MeV indicate that this flux is overpredicted by ~10% behind 5 ft of sodium, by ~40% behind 10 ft of sodium, and by ~60% behind 12.5 ft of sodium. By examining the spectral comparisons in the figure, additional insight can be obtained as to the energy regions where ENDF-III is probably deficient.

D. Conclusions and Recommendations

From comparisons of calculation with measurement for SDT1-5, the following specific conclusions about deficiencies in the ENDF-IV total neutron cross section can be made. For iron, lower total cross sections are certainly indicated for the regions 1.3 - 1.6 MeV, 2.5 - 3 MeV, and 4 - 5 MeV, and perhaps in additional regions between 1 and 2.5 MeV. For the latter two regions, a

constant reduction in σ_T by about 6% and 4% over the region is indicated. For the former region, where many minima are known to exist, a constant reduction by about 5% in σ_T would result in agreement with experiment. For oxygen, an average reduction of about 4% in σ_T in the energy ranges 4.3 - 4.7 and 5.5 - 5.9 MeV is indicated. For nitrogen, average increases in σ_T of about 5%, 7%, and 10% are indicated in the regions 0.8 - 1.2 MeV, 1.6 - 1.9 MeV, and 3.2 - 3.8 MeV respectively, and a decrease of about 7% is indicated in the region 4.2 - 4.6 MeV. For sodium, average increases of about 8% and 10% are indicated in the regions 1 - 1.5 MeV and 3.2 - 3.7 MeV. Everywhere else in the region 1 - 10 MeV, σ_T should be increased by about 5%. It should be pointed out at this time that additional conclusions can be made regarding the accuracy of the ENDF-IV nickel and chromium total cross sections based on comparisons with the results of similar "broomstick" experiments not yet incorporated into the SDT benchmark series.[1] For nickel, discrepancies in the range of 4 to 20% in σ_T are apparent in the region 38 keV - 4.6 MeV, and for chromium, discrepancies in the range of 5 - 20% in σ_T are apparent in the region 10 keV - 5 MeV. Evaluators are urged to consult Ref. 1 for a more complete resume of suspected deficiencies in the ENDF-IV values of σ_T.

The comparisons with SDT6 indicate the ENDF-IV thermal-neutron capture gamma-ray-production files are in reasonably good shape for iron, stainless steel, nitrogen, and sodium. More results are soon to be included in the SDT6 series, since these experiments covered a wider range of materials than has so far been described in SDT6. Comparisons of these results with ENDF-IV show that aluminum, silicon, potassium, and calcium are in reasonably good shape, that nickel should be reduced uniformly throughout the gamma-ray energy range 1.5 - 9 MeV by about 7%, and that chlorine, copper and titanium should be re-evaluated.

The comparisons with SDT7 indicate that sodium production cross sections for neutrons in the MeV range need to be re-evaluated. For other materials yet to be included in SDT7, it appears that aluminum, nickel, and titanium are adequate, but that copper, calcium, potassium, and silicon need to be re-evaluated

---

1. R. E. Maerker and F. J. Muckenthaler, "Neutron Total Cross Section Checks for Iron, Chromium, Nickel, Stainless Steel, Sodium and Carbon," ORNL-5013 (to be published).

The calculations with SDT10 show that there are significant discrepancies in lead, tungsten, and magnesium, and by inference in most materials not actually measured in SDT10.

The most serious discrepancy in the sodium neutron cross section set that may be deduced from SDT12 is that the total cross sections in the MeV range are a few percent too low, as witnessed by the comparisons shown in Table SDT12-2. By re-evaluating only these cross sections, the remaining disagreements summarized in Tables SDT12-1 and SDT12-3 may well be significantly reduced as well, although other cross sections (particularly in the vicinity of the 300-keV window) may be in error also. This important conclusion is consistent with that deduced from SDT4, the sodium "broomstick" experiment.

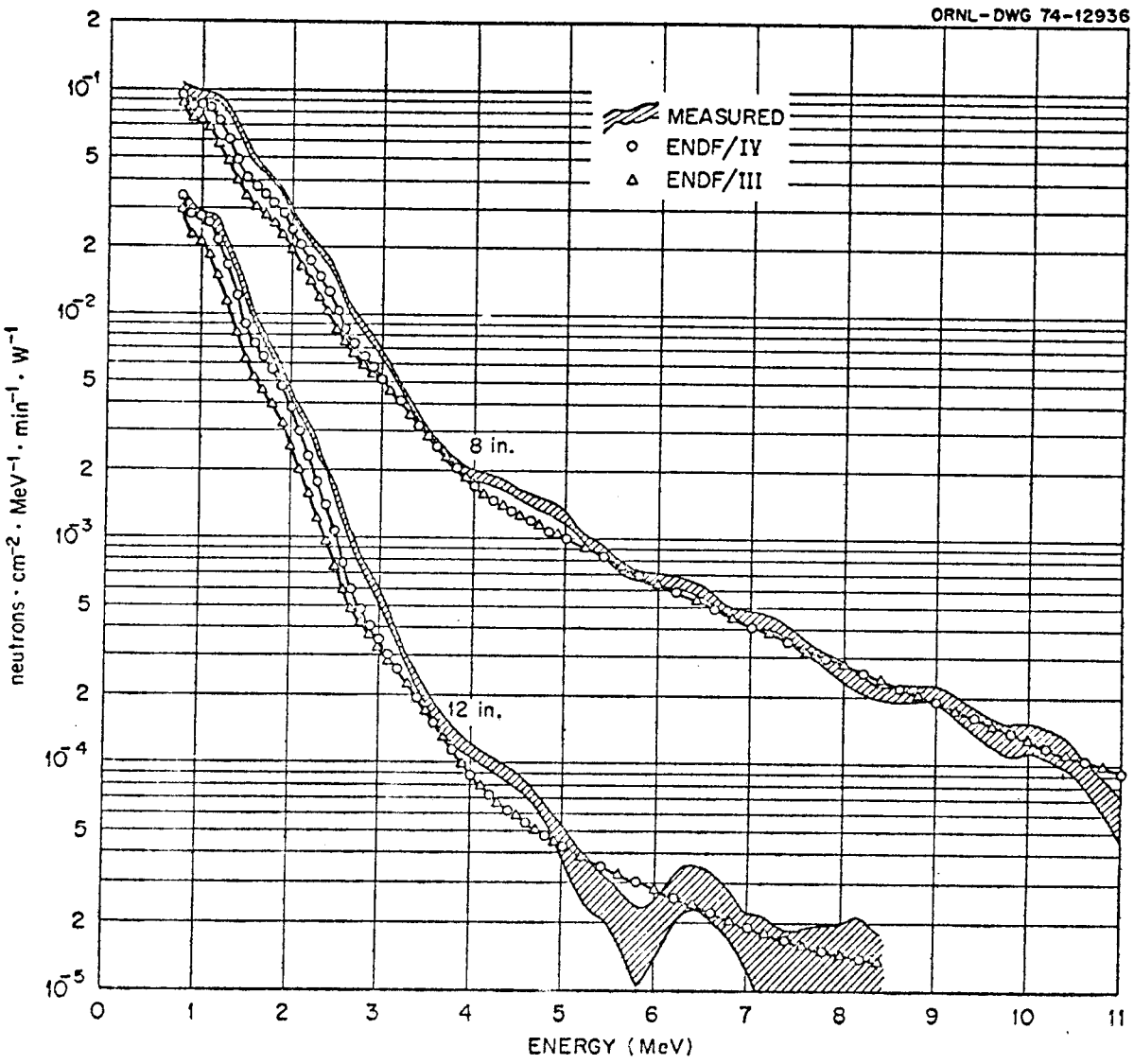

Fig. SDT1. Comparison of Measured and Calculated Transmitted Fluxes Behind 8 and 12 in. of Iron.

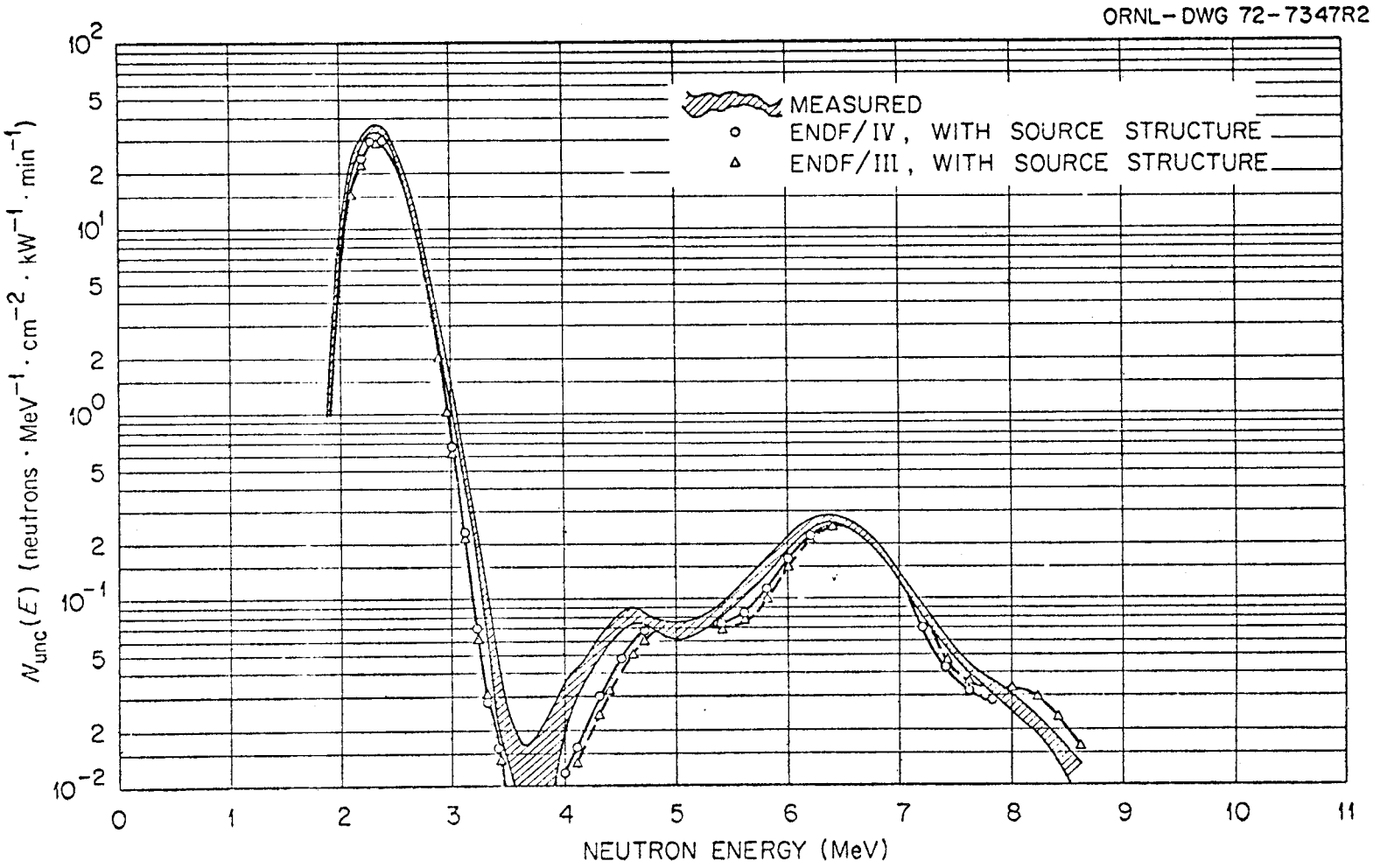

Fig. SDT2. Comparison of Measured and Calculated Transmitted Fluxes Behind 5 ft of Liquid Oxygen.

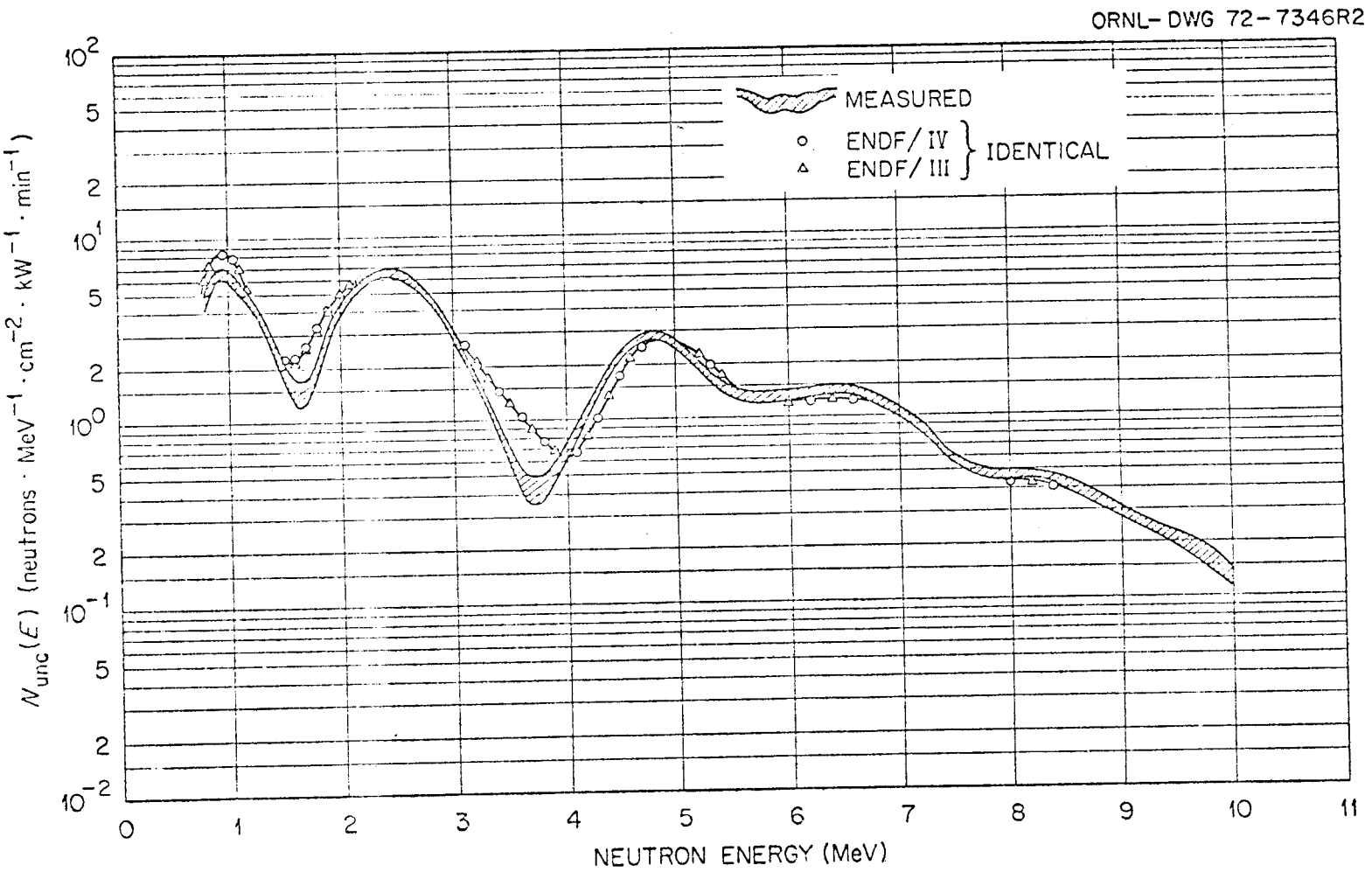

Fig. SDT3. Comparison of Measured and Calculated Transmitted Fluxes Behind 3 ft of Liquid Nitrogen.

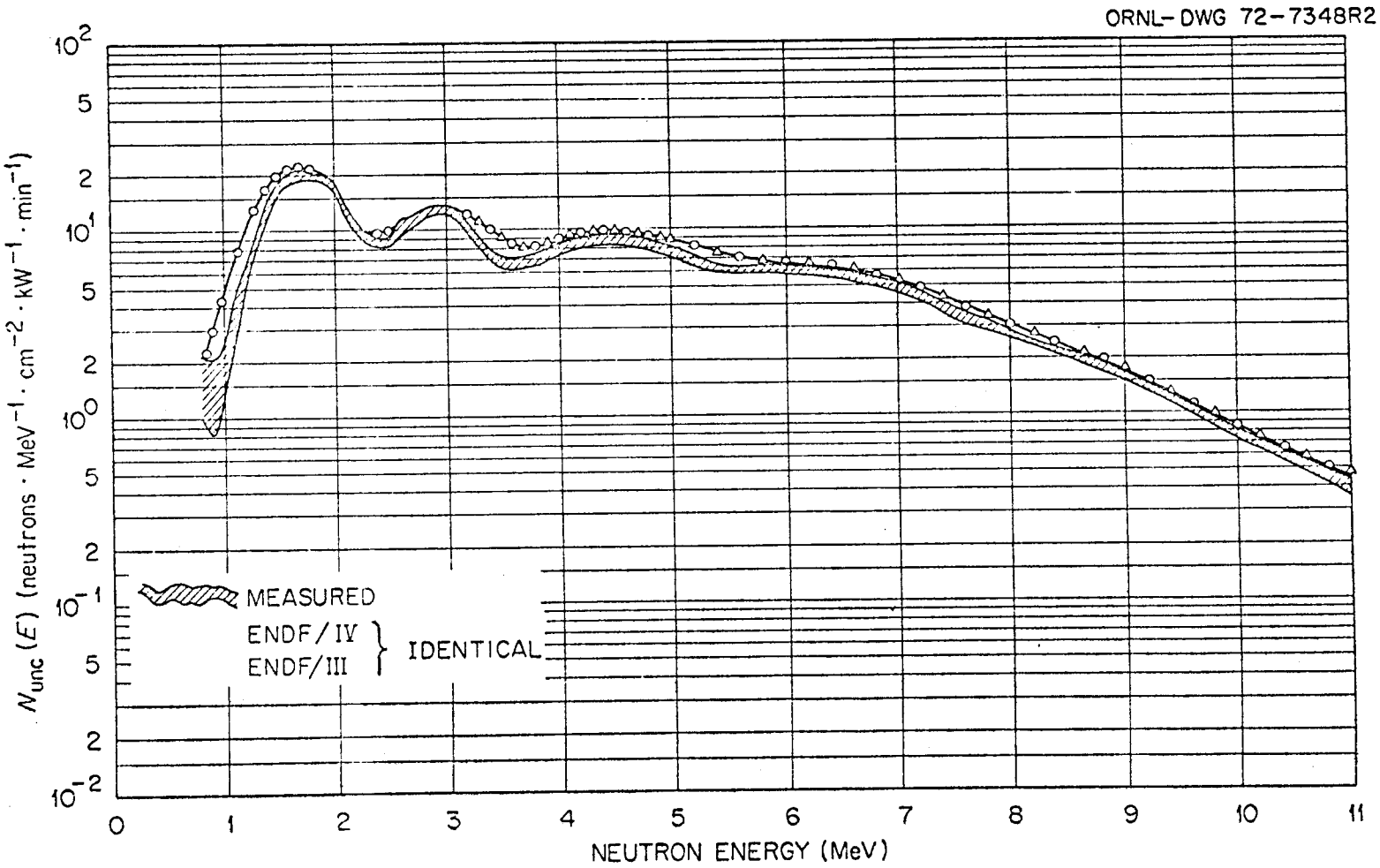

Fig. SDT4. Comparison of Measured and Calculated Transmitted Fluxes Behind 2 ft of Sodium.

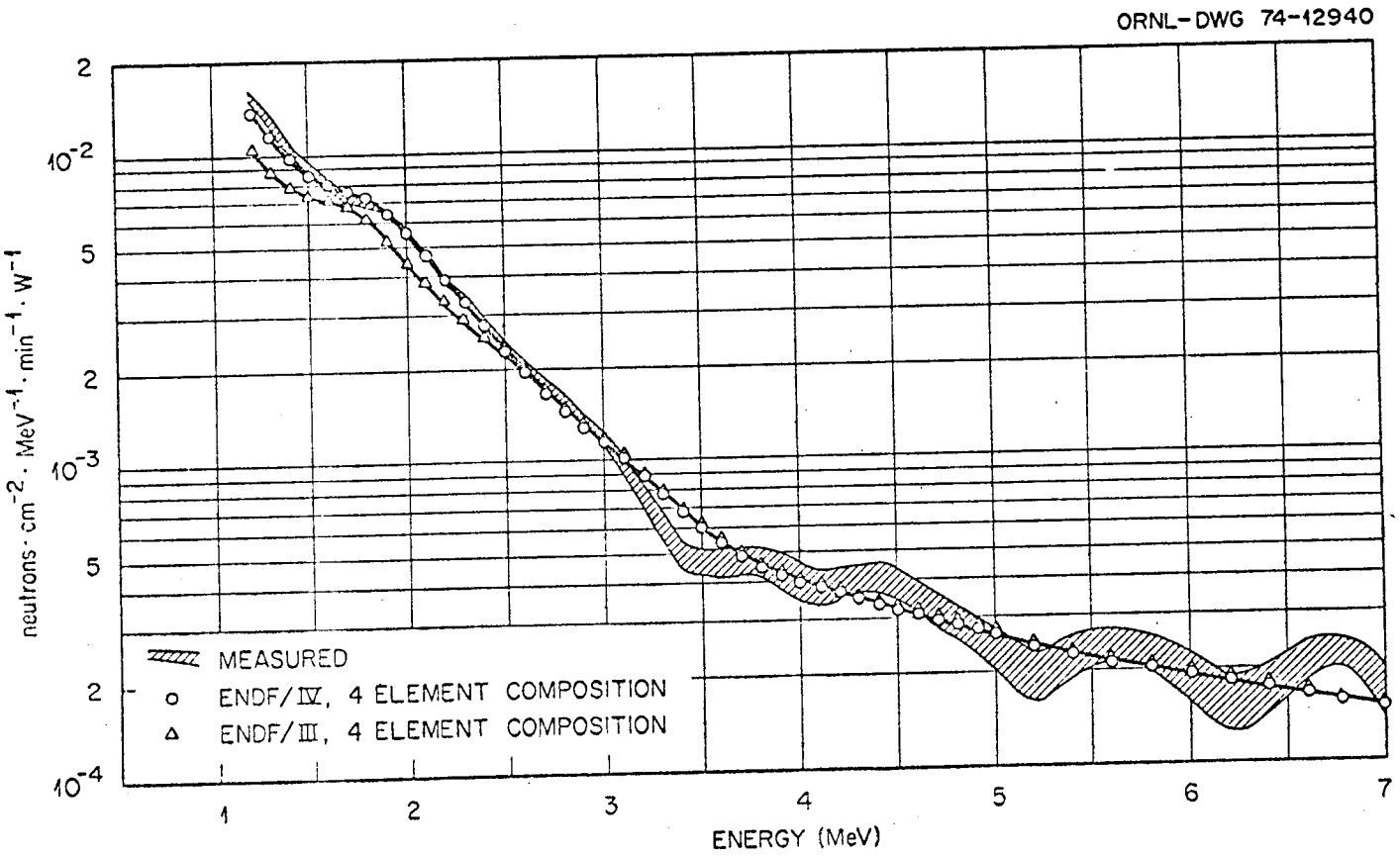

Fig. SDT 5. Comparison of Measured and Calculated Transmitted Fluxes Behind 8 in. of Type 310 Stainless Steel.

Table SDT6-1. Secondary Gamma-Ray-Production Cross Sections for Thermal-Neutron Capture in Iron

ΔE_γ (MeV)	Cross Section (mb)					Ratio:
		ENDF-III		ENDF-IV		
	Measured	LAPHANO Processed	LAPHFOR Processed	LAPHANO Processed	AMPX Processed	ENDF-IV(AMPX) / Measured
1.15-1.5	126	152	184	125	128	1.02
1.5-2	455	336	356	369	379	0.83
2-2.5	99	163	164	151	155	1.57[a]
2.5-3	152	181	182	239	240	1.58[a]
3-3.5	233	302	302	291	290	1.24[a]
3.5-4	88	194	197	82	82	0.93
4-4.5	182	271	269	237	237	1.30[a]
4.5-5	83	60	61	113	112	1.35[a]
5-5.5	25	35	36	32	31	1.24
5.5-6	250	151	148	241	235	0.94
6-6.5	255	236	243	227	235	0.92
6.5-7	13	7	8	3	3	0.23
7-7.5	139	125	125	123	123	0.88
7.5-8	1280	1268	1293	1273	1294	1.01
8-9	20	25	23	17	16	0.80
≥9	83	102	133	71	93	1.12
Sum	3483	3608	3724	3594	3653	1.05

a. Outside experimental error.

Table SDT6-2. Secondary Gamma-Ray-Production Cross Sections for Thermal-Neutron Capture in Stainless Steel

ΔE_γ (MeV)	Cross Section (mb)		Ratio: ENDF-IV(AMPX) / Measured
	Measured	ENDF-IV,[a] AMPX Processed	
1.0-1.5	442	131	0.30[b]
1.5-2	355	391	1.10
2-2.5	186	249	1.34[b]
2.5-3	134	223	1.66[b]
3-3.5	226	248	1.10
3.5-4	113	107	0.95
4-4.5	177	190	1.07
4.5-5	98	120	1.22
5-5.5	107	102	0.95
5.5-6	287	261	0.91
6-6.5	229	218	0.95
6.5-7	125	118	0.94
7-7.5	259	256	0.99
7.5-8	1025	1021	1.00
8-8.5	110	551	1.07
8.5-9	372		
9-9.5	58	132	1.17
9.5-10	55		
≥ 10	0	0	—
Sum	4358	4282	0.98

a. ENDF-III not included since there were no production files for nickel, chromium, and manganese in ENDF-III.

Table SDT6-3. Secondary Gamma-Ray-Production Cross Sections for Thermal-Neutron Capture in Nitrogen

ΔE_γ (MeV)	Cross Section (mb)					Ratio:
		ENDF-III[a]		ENDF-IV[a]		
	Measured	LAPHANO Processed	LAPHFOR Processed	LAPHANO Processed	AMPX Processed	ENDF-IV(AMPX) / Measured
1-1.5	0	0.2	0.2	0.2	0.1	
1.5-2	30	25.9	25.9	25.9	25.5	0.85
2-2.5	0	0.1	0.1	0.1	0.1	
2.5-3	6.4	5.9	5.9	5.9	5.8	0.91
3-3.5	0	0.7	0.7	0.7	0.7	
3.5-4	22.8	20.3	20.3	20.3	20.0	0.88
4-4.5	0	0	0	0	0	
4.5-5	13.4	12.4	12.4	12.4	12.2	0.91
5-5.5	43.3	38.7	38.7	38.7	38.1	0.88
5.5-6	25.2	21.8	21.8	21.8	21.4	0.85
6-6.5	15.2	14.3	14.3	14.3	14.0	0.92
6.5-7	0	0	0	0	0	
7-7.5	7.8	7.4	7.4	7.4	7.3	0.94
7.5-8	0	0	0	0	0	
8-8.5	3.5	3.4	3.4	3.4	3.4	0.93
8.5-9	0.17	0.1	0.1	0.1		
9-9.5	1.6	1.1	1.1	1.1	11.0	0.87
9.5-10	0	0.1	0.1	0.1		
10-10.5	0	0	0	0		
10.5-11	11	10.0	10.0	10.0		
≥ 11	0	0	0	0	0	
Sum	180.37	162.4	162.4	162.4	159.6	0.88

Table SDT6-4. Secondary Gamma-Ray-Production Cross Sections for Thermal-Neutron Capture in Sodium

ΔE_γ (MeV)	Cross Section (mb)		Ratio:
	Measured	ENDF-III&IV,[a] All Codes	ENDF-III&IV / Measured
1-1.5	79	90	1.18
1.5-2	76	48	0.63[b]
2-2.5	143	132	0.92
2.5-3	254	232	0.91
3-3.5	76	92	1.21
3.5-4	182	199	1.09
4-4.5	34	15	0.44[b]
4.5-5	14	3	0.21[b]
5-5.5	12	6	0.50[b]
5.5-6	31	33	1.06
6-6.5	115	118	1.03
$\geq$ 6.5	0	0	----
Sum	1016	968	0.95

a. ENDF-III and ENDF-IV are identical and all three processing codes give the same results.

b. Outside experimental error.

Table SDT7-1. Secondary Gamma-Ray-Production Cross Sections for Iron Averaged over a Neutron Spectrum from 1 - 14 MeV

ΔE_γ (MeV)	Cross Section (mb)					Ratio:
		ENDF-III		ENDF-IV		
	Measured	LAPHANO Processed	LAPHFOR Processed	LAPHANO Processed	AMPX Processed	ENDF-IV(AMPX) / Measured
1-1.5	278	252	258	211	210	0.76
1.5-2	132	100	98	110	106	0.80
2-2.5	101	94	98	99	101	1.00
2.5-3	74	84	86	63	64	0.86
3-3.5	44	31	30	46	46	1.05
3.5-4	33	24	25	38	39	1.18
4-4.5	8.7	2.9	2.9	8.0	8.0	0.92
4.5-5	5.6	3.1	3.1	4.9	5.0	0.89
5-5.5	3.8	2.8	2.9	4.1	4.1	1.08
5.5-6	2.4	2.4	2.4	2.4	2.4	1.00
6-6.5	< 2.1	0.7	0.7	1.9	1.9	~ 0.90
6.5-7	< 0.6	0.5	0.5	1.3	1.3	~ 2.2[a]
7-7.5	< 1.5	0.3	0.3	0.8	0.8	~ 0.5
≥ 7.5	0	0.8	0.8	1.1	1.4	
Sum	≲ 686.7	598.5	608.6	591.5	590.9	0.86

a. Outside experimental error.

Table SDT7-2. Secondary Gamma-Ray-Production Cross Sections for Stainless Steel Averaged over a Neutron Spectrum from 1 - 14 MeV

ΔE_γ (MeV)	Cross Section (mb)		Ratio: ENDF-IV(AMPX) / Measured
	Measured	ENDF-IV,[a] AMPX Processed	
1-1.5	383	280	0.73
1.5-2	139	122	0.88
2-2.5	84	93	1.11
2.5-3	53	59	1.11
3-3.5	43	42	0.98
3.5-4	25	32	1.28
4-4.5	8.8	8.4	0.95
4.5-5	5.8	5.0	0.86
5-5.5	5.1	3.7	0.73
5.5-6	3.0	2.2	0.73
6-6.5	<2.6	1.7	~ 0.65
6.5-7.5	<4.9	1.8	~ 0.37
≥ 7.5	0	1.3	
Sum	$\lesssim 757.2$	652.1	0.86

a. ENDF-III not included since there were no production files for nickel, chromium, and manganese in ENDF-III.

Table SDT7-3. Secondary Gamma-Ray-Production Cross Sections for Oxygen Averaged over a Neutron Spectrum Above 6.5 MeV

E_γ (MeV)	Cross Section (mb)			Ratio: ENDF-IV / Measured
	Measured	ENDF-III[a]	ENDF-IV[a]	
6.13	90	80	87	0.97
6.92+7.12	55	47	47	0.85
Sum	145	127	134	0.92

a. Processed by LAPHANO.

Table SDT7-4. Secondary Gamma-Ray-Production Cross Sections for Sodium Averaged over a Neutron Spectrum from 1 - 14 MeV

ΔE_γ (MeV)	Cross Section (mb)		Ratio:
	Measured	ENDF-III&IV,[a] All Codes	ENDF-IV / Measured
1.1-1.5	59	2.4	0.04[b]
1.5-2	131	99	0.76
2-2.5	47	37	0.79
2.5-3	50	60	1.20
3-3.5	22	8.3	0.38[b]
3.5-4	15	12	0.80
4-4.5	7.3	9.3	1.27
4.5-5	4.6	1.3	0.28[b]
5-5.5	2.9	1.0	0.34[b]
5.5-6	3.7	4.1	1.11
6-6.5	4.2	1.5	0.36[b]
6.5-7.5	2.4	0.3	0.13[b]
$\geq$ 7.5	0	0	
Sum	349.1	236.2	0.68[b]

a. ENDF-III and ENDF-IV are identical and all three processing codes give the same results.

b. Outside experimental error.

Table SDT10-1. Pulsed Sphere Calculations Using ENDF-IV-P Data for 30-deg Measurement — Comparison of Integrals Under Elastic Peak, Total Integral and Integral from Elastic Peak to 1.9 MeV

(Units are neutrons per source neutron.)

Material	$\int_0^{161} N(t)\,dt$ Exp.	$\int_0^{161} N(t)\,dt$ Calc.	Calc.-Exp. / Exp.	$\int_0^{401} N(t)dt$ Exp.	$\int_0^{401} N(t)dt$ Calc.	Calc.-Exp. / Exp.	$\int_{161}^{401} N(t)dt$ Exp.	$\int_{161}^{401} N(t)dt$ Calc.	Calc.-Exp. / Exp.
H_2O[a]	0.307	0.321	+4.5%	0.508	0.562	+11%	0.201	0.241	+15%
D_2O	0.297	0.303	+1.3%	0.298	0.299	+0.3%	0.595	0.602	+1.2%
^6Li	0.795	0.804	+1.1%	0.962	0.937	-2.6%	0.167	0.133	-20%
^7Li	0.798	0.806	+0.9%	0.963	0.947	-1.7%	0.165	0.141	-15%
^9Be	0.718	0.697	-2.9%	0.975	0.970	-0.5%	0.257	0.273	+6.2%
^{12}C	0.757	0.763	+0.8%	0.907	0.885	-2.4%	0.150	0.122	-19%
^{14}N	0.645	0.592	-8.2%	0.816	0.783	-4.0%	0.171	0.191	+12%
^{16}O	0.723	0.715	-1.1%	0.879	0.891	+1.4%	0.156	0.176	+13%
Mg	0.664	0.770	+16%	0.800	0.853	+6.6%	0.136	0.083	-39%
^{27}Al	0.590	0.576	-2.4%	0.786	0.747	-5.0%	0.196	0.171	-13%
Ti	0.520	0.553	+6.3%	0.728	0.700	-4.0%	0.208	0.147	-29%
Fe	0.609	0.626	+2.8%	0.796	0.775	-2.6%	0.187	0.149	-20%
W	0.688	0.653	-5.1%	0.812	0.731	-10%	0.124	0.078	-37%
Pb	0.545	0.493	-9.5%	0.878	0.702	-20%	0.333	0.209	-37%
^{235}U	0.646	0.703	+8.8%	1.180	1.175	-0.4%	0.534	0.472	-11.6%
^{238}U	0.643	0.656	+2.0%	0.907	0.870	-4.1%	0.264	0.214	-19%
^{239}Pu	0.638	0.729	+14%	1.470	1.440	-2.0%	0.832	0.711	-14%

a. The results of the water-pulsed sphere are off by several time channels.

Table SDT12-1. Comparison of Calculated and Measured Bonner Ball Counting Rates on Center Line 24 in. Behind Various Thicknesses of Sodium[a]

Bonner Ball	Ratio: Calculated/Measured		
	10 ft Na	12.5 ft Na	15 ft Na
Cd-covered	0.83	0.84	0.72
3-in.	0.90	0.94	0.74
4-in.	0.85	0.88	0.71
5-in.	0.89	0.91	0.75
6-in.	0.87	0.89	0.72
8-in.	0.86	0.85	0.70
10-in.	0.81	0.81	0.63
12-in.	0.81	0.72	0.58
Mod. 3-in.	1.37	1.33	1.09

a. The calculations were performed with DOT using a 100-group GAM II structure based on ENDF-III. There is no difference in the energy region below 15 MeV between ENDF-III and ENDF-IV.

Table SDT12-2. Comparison of Calculated and Measured NE-213 Spectrometer Responses Behind Sodium[a]

(Entries are calculated-to-measured ratios of $\int_{1\ \mathrm{MeV}}^{12\ \mathrm{MeV}} \phi(E)dE.$)

Location	Ratio
On center line, 359 in. behind 5 ft of Na	1.24
96 in. off center line, 359 in. behind 5 ft of Na	1.17
On center line, 24 in. behind 10 ft of Na	1.28

a. The calculations were performed with DOT using a 100-group GAM II structure based on ENDF-III. There is no difference in the energy region below 15 MeV between ENDF-III and ENDF-IV.

Table SDT12-3. Comparison of Calculated and Measured Benjamin Counter Responses Behind Sodium[a]

(Entries are calculated-to-measured ratios of $\int_{74\ \mathrm{keV}}^{1.35\ \mathrm{MeV}} \phi(E)dE.$)

Location	Ratio
On center line, 24 in. behind 5 ft of Na	1.13
On center line, 359 in. behind 5 ft of Na	1.07
96 in. off center line, 359 in. behind 5 ft of Na	1.04
On center line, 24 in. behind 10 ft of Na	1.39
On center line, 24 in. behind 12.5 ft of Na	1.61

a. See footnote a of Table SDT12-2 above.

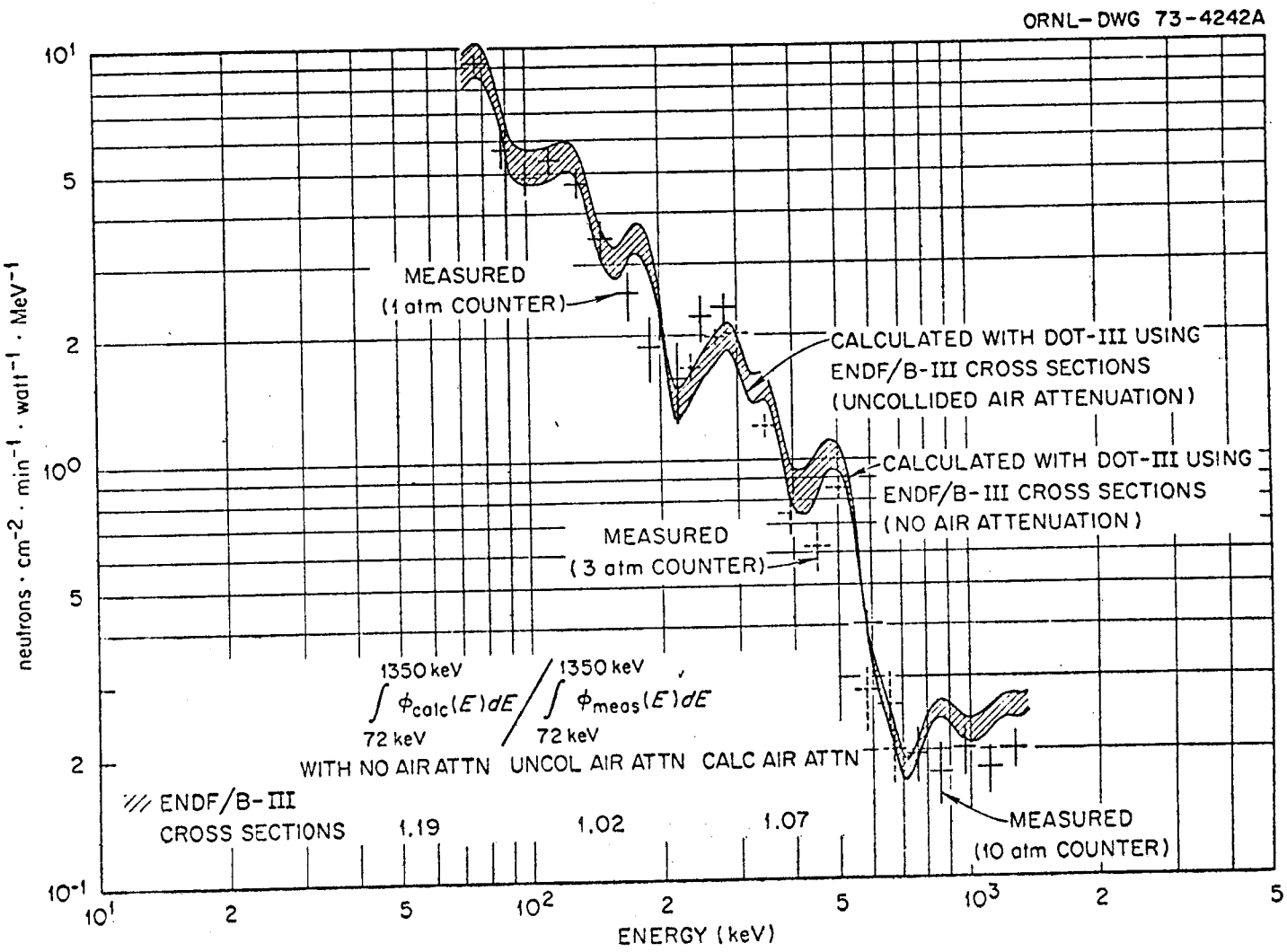

Fig. SDT12-1. Comparison of Measured and Calculated Transmitted Fluxes in the Region 74 keV - 1.35 MeV Behind 5 ft of Sodium. Detector is on the center line 359 in. behind the sodium.

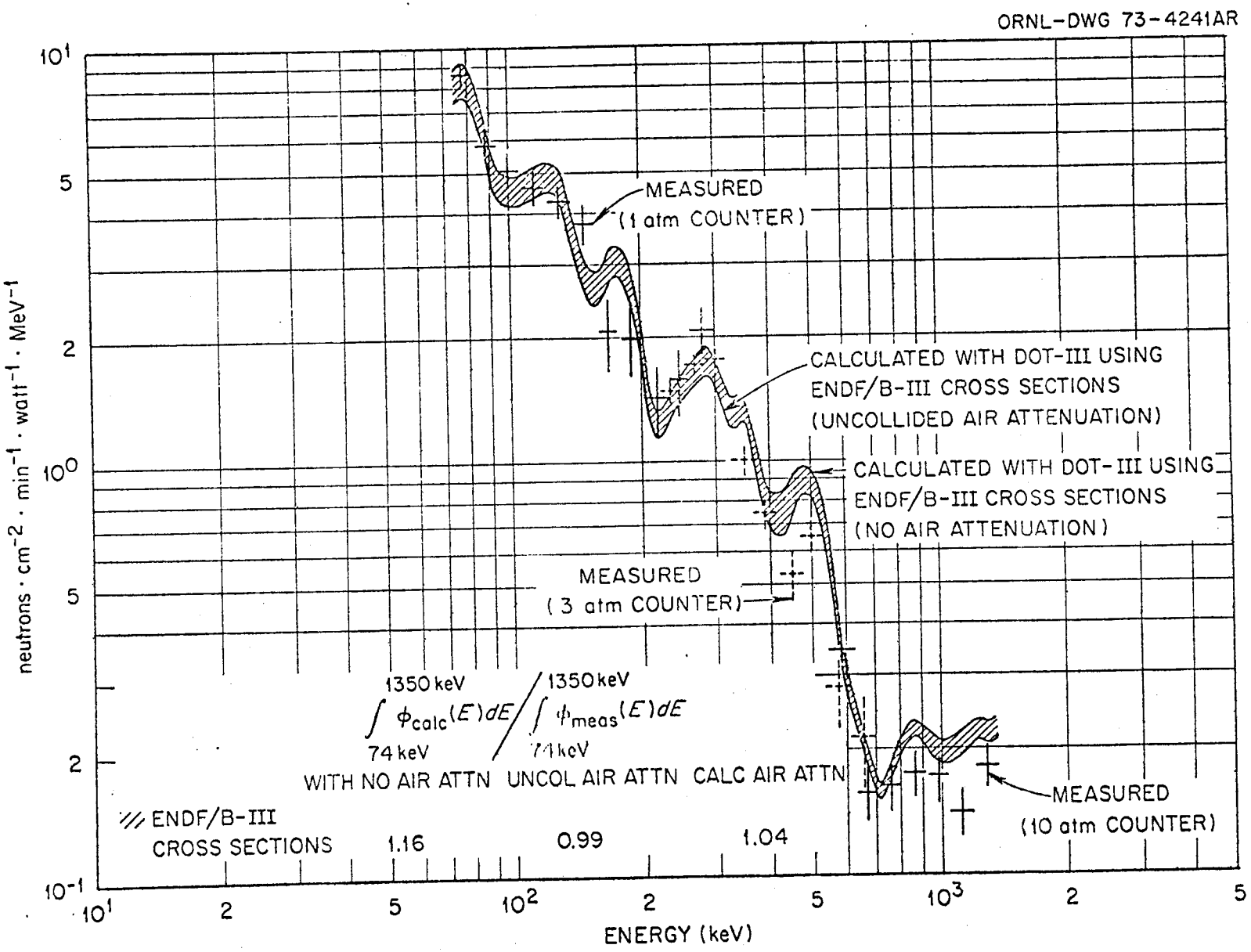

Fig. SDT12-2. Comparison of Measured and Calculated Transmitted Fluxes in the Region 74 keV - 1.35 MeV Behind 5 ft of Sodium. Detector is 96 in. off the center line and 359 in. behind the sodium.

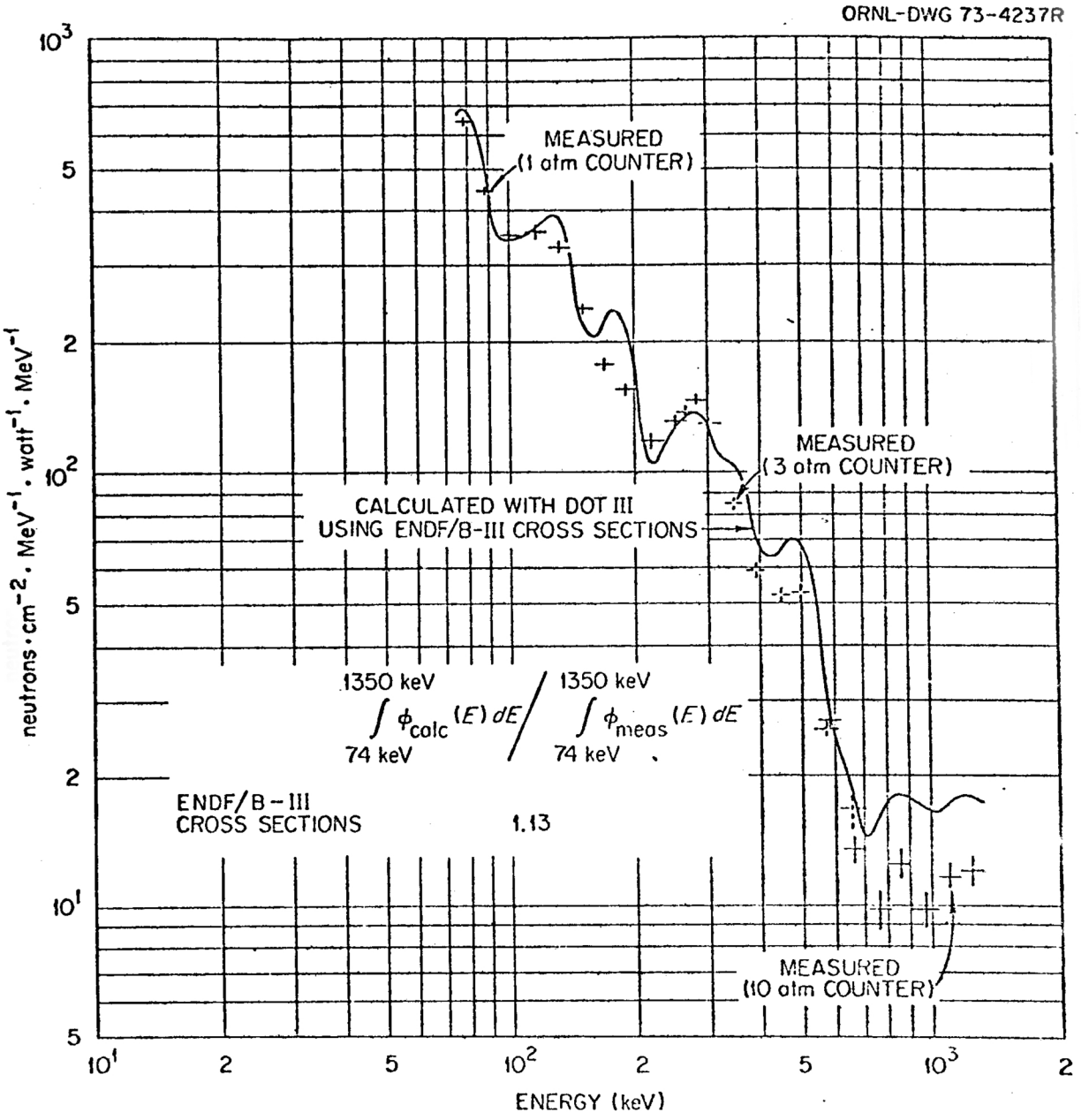

Fig. SDT12-3. Comparison of Measured and Calculated Transmitted Fluxes in the Region 74 keV - 1.35 MeV Behind 5 ft of Sodium. Detector is on the center line 24 in. behind the sodium.

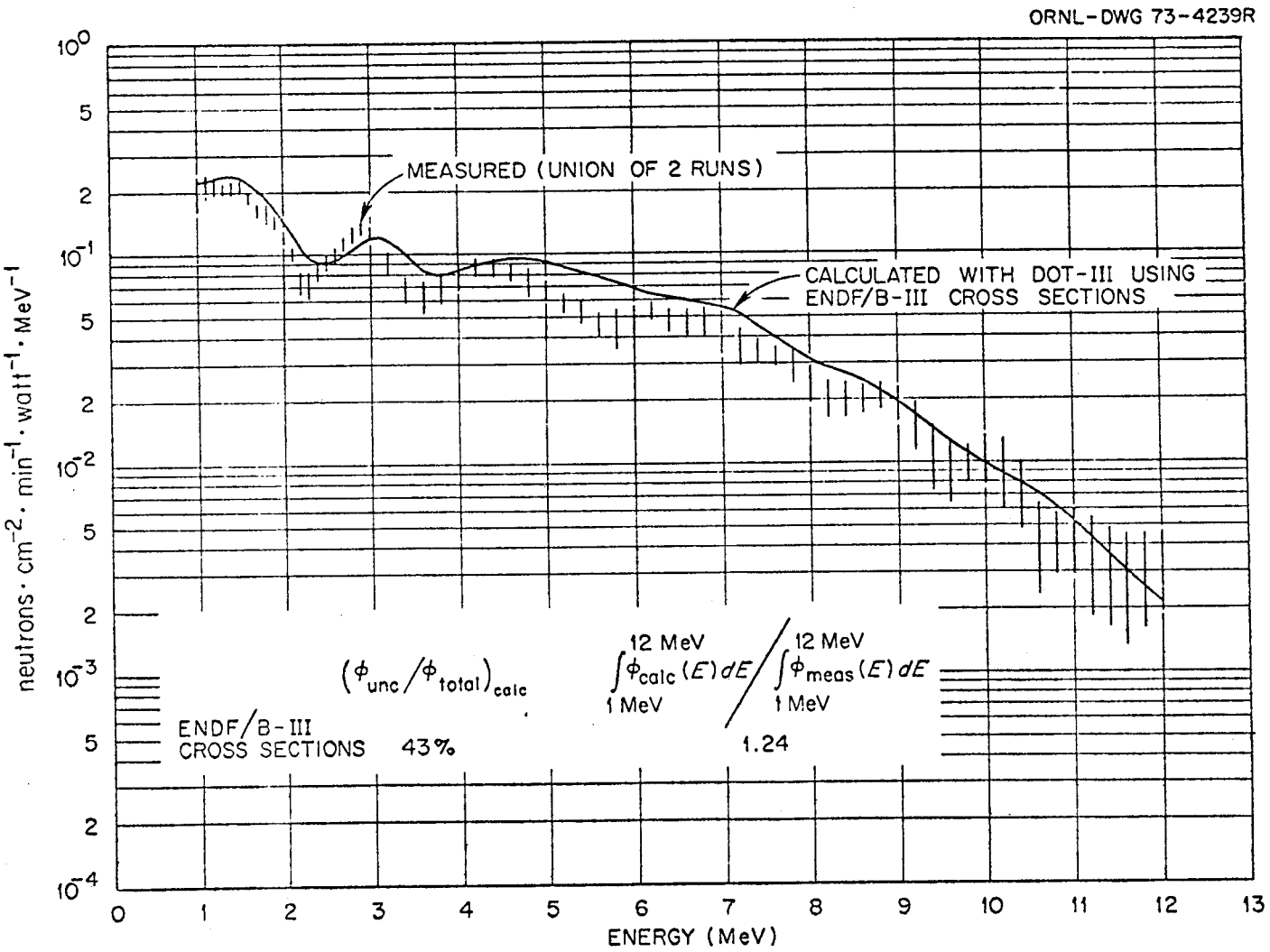

Fig. SDT12-4. Comparison of Measured and Calculated Transmitted Fluxes in the Region 1 - 12 MeV Behind 5 ft of Sodium. Detector is on the center line 359 in. behind the sodium.

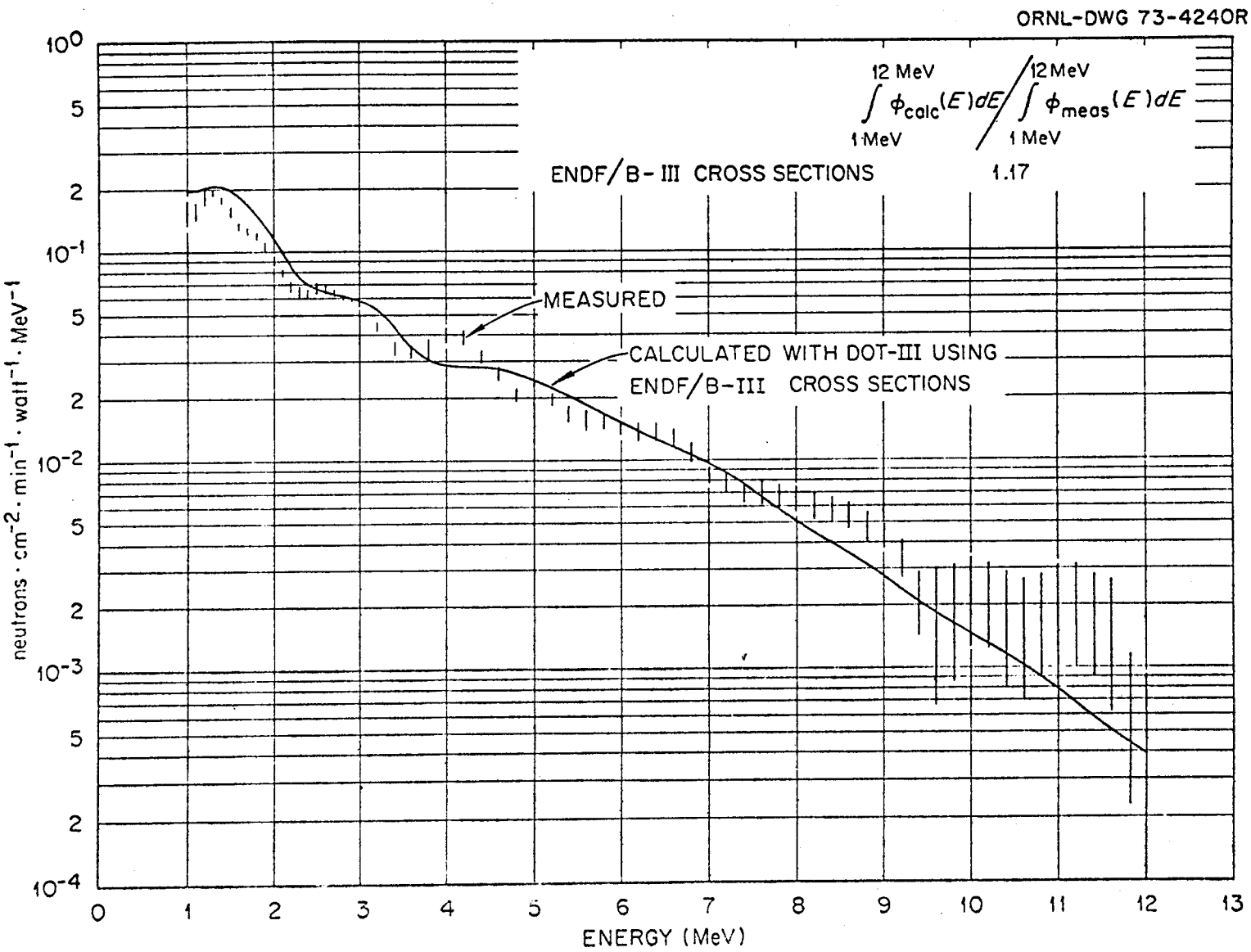

Fig. SDT12-5. Comparison of Measured and Calculated Transmitted Fluxes in the Region 1 - 12 MeV Behind 5 ft of Sodium. Detector is 96 in. off the center line and 359 in. behind the sodium.

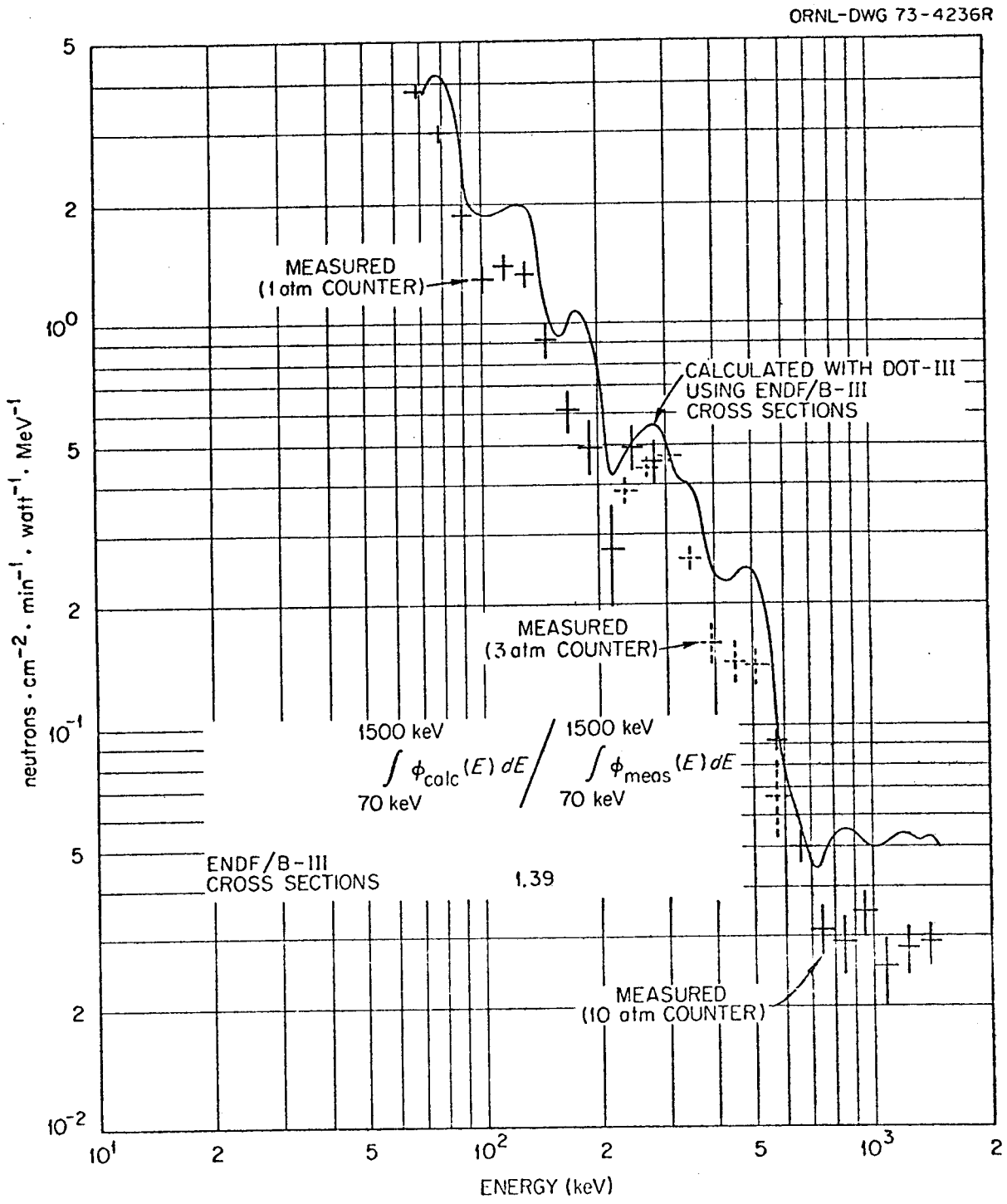

Fig. SDF12-6. Comparison of Measured and Calculated Transmitted Fluxes in the Region 70 keV - 1.5 MeV Behind 10 ft of Sodium. Detector is on the center line 2¼ in. behind the sodium.

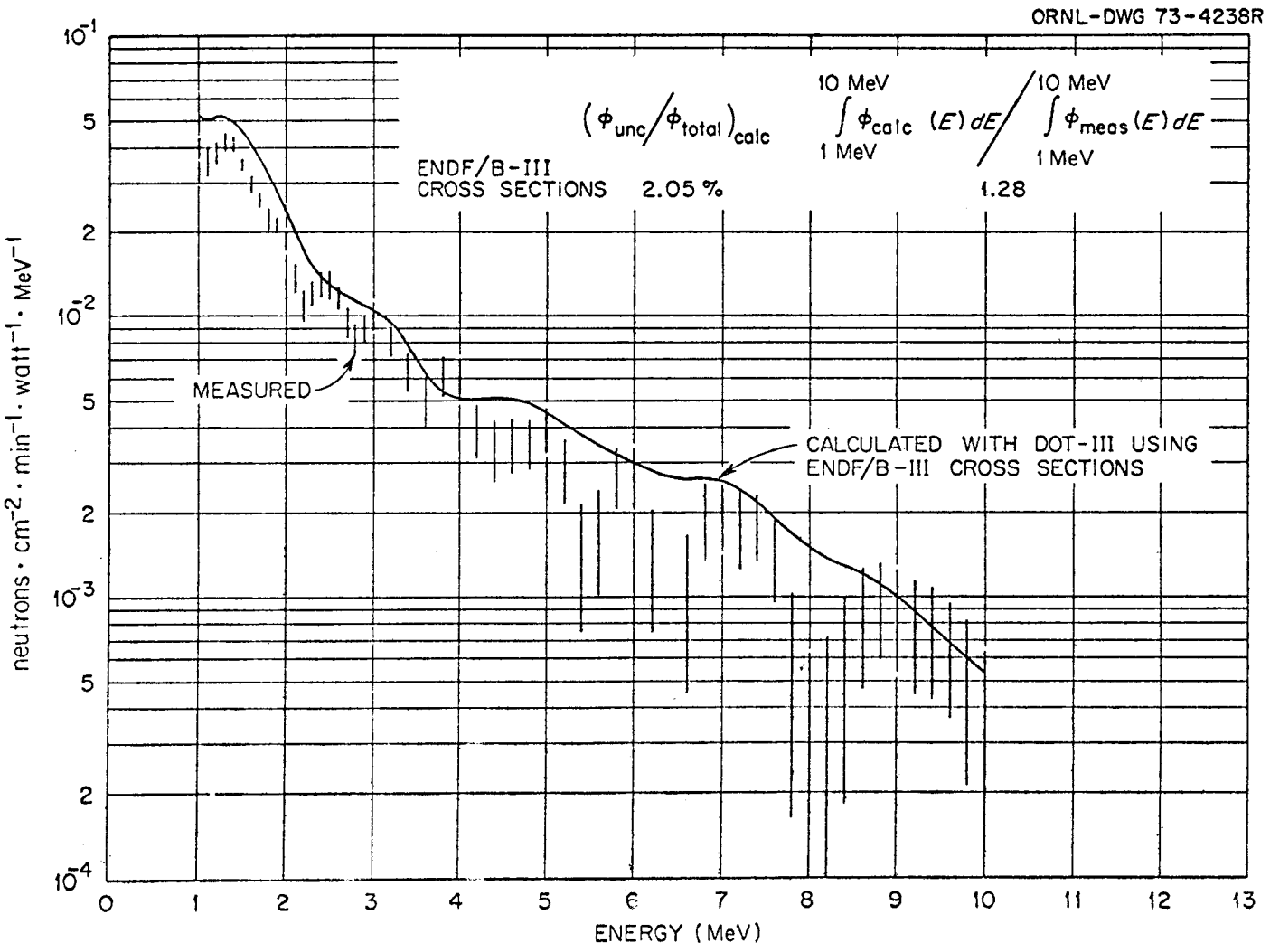

Fig. SDT12-7. Comparison of Measured and Calculated Transmitted Fluxes in the Region 1 - 10 MeV Behind 10 ft of Sodium. Detector is on the center line 24 in. behind the sodium.

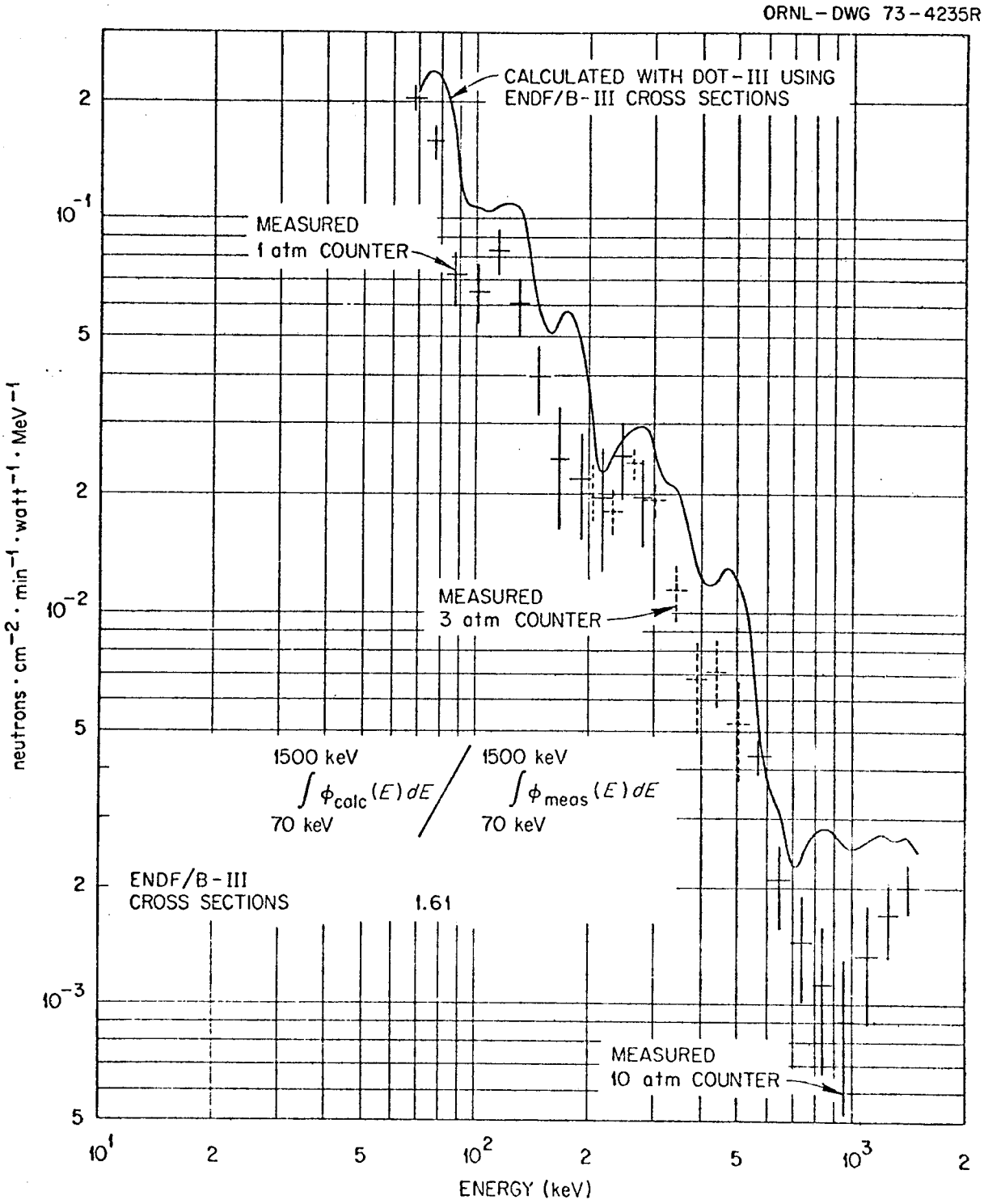

Fig. SDT12-8. Comparison of Measured and Calculated Transmitted Fluxes in the Region 70 keV - 1.5 MeV Behind 12.5 ft of Sodium. Detector is on the center line 24 in. behind the sodium.

DOSIMERTY

V. DOSIMETRY

A. Introduction

A dosimetry benchmark experiment consists of reaction rate measurements in a well defined neutron spectrum. Three benchmark spectra have been specified: a fission neutron spectrum, and the fast reactor spectra of the ΣΣ and CFRMF facilities. The results of reaction rate measurements in these spectra are reported as spectrum averaged cross sections; i.e.,

$$\bar{\sigma} = \int_{10^{-5}\ \text{eV}}^{20\ \text{MeV}} \sigma(E)\ \phi(E)\ dE \Bigg/ \int_{10^{-5}\ \text{eV}}^{20\ \text{MeV}} \phi(E)\ dE. \qquad (1)$$

There are 36 reactions (for 26 isotopes) for which dosimetry measurements are available. The data covers a broad range of reaction types and spectral indices.

The participants in the ENDF/B-IV dosimetry file data testing are Aerojet Nuclear Corporation (ANC), Oak Ridge National Laboratory (ORNL), Brookhaven National Laboratory (BNL), and Hanford Engineering Development Laboratory (HEDL).

B. Computational Methods

The dosimetry data is tested very simply by computing the spectrum averaged cross section (e.g., Eq. 1) where the spectra for the three tests are given and are specified as follows:

1. ^{235}U fission spectrum (Maxwellian),

$$\phi(E) = 0.74\ E^{\frac{1}{2}} \exp\ (-E/T)$$

for

$$T = 1.29 \text{ MeV or } 1.32 \text{ MeV.}$$

2. ΣΣ central neutron spectrum specified as flux per unit lethargy in a 136-group structure.

3. CFRMF fast reactor neutron spectrum specified as flux per unit lethargy in a 69-group structure.

The calculation of the average reaction rate is obviously sensitive to the specification of the neutron spectrum. Ideally, the specification of the ΣΣ and CFRMF spectra would be derived from accurate measurements. But, since high precision measurements over the entire range of these spectra are not available, the specification of these spectra rely upon an evaluation of the spectra where the evaluation is based upon available spectrum measurements and calculations.[1,2]

ΣΣ SPECTRUM SPECIFICATION

The neutron spectrum in the center of the ΣΣ reactor has been measured with proton-recoil spectrometers, a $^{3}He(n,p)t$ spectrometer and a $^{6}Li(n,\alpha)t$ spectrometer. Details of the measurements and descriptions of the cross sections used have been reported.[3,4] A ±5% agreement was generally found among the various measured spectra for the energy range 20 keV to 4 MeV. The spectrum measurements are compared in Fig. 1. These measurements have been used to obtain an evaluated,

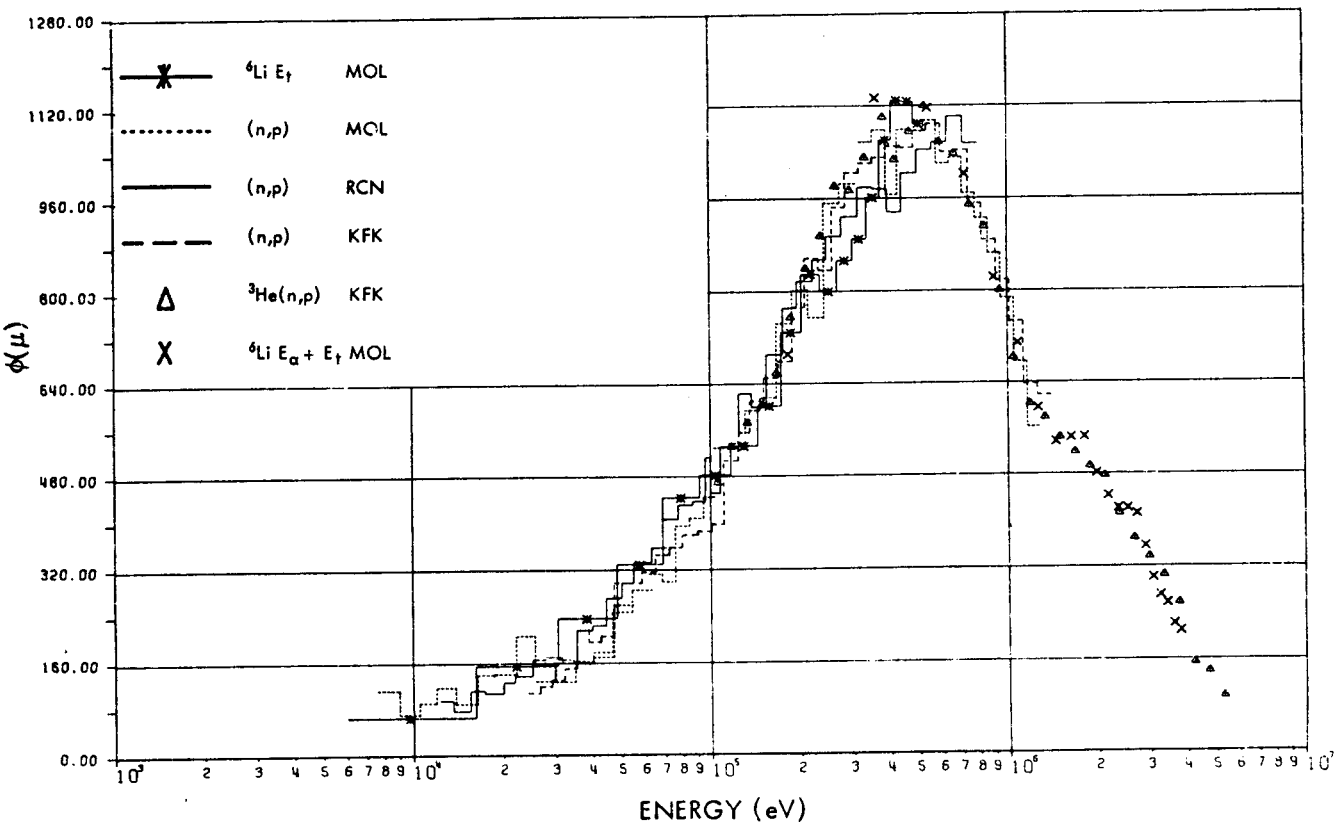

Fig. 1. ΣΣ Central-Neutron Field Flux Spectral Characterization by Interlaboratory Spectrometry Measurements.

smooth spectrum by applying a least-squares cubic spline procedure to the cumulative distribution of the experimental data in the energy interval 6 keV to 5.6 MeV. The estimated uncertainties in the evaluated, smoothed spectrum are taken to be ±5% based upon the consistency generally observed between the various independent measurements and techniques.

The ΣΣ spectrum has also been calculated with a discrete-ordinates transport theory code using ENDF/B-III nuclear data.[5] The departures between the measurements and this calculation never exceed ±5% and they are interpretable in terms of nuclear data inadequacies of the constituant materials of the ΣΣ composition. These departures have a nonneglible impact on dosimetry data testing, particularly for such important reactions as ^{237}Np(n,f) and ^{240}P(n,f). Above 5.6 MeV and below 6 keV, the ΣΣ spectrum is defined by the calculation.

The ΣΣ spectrum is a good benchmark test for fission and threshold reactions but the accuracy for capture reaction tests is somewhat questionable.

CFRMF SPECTRUM SPECIFICATION

The specifications of the CFRMF spectrum for ENDF/B-IV data testing is based upon proton-recoil measurements in the energy range 3 keV to 2.5 MeV and upon an extensive set of calculations. Three different methods have been used to compute the CFRMF spectrum: (a) a one-dimensional S_n transport code, SCAMP,[6] over the energy range 10 MeV to thermal; (b) a Monte Carlo code, RAFFLE;[7] and (c) a multiregion resonance absorption cross-section code, RABBLE.[8] Both RAFFLE and RABBLE were used for limited portions of the energy range.

The SCAMP and RAFFLE calculations were made with a 20-region concentric cylindrical cell model of the central portion of the CFRMF loading. These calculations were made in 69 energy groups with 0.25 lethargy spacing from 10 MeV

down. A 69-group library was prepared for these calculations using the PHROG code.[9] All cross sections were derived from ENDF/B-III except those of iron which came from ENDF/B-II.

The transport theory code with its flexibility and relatively short computing times was used for most of the spectrum calculations. The SCAMP computations were run as eigenvalue problems with a semi-isotropic reflective boundary condition at the outer boundary and a constant buckling (B^2 = 0.001769) for all regions. Calculations of a wide variety were made to refine the geometric representation of the model and to evaluate the effects of various assumptions made for the codes being used. Several outer boundary dimensions were tested in the calculations and the central spectrum was found to be relatively insensitive over the range of dimensions tested. The final calculations were made with an outer boundary giving a k_{eff} of unity.

The Monte Carlo code was used to calculate the CFRMF spectrum over the energy range from 10 MeV to 15 keV to examine the effects of material resonances (aluminum and oxygen) in the thermal driver spectrum on the spectrum at the center of the fast zone. These RAFFLE computations used pointwise elastic scatter cross sections for aluminum and oxygen and for the absorption cross section of ^{10}B to reduce possible spectrum smoothing effects due to group-averaging of the cross sections.

The resonance absorption code was used to calculate the CFRMF spectrum over the energy range from 52.5 keV to 0.876 eV to properly represent the effects of resonance absorption on the spectrum at the center of the fast zone. These RABBLE computations give group-averaged cross sections for the resonance energy range using space- and lethargy-dependent slowing down sources. Modifications were made

to allow a greater number of broad groups and regions, and subroutines were incorporated to handle the unresolved resonance cross sections. The broad group structure was the same as described above for Groups 22 through 65, where each broad group had 250 fine groups of equal lethargy width. Figure 2 compares the S_8 transport code calculated spectrum with the proton-recoil measurement. There are significant differences between the calculations and measurements, particularly at energies around 1.0 MeV, 225 keV, and below 90 keV. To test for possible smoothing effects due to the cross-section processing codes, a Monte Carlo calculation was made of this spectrum with pointwise cross sections for the materials expected to contribute to smoothing of the spectrum (Al and O elastic scatter, ^{10}B absorption). Only minor differences were found in the comparison of the transport and Monte Carlo calculations as depicted in Fig. 3.

Based on the general agreement between the widely varying computational approaches and the calculations and measurements, it is concluded that the 69-group spectrum from the transport theory computation is as good a representation of the neutron energy spectrum at the center of the CFRMF as can be obtained with the available cross-section sets and computational methods. It is this calculated spectrum that has been used for the dosimetry data testing.

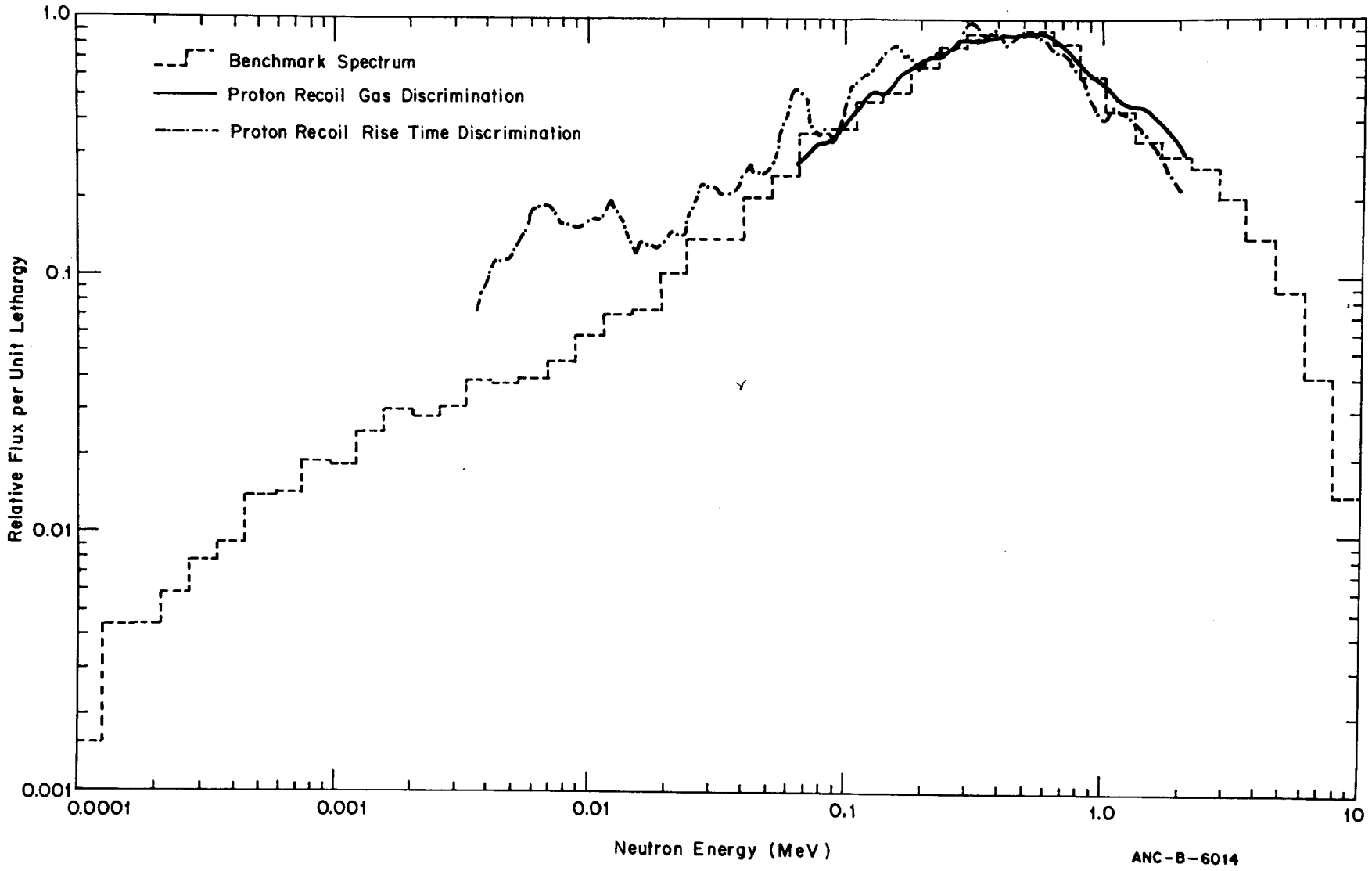

Fig. 2. Comparison of Transport Theory Calculated Spectrum and Proton-Recoil Measured Spectrum in CFRMF.

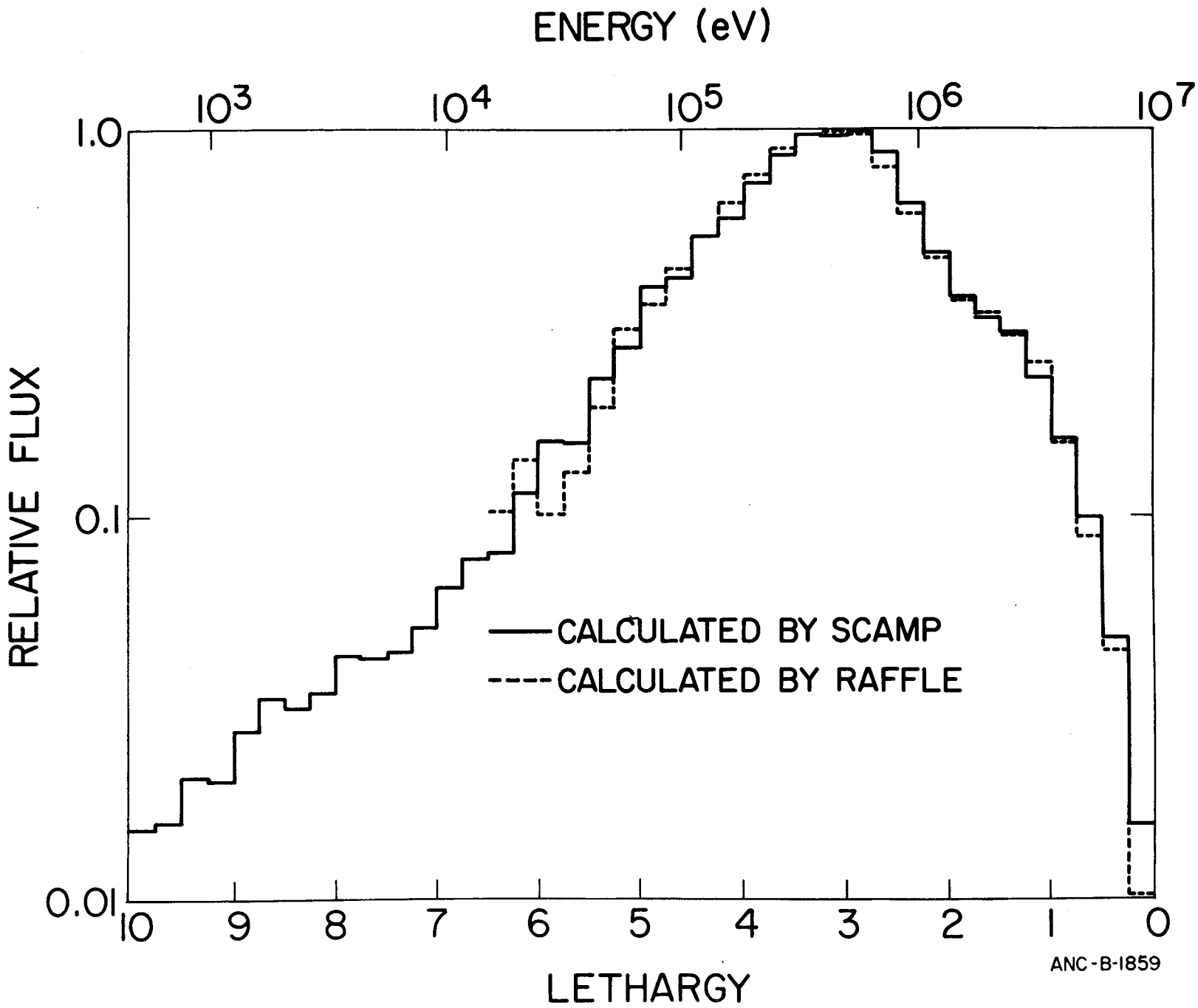

Fig. 3. Monte Carlo Calculation (RAFFLE) using Pointwise Cross Sections Compared to Transport Calculation (SCAMP, one dimensional, S_8, P-1) in CFRMF.

C. Testing Results

The calculated spectrum averaged cross-section for the three benchmark spectra using the "pointwise" cross sections as supplied in the ENDF/B dosimetry library are presented in Table I. All calculations in Table I were performed at BNL. Column 1 lists all the isotopes and reactions in the dosimetry file. Column 2 lists the calculated spectrum-averaged cross sections using the ΣΣ spectrum (Ref. 1). Column 2 is compared to the evaluated integral data as given by Fabry[10] in column 3. Column 4 gives the results calculated with use of the evaluated CFRMF spectrum (Ref. 2) for comparison with a spectrum-averaged cross section (column 5) deduced by McElroy[11] from reaction rate measurements in the CFRMF and a tentative value of absolute integral flux of $7.3_6 \times 10^{10} \pm 2.3\%$ n/(cm^2 sec). The CFRMF reaction rates were supplied by Atomics International (helium mass spectrometric measurements), National Bureau of Standards (fission chamber measurements), and Argonne National Laboratory (ANL), Aerojet Nuclear Company (ANC), Atlantic Richfield Hanford Company, and Hanford Engineering Development Laboratory (HEDL) (radiometric measurements). Columns 6 and 7 contain the fission-spectrum-averaged cross section with two temperatures. Column 6 has T = 1.29, as suggested by McElroy,[11] and column 7, T = 1.32, the value in the ENDF/B general purpose file. Finally, in column 8, the evaluated fission spectrum measurements as supplied by Fabry[12] are listed.

Some of the reactions on the dosimetry file have their resonance regions represented by resonance parameters and background cross sections. These parametric representations were converted to pointwise data for the above calculations by the code RESEND.[13] Because of the voluminous output of RESEND for some isotopes (e.g. ^{238}U) and the resulting difficulties encountered in data testing

TABLE I. Calculated and Measured Average Reaction Rates in the Three Dosimetry Benchmark Experiments[1]

Isotope/ Reaction	$\hat{\sigma}(\Sigma\Sigma)$ Dosimetry File (mb)	$\hat{\sigma}(\Sigma\Sigma)$ (Ref. 10) (mb)	$\hat{\sigma}$(CRFMF) Dosimetry File (mb)	$\hat{\sigma}$(CFRMF) (Ref. 11) (mb)	$\hat{\sigma}_f$(T = 1.29) Dosimetry File (mb)	$\hat{\sigma}_f$(T = 1.32) Dosimetry File (mb)	$\hat{\sigma}_f$ (Ref. 12) (mb)
^{6}Li(n, total He)	924.1		998.1	900 ± 39	486.9	486.0	
^{10}B(n, total He)	1605.0		1843.6	1940 ± 60	515.2	512.3	
^{23}Na(n,γ)	1.392		1.842		0.295	0.291	
^{27}Al(n,p)	1.047	1.033 ± 0.103	0.917	0.931 ± 0.033	3.926	4.222	4.0 ± 0.4
^{27}Al(n,a)	0.208	0.182 ± 0.005	0.156	0.172 ± 0.053	0.709	0.801	0.73 ± 0.02
^{32}S(n,p)	16.32		13.90		61.32	63.87	69 ± 2
^{45}Sc(n,γ)	18.79		20.06	25.0 ± 0.009	5.982	5.879	
^{46}Ti(n,p)	2.523		2.195	2.78 ± 0.097	9.503	10.24	12.3 ± 0.3
^{47}Ti(n,np)	5×10^{-4}		0.0				
^{47}Ti(n,p)	5.712		4.78	4.44 ± 0.02	20.62	21.40	20.0 ± 2.0
^{48}Ti(n,np)	5×10^{-4}		0.0				
^{48}Ti(n,p)	0.0510		0.034	0.073 ± 0.003	0.171	0.194	0.32 ± 0.02
^{55}Mn(n,2n)	0.080		0.0		0.302	0.367	0.25 ± 0.01
^{54}Fe(n,p)	19.56		16.85	18.6 ± 0.58	74.04	77.67	82.5 ± 2.0
^{56}Fe(n,p)	0.296	0.273 ± 0.008	0.238		1.033	1.145	1.07 ± 0.06
^{58}Fe(n,γ)	5.093		6.13	6.52 ± 0.22	1.709	1.695	
^{59}Co(n,2n)	0.056		0.0		0.215	0.262	
^{59}Co(n,γ)	55.60		89.88	97.6 ± 3.6	6.517	6.433	
^{59}Co(n,a)	0.043		0.033		0.149	0.168	0.156 ± 0.006
^{58}Ni(n,2n)	6.88×10^{-4}		0.0		3.9×10^{-3}	4.9×10^{-3}	
^{58}Ni(n,p)	26.23	28.8 ± 0.7	22.26	25.6 ± 0.8	97.21	101.5	113 ± 3
^{60}Ni(n,p)	0.683		0.569		2.413	2.658	
^{63}Cu(n,γ)	41.53	40.0 ± 2.0	48.63	48.4 ± 2.6	11.15	11.01	10.1 ± 1.5
^{63}Cu(n,a)	0.104		0.080		0.354	0.396	0.50 ± 0.05
^{85}Cu(n,2n)	0.102		0.0		0.383	0.464	
^{115}In(n,n')	54.37	58.6 ± 1.2	44.033	53 ± 3	163.9	166.8	188 ± 4
^{115}In(n,γ)	276.97	261 ± 9	301.4	300 ± 11	138.4	136.6	146 ± 5
^{127}I(n,2n)	0.393		0.068		1.379	1.368	1.09 ± 0.05
^{197}Au(n,γ)	331.41	442 ± 8	414.87	452 ± 14	86.35	84.92	88 ± 5
^{232}Th(n,f)	19.77	21.0 ± 1.3	16.08		67.25	69.01	83.0 ± 3.5
^{232}Th(n,γ)	261.37		286.26		105.4	103.8	
^{235}U(n,f)	1598.3	1589 ± 55	1588.0	1659 ± 53	1243.2	1243.2	1250 (REF)
^{238}U(n,f)	86.46	87.4 ± 3.1	70.04	81.0 ± 0.3	288.9	295.4	328 ± 10
^{238}U(n,γ)	223.16	194 ± 8	231.76	196 ± 11	76.79	75.60	
^{237}Np(n,f)	625.52	634 ± 22	551.01	591 ± 21	1313.2	1322.8	1370 ± 75
^{239}Pu(n,f)	1753.3	1875 ± 66	1771.4	1930 ± 60	1780.1	1782.4	1859 ± 60

[1]All calculations performed with pointwise data from dosimetry file by BNL.

calculations, all reactions were converted into 620 group average cross sections by the code INTEND.[14] These group averaged cross sections were used by most of the testers and the calculations are summarized in Table II. The BNL tests were also rerun with the 620 group cross section set and compared in Table II to the calculations done by HEDL, ANC and ORNL.

Table II compares the $\Sigma\Sigma^1$ spectrum averaged cross sections calculated at BNL, HEDL,[15] and ORNL[16] using 620 group averaged cross sections as input with reference measured cross sections as supplied by Fabry,[1] the CFRMF spectrum averaged cross sections calculated by BNL, HEDL,[15] and ANC[17] using 620 group averaged cross section as input with reference cross sections supplied by McElroy,[11] and also compares the ^{235}U fission spectrum averaged cross sections calculated at BNL, HEDL,[15] and ORNL[16] using 620 group averaged cross sections as input with the reference cross sections as supplied by Fabry.[12] Differences have been noted among the data testers due, in part, to the manner in which the calculations were performed. In some cases, the tester modified the neutron flux spectrum to the 620 group structure of the cross sections, and in other cases, the 620 group cross sections were averaged to the group structure of the neutron spectra. A uniform procedure was not followed, and, hence the variation among testers. For the two BNL calculations ("pointwise" cross sections in Table I and 620 group cross sections in Table II), most of the results agree closely but there are some important, unexplained differencess [e.g., $^{10}B(n,\alpha)$, $^{235}U(n,f)$].

From the results of Tables I and II, it can be concluded that these tests indicate acceptable agreement for a few reactions but there does exist a wide range of disagreement, especially for some of the important reactions. Of the

TABLE II. Calculated Average Reaction Rates in the Three Dosimetry Benchmarks Using 620 Group Cross-Sections

	ΣΣ			
Isotope/Reaction	BNL (mb)	HEDL (mb)	ORNL (mb)	Ref. 10 (mb)
^{6}Li (n, total He)	914.30	923.3	922.9	
^{10}B (n, total He)	1497.5	1514	1507	
^{23}Na (n,γ)	1.391	1.405	1.405	
^{27}Al (n,p)	1.047	0.869	0.8699	1.033 ± 0.103
^{27}Al (n,α)	0.208	0.153	0.1537	0.182 ± 0.005
^{32}S (n,p)	16.32	14.53	14.50	
^{45}Sc (n,γ)	18.79	19.01	18.96	
^{46}Ti (n,p)	2.524	2.075	2.073	
^{47}Ti (n,np)	5×10^{-4}	0.96×10^{-3}	2.75×10^{-4}	
^{47}Ti (n,p)	5.713	5.174	5.174	
^{48}Ti (n,np)	5×10^{-4}	4.9×10^{-4}	2.93×10^{-4}	
^{48}Ti (n,p)	0.0510	0.0379	0.0377	
^{55}Mn (n,2n)	0.080	0.0554	0.0493	
^{54}Fe (n,p)	19.56	17.20	17.22	
^{56}Fe (n,p)	0.296	0.230	0.2299	0.273 ± 0.008
^{58}Fe (n,γ)	4.874	5.377	5.433	
^{59}Co (n,2n)	0.056	0.0392	0.0339	
^{59}Co (n,γ)	55.60	46.21	40.61	
^{59}Co (n,α)	0.043	0.0326	0.0326	
^{58}Ni (n,2n)	1.89×10^{-4}	7.07×10^{-4}	3.8×10^{-4}	
^{58}Ni (n,p)	26.23	23.33	23.34	28.8 ± 0.7
^{60}Ni (n,p)	0.683	0.5376	0.5389	
^{63}Cu (n,γ)	39.39	38.76	39.16	40.0 ± 2.0
^{63}Cu (n,α)	0.104	0.0779	0.0782	
^{65}Cu (n,2n)	0.103	0.0708	0.0635	
^{115}In (n,n')	53.47	50.79	50.71	58.6 ± 1.2
^{115}In (n,γ)	276.74	283.6	278.0	261 ± 9
^{127}I (n,2n)	0.393	0.2645	0.2537	
^{197}Au (n,γ)	336.7	371.2	348.7	442 ± 8
^{232}Th (n,f)	19.78	18.50	18.51	21.0 ± 1.3
^{232}Th (n,γ)	261.67	263.3	259.8	
^{235}U (n,f)	1516.1	1518	1518	1589 ± 55
^{238}U (n,f)	86.47	81.57	81.59	87.4 ± 3.1
^{238}U (n,γ)	222.68	220.8	214.1	194 ± 8
^{237}Np (n,f)	625.62	607.4	607.2	634 ± 22
^{239}Pu (n,f)	1753.2	1750	1754	1875 ± 66

TABLE II. (Cont'd)

	CFRMF			
Isotope/Reaction	BNL (mb)	HEDL (mb)	ANC (mb)	Ref. 11 (mb)
^{6}Li (n, total He)	986.7	989.4	988.9	900 ± 39
^{10}B (n, total He)	1692.7	1695	1695	1940 ± 60
^{23}Na (n,γ)	1.843	1.83	1.831	
^{27}Al (n,p)	0.917	0.860	0.894	0.931 ± 0.033
^{27}Al (n,α)	0.156	0.144	0.171	0.172 ± 0.053
^{32}S (n,p)	13.89	13.56	13.67	
^{45}Sc (n,γ)	20.08	20.11	20.11	25.0 ± 0.1
^{46}Ti (n,p)	2.196	2.09	2.168	2.78 ± 0.97
^{47}Ti (n,np)	-*	0.95×10^{-3}	1.43×10^{-3}	
^{47}Ti (n,p)	4.78	4.67	4.73	4.44 ± 0.02
^{48}Ti (n,np)	-*	50×10^{-4}	7.2×10^{-4}	
^{48}Ti (n,p)	0.034	0.037	0.0425	0.073 ± 0.003
^{55}Mn (n,2n)	-*	0.0574	0.7638	
^{54}Fe (n,p)	16.86	16.36	16.35	18.60 ± 0.58
^{56}Fe (n,p)	0.238	0.233	0.2450	
^{58}Fe (n,γ)	6.23	6.02	6.13	6.52 ± 0.22
^{59}Co (n,2n)	-*	0.0408	0.0546	
^{59}Co (n,γ)	86.49	74.10	85.51	97.6 ± 3.6
^{59}Co (n,α)	0.033	0.031	0.0357	
^{58}Ni (n,2n)	-*	7.17×10^{-4}	10.2×10^{-4}	
^{58}Ni (n,p)	22.29	21.77	21.97	25.6 ± 0.8
^{60}Ni (n,p)	0.569	0.522	0.5683	
^{63}Cu (n,γ)	47.08	47.62	47.26	48.4 ± 2.6
^{63}Cu (n,α)	0.080	0.0740	0.0846	
^{65}Cu (n,2n)	-*	0.0729	0.0967	
^{115}In (n,n')	44.09	43.57	43.59	53 ± 3
^{115}In (n,γ)	300.97	300.8	301.0	300 ± 11
^{127}I (n,2n)	0.068	0.264	0.3433	
^{197}Au (n,γ)	412.33	416.3	413.2	457 ± 14
^{232}Th (n,f)	16.12	15.84	15.93	
^{232}Th (n,γ)	286.73	285.1	285.5	
^{235}U (n,f)	1587.8	1587	1588	1659 ± 53
^{238}U (n,f)	70.13	69.22	69.48	81.0 ± 0.3
^{238}U (n,γ)	232.9	230.2	229.4	196 ± 11
^{237}Np (n,f)	551.2	547.5	547.9	591 ± 21
^{239}Pu (n,f)	1771.7	1771	1771	1930 ± 60

*Because of the sharp cutoff at 10 MeV of CFRMF spectrum, high energy threshold reaction cross sections cannot be calculated.

TABLE II. (Cont'd)

^{235}U Fission Spectrum						
Isotope/ Reaction	BNL (mb)		HEDL (mb)		ORNL (mb)	Ref. 12 (mb)
	(T=1.29)	(T=1.32)	(T=1.29)	(T=1.32)	(T=1.29)	
^{6}Li (n, total He)	487.0	486.1	487.1	486.2	487.7	
^{10}B (n, total He)	514.4	511.5	515.0	512.2	515.5	
^{23}Na (n,γ)	0.294	0.291	0.295	0.291	0.295	
^{27}Al (n,p)	3.930	4.226	3.93	4.22	3.916	4.0 ± 0.4
^{27}Al (n,α)	0.710	0.801	0.710	0.801	0.7058	0.73 ± 0.02
^{32}S (n,p)	61.35	63.89	61.35	63.89	61.24	69 ± 2
^{45}Sc (n,γ)	5.98	5.87	5.98	5.88	5.99	
^{46}Ti (n,p)	9.513	10.25	9.51	10.24	9.477	12.3 ± 0.3
^{47}Ti (n,np)	-	-	4.95×10^{-3}	6.3×10^{-3}	4.9×10^{-3}	
^{47}Ti (n,p)	20.65	21.43	20.64	21.42	20.60	20.0 ± 2.0
^{48}Ti (n,np)	-	-	2.62×10^{-3}	3.3×10^{-3}	2.6×10^{-7}	
^{48}Ti (n,p)	0.177	0.200	0.177	0.200	0.1758	0.32 ± 0.02
^{55}Mn (n,2n)	0.300	0.364	0.300	0.363	0.2971	0.25 ± 0.01
^{54}Fe (n,p)	74.09	77.72	74.07	77.69	73.91	82.5 ± 2.0
^{56}Fe (n,p)	1.034	1.15	1.033	1.145	1.029	1.07 ± 0.06
^{58}Fe (n,γ)	1.708	1.695	1.71	1.69	1.713	
^{59}Co (n,2n)	0.213	0.260	0.213	0.259	0.2112	
^{59}Co (n,γ)	6.513	6.429	6.59	6.50	6.590	
^{59}Co (n,α)	0.149	0.168	0.149	0.168	0.1486	0.156 ± 0.006
^{58}Ni (n,2n)	3.8×10^{-3}	4.7×10^{-3}	3.75×10^{-3}	4.7×10^{-3}	3.71×10^{-3}	
^{58}Ni (n,p)	97.27	101.6	97.24	101.5	97.05	113 ± 3
^{60}Ni (n,p)	2.415	2.660	2.414	2.659	2.404	
^{63}Cu (n,γ)	11.14	11.0	11.18	11.04	11.19	10.1 ± 1.3
^{63}Cu (n,α)	0.354	0.396	0.354	0.396	0.352	0.50 ± 0.05
^{65}Cu (n,2n)	0.381	0.460	0.380	0.460	0.377	
^{115}In(n,n')	163.9	165.9	163.8	166.7	163.5	188 ± 4
^{115}In(n,γ)	138.3	136.5	138.5	136.7	138.6	
^{127}I (n,2n)	1.378	1.636	1.377	1.635	1.367	1.09 ± 0.05
^{197}Au (n,γ)	86.28	84.85	86.58	85.15	86.69	88 ± 5
^{232}Th (n,f)	67.28	69.04	67.26	69.02	67.19	
^{232}Th (n,γ)	105.4	103.8	105.5	103.9	105.7	83.0 ± 3.5
^{235}U (n,f)	1242.99	1242.98	1243	1243	1243	1205 (Ref)
^{238}U (n,f)	289.0	2955	288.9	295.4	288.6	328 ± 10
^{238}U (n,γ)	76.74	75.86	76.87	75.68	76.97	
^{237}Np(n,f)	1313.5	1323.1	1313	1323	1312	1370 ± 75
^{239}Pu(n,f)	1780.3	1782.7	1780	1783	1780	

integral spectrum reactions used as broad energy range indices, only ^{115}In shows some degree of agreement. $^{238}U(n,\gamma)$ is overpredicted by ∿13% in both ΣΣ and CFRMF and $^{197}Au(n,\gamma)$ is underpredicted by ∿30% in ΣΣ. For the important fission cross sections, $^{235}U(n,f)$ is computed ∿4% low in CFRMF while $^{239}Pu(n,f)$ is consistently computed a few percent low in all three spectra. For the threshold fission reactions, $^{232}Th(n,f)$, $^{238}U(n,f)$ and $^{237}Np(n,f)$ are consistently calculated low with the greatest disagreement (∿10-12%) in the fission spectrum. For the low energy absorbers, the standard cross sections $^{10}B(n,\alpha)$ and $^{6}Li(n,\alpha)$ disagree by 5% and 10% respectively with the measurements in CFRMF. It should be noted that the results of these dosimetry tests are consistent with similar tests in the fast reactor benchmarks; i.e., $^{239}Pu(n,f)$ is calculated lower than $^{235}U(n,f)$ and $^{238}U(n,\gamma)$ is calculated too high.

The major uncertainty associated with dosimetry tests is the specification of the neutron spectrum. The spectra in ΣΣ and CFRMF were specified for the tests above based on calculations using ENDF/B-III. Results of dosimetry tests using a spectrum specified with calculations using ENDF/B-IV are available for CFRMF and these are presented in Table III. The first column in Table III lists the C/E ratios for the calculations presented in Table II, i.e., the CFRMF spectrum computed with the SCAMP code using ENDF/B-III cross sections and an approximate model for the core geometry. The second column lists the same results computed with a more exact core geometry model. The third column lists the results obtained with the full core model and ENDF/B-IV cross sections. Two observations are made: (1) the modelling of the core geometry makes little difference and (2) the use of ENDF/B-IV to compute the CFRMF spectrum yields nearly the same results as ENDF/B-III but with notable improvement in the threshold fissioning isotopes ($^{237}Np(n,f)$ and and $^{238}U(n,f)$) and in $^{115}In(n,n')$.

D. Conclusions and Recommendations

For most of the dosimetry tests, the general order of disagreement between calculated and measured reaction rates is a few percent or more and is outside the range of uncertainty reported for the measurements. From the wide range of disagreement between calculations and measurements, it is clear that not only are some of the cross sections in the dosimetry file in error, but the benchmark spectra are not well enough known. There is a need to improve the testing procedure. The measured reaction rates must be carefully evaluated and documented. Corrections for various measurement techniques must be investigated (fission chambers, radiometric techniques) and heterogeneity effects in the measurements must be specified. The benchmark testing procedures must be evaluated. The specification of the benchmark spectra, either with improved measurements or calculations, is necessary. Group collapsing schemes (e.g., to 620 group structure) must be carefully specified to preserve reaction rates. Finally, new spectra such as BIG-10[18] should be investigated for future use with the dosimetry file.

TABLE III. Calculated-to-Experimental (C/E) Ratios for Dosimetry Tests in CFRMF Using Three Different Spectrum Calculations[a]

	Reactor Cell Model, ENDF/B-III	Full Core Model, ENDF/B-III	Full Core Model, ENDF/B-IV
$^{6}Li(n,\alpha)^{3}H$	1.10	1.10	1.08
$^{10}B(n,\alpha)^{7}Li$	0.88	0.90	0.87
$^{235}U(n,f)f.p.$	0.96	0.96	0.96
$^{239}Pu(n,f)f.p.$	0.92	0.91	0.92
$^{237}Np(n,f)f.p.$	0.92	0.92	0.98
$^{238}U(n,f)f.p.$	0.86	0.85	0.95
$^{45}Sc(n,\gamma)^{46}Sc$	0.80	0.81	0.80
$^{58}Fe(n,\gamma)^{59}Fe$	0.94	0.95	0.94
$^{59}Co(n,\gamma)^{60}Co$	0.87	0.93	0.92
$^{115}In(n,\gamma)^{116m}In$	1.00	1.01	1.01
$^{197}Au(n,\gamma)^{198}Au$	0.91	0.93	0.92
$^{27}Al(n,p)^{27}Mg$	0.96	0.94	1.01
$^{27}Al(n,\alpha)^{24}Na$	0.98	0.97	1.03
$^{46}Ti(n,p)^{46}Sc$	0.77	0.76	0.82
$^{47}Ti(n,p)^{47}Sc$	1.06	1.05	1.15
$^{48}Ti(n,p)^{48}Sc$	0.58	0.57	0.59
$^{54}Fe(nmp)^{54}Mn$	0.89	0.88	0.95
$^{58}Ni(n,p)^{58}Co$	0.86	0.85	0.92
$^{115}In(n,n')^{115m}In$	0.82	0.81	0.90
$^{63}Cu(n,\gamma)^{64}Cu$	0.98	0.99	0.99

[a]All calculations were performed with the SCAMP code at ANC.

Section V. REFERENCES

1. A. Fabry, G. DeLeeuw, and S. DeLeeuw, "The MOL-ΣΣ Secondary Intermediate-Energy Standard Neutron Field," Nucl. Tech. 25, 349 (1975); Trans. Am. Nucl. Soc. 17, 527 (1973); Private Communication to Data Testing Subcommittee, CSEWG (January 1974).
2. J. W. Rogers, D. A. Millsap, and Y. D. Harker, "CFRMF Neutron Field Flux Spectral Characterization," Nucl. Tech. 25, 330 (1975); Trans. Am. Nucl. Soc. 17, 527 (1973).
3. H. Bluhm, et al., "Intercomparison of Differential Neutron Spectrometry Techniques in the MOL-ΣΣ Fast Assembly," KFK 1658, RCN 172, Blg 471 (July 1972).
4. R. Billiau, K. Bobin, W. Drent, and L. Hespeels, Eds., CEN-SCK Annual Scientific Report 1972, Centre d'Etude de l'Energie Nucleaire, Blg 481/73, Mol, 4.66 (1973).
5. W. N. McElroy, Ed., "LMFBR Reaction Rate and Dosimetry Quarterly Progress Report, June, July, August 1972," HEDL-TME 72-129 (September 1972).
6. C. L. Beck, Idaho Nuclear Corporation, Private Communication (February 1968).
7. W. E. Vesley, F. J. Wheeler, and R. S. Marsden, "The RAFFLE General Purpose Monte Carlo Code," ANCR-1022, Aerojet Nuclear Company (April 1973).
8. P. H. Kier and A. A. Robba, "RABBLE, A Program for Computation of Resonance Absorption in Multiregion Reactor Cells," ANL-7326, Argonne National Laboratory (1967).
9. R. L. Curtis, F. J. Wheeler, G. L. Singer, and R. A. Grimesey, "PHROG--A Fortran IV Program to Generate Fast Neutron Spectra and Average Multigroup Constants," IN-1435, Idaho Nuclear Corporation (April 1971).

Section V. REFERENCES (Contd.)

10. A. Fabry, Private Communication to W. N. McElroy; documented in HEDL-TME 72-129, Hanford Engineering and Development Laboratory.

11. W. N. McElroy, Private Communication to H. Alter (Data Testing Subcommittee Chairman), CSEWG (February 22, 1973), Subsequent Corrections to B. Magurno (July 1974).

12. A. Fabry, "Evaluation of Microscopic Integral Cross Sections Averaged in a ^{235}U Thermal Fission Neutron Spectrum (for 29 Nuclear Reaction Relevant to Neutron Dosimetry and Fast Reactor Technology)," Blg 465, Centre d'Etude de l'Energie Nucleaire (1972).

13. O. Ozer, "RESEND," BNL-17134, Brookhaven National Laboratory (1972).

14. O. Ozer, "INTEND," (to be published as a BNL report).

15. E. P. Lippincott and W. N. McElroy, Private Communication to B. A. Magurno, ENDF/B-IV Dosimetry File Phase II Data Testing (October 21, 1974).

16. F. B. K. Kam, Private Communication to B. A. Magurno (October 14, 1974).

17. Y. Harker, Private Communication to B. A. Magurno (October 1974).

18. L. J. Sapir, H. H. Helmick, and J. D. Orndoff, "BIG TEN, A 10% Enriched Uranium Critical Assembly: Kinetic Studies," Trans. Am. Nucl. Soc. 15, 312 (1972); E. J. Lozito and E. J. Dowdy, "A Measurement of the Central Neutron Spectrum of 'BIG-10' Critical Assembly," Trans. Am. Nucl. Soc. 17, 529 (1973).

FISSION PRODUCTS

VI. FISSION PRODUCTS

A. Introduction

The fission product file on ENDF/B-IV contains cross sections and decay data for 824 nuclides. In addition, fission yield data is given for six fissionable nuclides. The cross section and decay parameters (half lives, β and γ energies, branching, etc.) constitute a collection of about 300000 data entries and the fission yields, 13000 entries. The objectives of benchmark testing have been to infer the accuracy of this extensive set of data and, if possible, to indicate where readjustment of the data may be made according to differential measurements or theoretical uncertainty tolerances. This should be done at least for the more important fission product nuclide contributors (in general, isotopes with large cumulative yields).

Benchmark testing of ENDF/B-IV FP data falls into the following four areas:

- decay heat following "burst" or long-time-exposure fission
- β and γ spectra production
- fission product absorption
- delayed and prompt neutron yields.

In this report comparisons are made in the above four categories between ENDF/B-IV calculations and several recent and past integral measurements. Most of the comparisons presented are in the "decay heat" area. Nine testers participated in the ENDF/B-IV FP benchmark testing. They include J. C. Connor (WNES), J. K. Dickens (ORNL), T. R. England (LASL), S. B. Gunst (BAPL), G. W. Morrison (ORNL), R. E. Schenter (HEDL), F. Schmittroth (HEDL), W. H. Walker (CRNL), and C. R. Weisbin (ORNL).

B. Computational Methods

Decay heat calculations with no flux effects were made using the particular code being implemented and developed by the participating laboratory. These codes are CINDER-10 (a modified version of CINDER-7[1]), FISSPROD-2,[2] ORIGEN,[3] RIBD-II,[4] and ZPOWR.[5] All the codes gave essentially identical results for the benchmark testing presented in this report. Consequently, calculational results are indicated by the input data used (e.g. ENDF/B-IV) and not the codes which produced the values. The good agreement obtained between these codes even though they use different mathematical procedures has been previously reported.[6] High flux absorption and decay heat calculations were made with FISSPROD-2. Uncertainty results for decay heat were calculated using the codes ZPOWR and ZVAR which are based on the uncertainty analyses of Schmittroth.[5] ORIGEN and CINDER-10 were used for spectra calculations. Resonance integrals and CFRMF effective capture cross sections were calculated using ETOX-4 (a modified version of ETOX[7]).

C. Testing Results

DECAY HEAT

The decay heat benchmarks used to test ENDF/B-IV are divided into two categories. They include recently reported experimental results which have been published since 1973 and experimental results released previous to 1973. Four sets of measurements comprise the recent work. They are described as: 1) gamma power for short exposure (2.4s and 100.4s) and short cooling times (3-14,400s) at ORNL by Dickens et al.[8], 2) beta power for short exposure (10s and 100s) and extremely short cooling times (.2-26.s) by Alam and Scobie[9] at SURRC, 3) total decay power calorimetry for intermediate time exposures (100s, 1000s, and 5000s) and cooling times (70-70,000s) by Lott et al.[10] at Fontenay-aux-Roses, and 4) total decay power calorimetry for samples irradiated in high neutron fluxes (> 10^{14} n/cm^{2}s) for long irradiation and long cooling times (14.-4600.h) at BAPL by Gunst et al.[11,12] The pre-1973 experiments have been evaluated by Perry et al.[13] and comparisons will be made of ENDF/B-IV summation calculations with these evaluations. All the decay heat measurements considered in this report are for U235 thermal fission.

1) Gamma Power - ORNL (1975)[8]

Gamma-ray energy release from fission product decay following thermal-neutron fission of U235 was obtained and reduced for cooling times between 3 and 14,400 sec. The data were obtained as pulse-height spectra for photon energies between 0.05 and 8 MeV using a NaI spectrometer, and were unfolded to give photon-energy spectra of moderate resolution. Energy release values were obtained by integrating the spectra.

Table I gives these data compared with ENDF/B-IV calculations for 27 combinations of exposure, cooling and counting times. The ENDF/B-IV values are outside the one sigma experimental uncertainty limits for very short cooling times (< 7s) and

Table I. Gamma Decay Energy Following Thermal Neutron Fission of U235

Exposure (sec)	Cooling Time (sec)	Counting Time (sec)	Energy Release (MeV/Fission) Experiment (ORNL)	Calculation (ENDF/B-IV)	C-E
2.4	3	2	.219±.026	.187	-.032
2.4	5	2	.164±.013	.143	-.021
2.4	7	2	.133±.011	.118	-.015
2.4	9	5	.242±.023	.229	-.013
2.4	14	5	.178±.011	.173	-.005
2.4	19	10	.260±.015	.257	-.003
2.4	29	10	.190±.011	.189	-.001
2.4	39	20	.278±.016	.272	+.006
2.4	59	20	.195±.011	.194	+.001
2.4	79	20	.149±.008	.148	+.001
2.4	99	50	.254±.014	.258	+.004
2.4	149	50	.163±.009	.170	+.007
2.4	199	100	.206±.012	.219	+.013
2.4	299	301	.307±.020	.337	+.030
100.4	10	20	.227±.022	.241	+.014
100.4	30	20	.161±.013	.168	+.005
100.4	50	50	.266±.018	.277	+.011
100.4	100	50	.169±.010	.177	+.008
100.4	150	100	.212±.012	.226	+.014
100.4	250	100	.138±.008	.145	+.007
100.4	350	200	.186±.010	.194	+.008
100.4	550	200	.129±.007	.138	+.009
100.4	750	200	.101±.006	.109	+.008
100.4	950	500	.185±.010	.208	+.023
100.4	1450	500	.132±.007	.155	+.023
100.4	1950	500	.100±.006	.124	+.024
100.4	2450	11950	.636±.041	.830	+.194

the longest cooling times (> 300s). For the intermediate times, the two results essentially overlap. For the last counting time intervals the ENDF/B-IV summation result is 30% greater than the measured one, outside the three sigma experimental uncertainty limit. Because of this large difference, the basic ENDF/B-IV data was reexamined and found to have an error in the decay branching of Zr98 to the long lived (51m) and short lived (2.8s) states of Nb98.* Figure 1 shows the effect of the Zr98 branching correction for the "burst" exposure case. Also shown in Figure 1 are symbols representing the ORNL measurement values and uncertainties given in Table I, the nominal values being equal to a double integral of the "burst" function $[f(t_c)]$. The plotted cooling time value $\bar{t}_c$ for each of the ORNL points is the "logrithmic time average" $[\bar{t}_c = \sqrt{t_c(t_{exp}+t_c+t_{count})}]$ of the time range of the double integral. The ordinate values are obtained by using the same percentage differences in energy release as given in Table I for each corresponding $f(\bar{t}_c)$.

In order to properly assess if there remains a discrepancy between experiment and calculation, it is useful to have an uncertainty analysis for the calculation. This analysis is also useful in determining which particular piece of input data might need possible adjustment or reexamination.

Figures 2 and 3 show the results of such an uncertainty analysis as applied to the ORNL results. Plotted in Figure 2 are the calculated gamma decay power curves for the two exposures of ORNL experiment. Also given are the ORNL points which represent the "average" gamma power consistent with the results of Table I. The

---

*The error occurred due to not taking into account a change in ground versus isomeric state assignment when combining data from two different sources in constructing the ENDF/B-IV files. The shape of the gamma "burst" (energy release from a single instantaneous fission) curve was a major clue in finding the branching error. The ENDF/B-IV curve (see Figure 1) has a large "bump" when plotted as $t_c f(t_c)$ at a cooling time of about 3000s. Decay branching to metastable versus ground state has a significant effect on the shape of this "bump" as explicitly shown in Figure 12 of Reference 5.

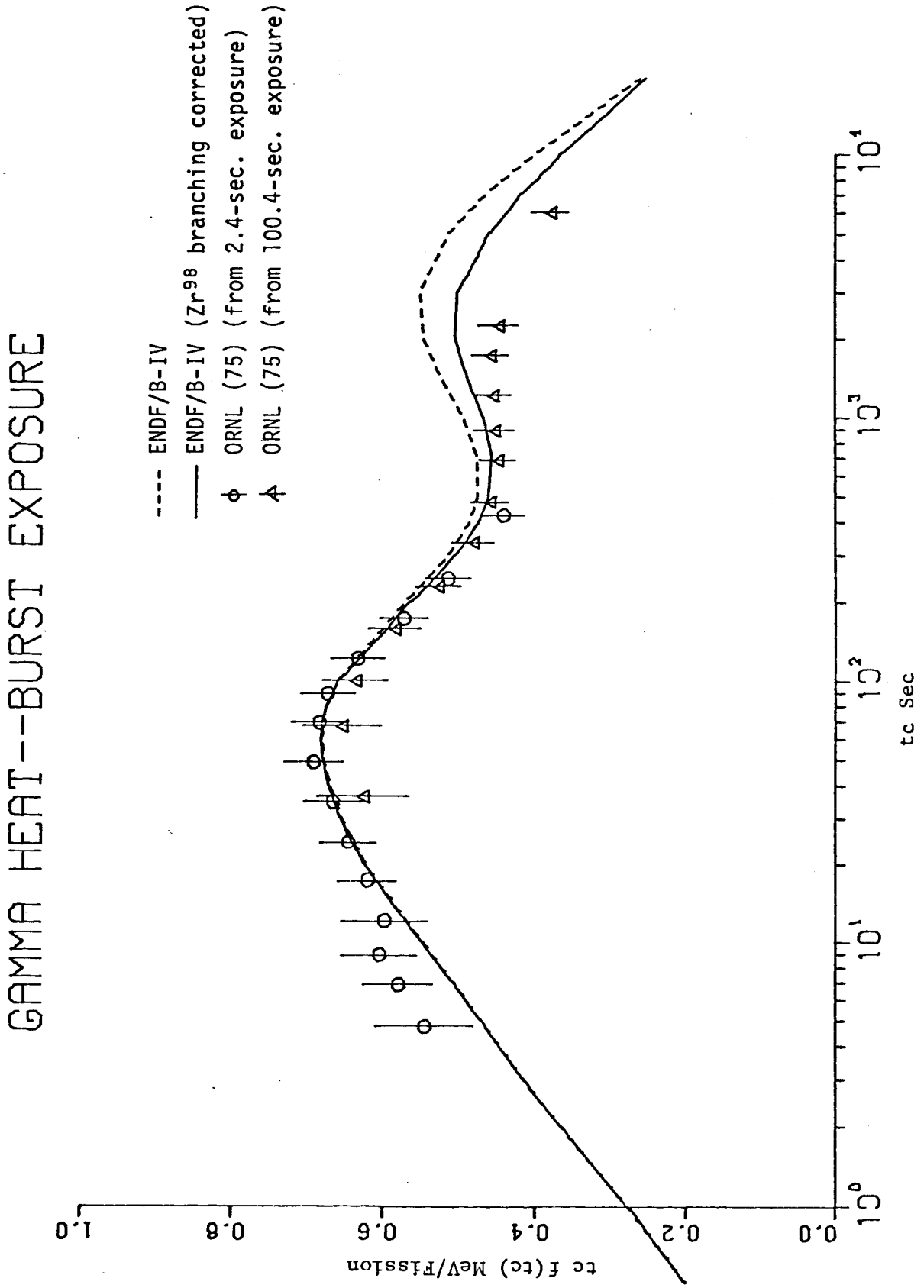
GAMA HEAT--BURST EXPOSURE
---- ENDF/B-IV
—— ENDF/B-IV (Zr^{98} branching corrected)
ORNL (75) (from 2.4-sec. exposure)
ORNL (75) (from 100.4-sec. exposure)
tc f(tc) MeV/Fission
0.0
0.2
0.4
0.6
0.8
1.0
10^0
10^1
10^2
10^3
10^4
tc Sec

Figure 1.

calculated one-sigma uncertainty bands in Figure 2 were obtained from the code ZVAR which represents the implementation of the formalism of Reference 5. A breakdown of the various contributors to the overall uncertainty is shown in Figure 3 for the 2.4 sec exposure depicted in Figure 2. Clearly, uncertainties in the decay energies are a dominant effect, especially for the short cooling times represented in the ORNL experiment. This dominance is due partly to the fact the average gamma decay energies, appropriate here, are more uncertain than the total decay energies, and partly because the fission-product yields for the thermal fission of U235 are relatively well known. The individual uncertainties are added quadratically to give the total. Also, to account for possible errors in branching ratios, the total uncertainty contains one other component (not shown) that varies from about 4% at short cooling times to less than 1% at long times. The large uncertainties at the very short times, typical of a short exposure, are 2-3 times greater than those for a typical reactor exposure.

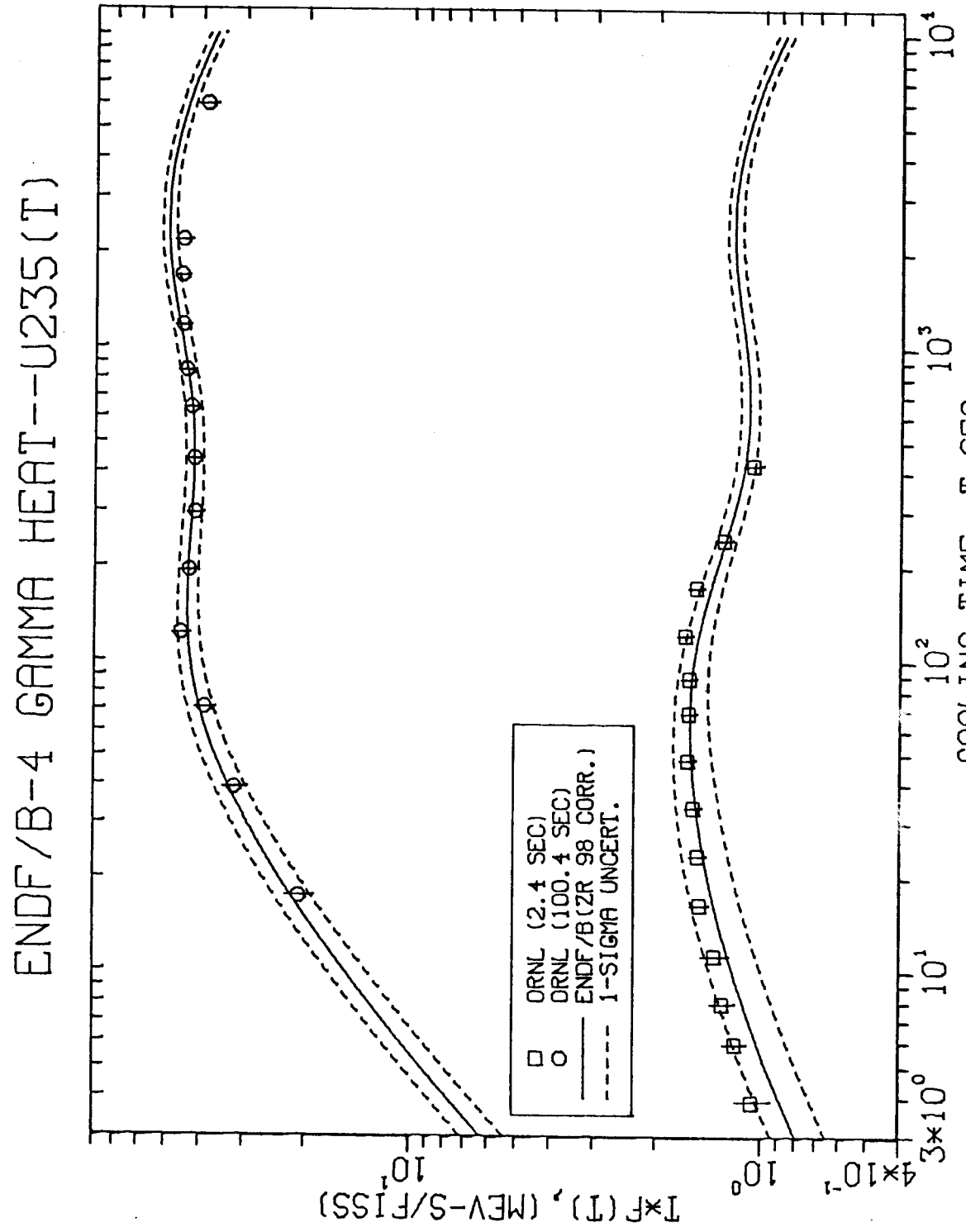
ENDF/B-4 GAMMA HEAT--U235(T)
T*F(T), (MEV-S/FISS)
COOLING TIME--T,SEC
ORNL (2.4 SEC)
ORNL (100.4 SEC)
ENDF/B(ZR 98 CORR.)
1-SIGMA UNCERT.

Figure 2.

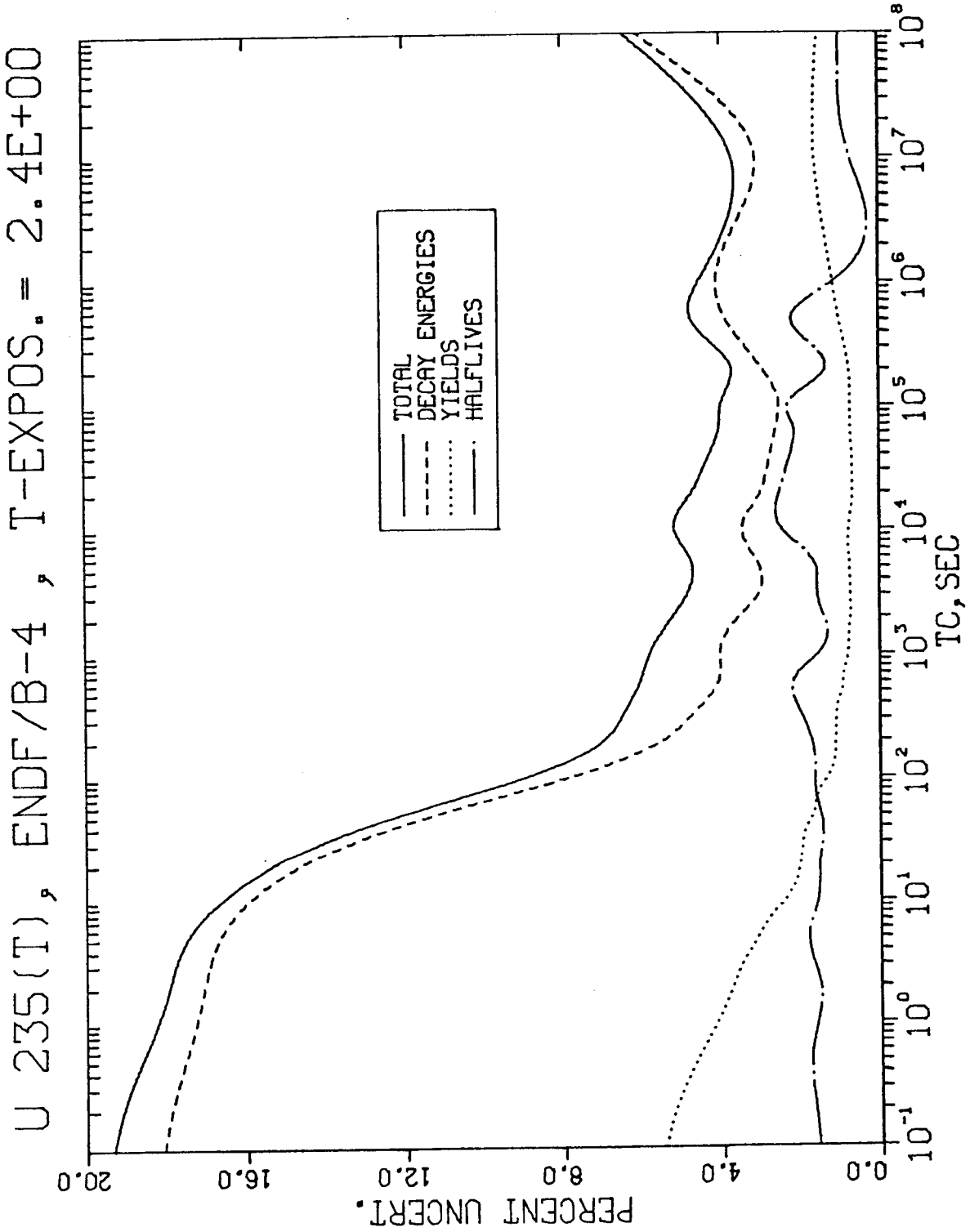
U 235(T), ENDF/B-4 , T-EXPOS.= 2.4E+00
TOTAL
DECAY ENERGIES
YIELDS
HALFLIVES
PERCENT UNCERT.
0.0
4.0
8.0
12.0
16.0
20.0
10^{-1}
10^{0}
10^{1}
10^{2}
10^{3}
10^{4}
10^{5}
10^{6}
10^{7}
10^{8}
TC, SEC

Figure 3.

2) Beta Power - SURRC (1974)[9]

Previous measurements of the beta-energy release rate following fission were restricted by experimental limitations to cooling times greater than three seconds. In this experiment the "rabbit" was driven pneumatically instead of manually from the irradiation to the beta detector. Because of this, results were obtained for extremely short cooling times (.2-26s).

Figure 4 shows the SURRC results compared to the ENDF/B-IV summation calculations for the 10 and 100s irradiations. The Alam-Scobie results were normalized at 10s cooling time for both irradiations to the previous beta power measurements of MacMahon et al.[14] Also an 8% experimental uncertainty was estimated by the authors and these are given by the error bars shown in Figure 4. Uncertainty calculations using the methods described in the previous ORNL section were made and the one sigma bands are shown. The agreement between experiment and calculation for these very short cooling times is remarkably good (though not unreasonable as indicated by the small calculated uncertainty bands) except for times greater than 20s for the 100s irradiation. The precise determination of the normalization value at 10s cooling time for the 100s irradiation case is critical to further more detailed comparisons of experiment to summation calculation.

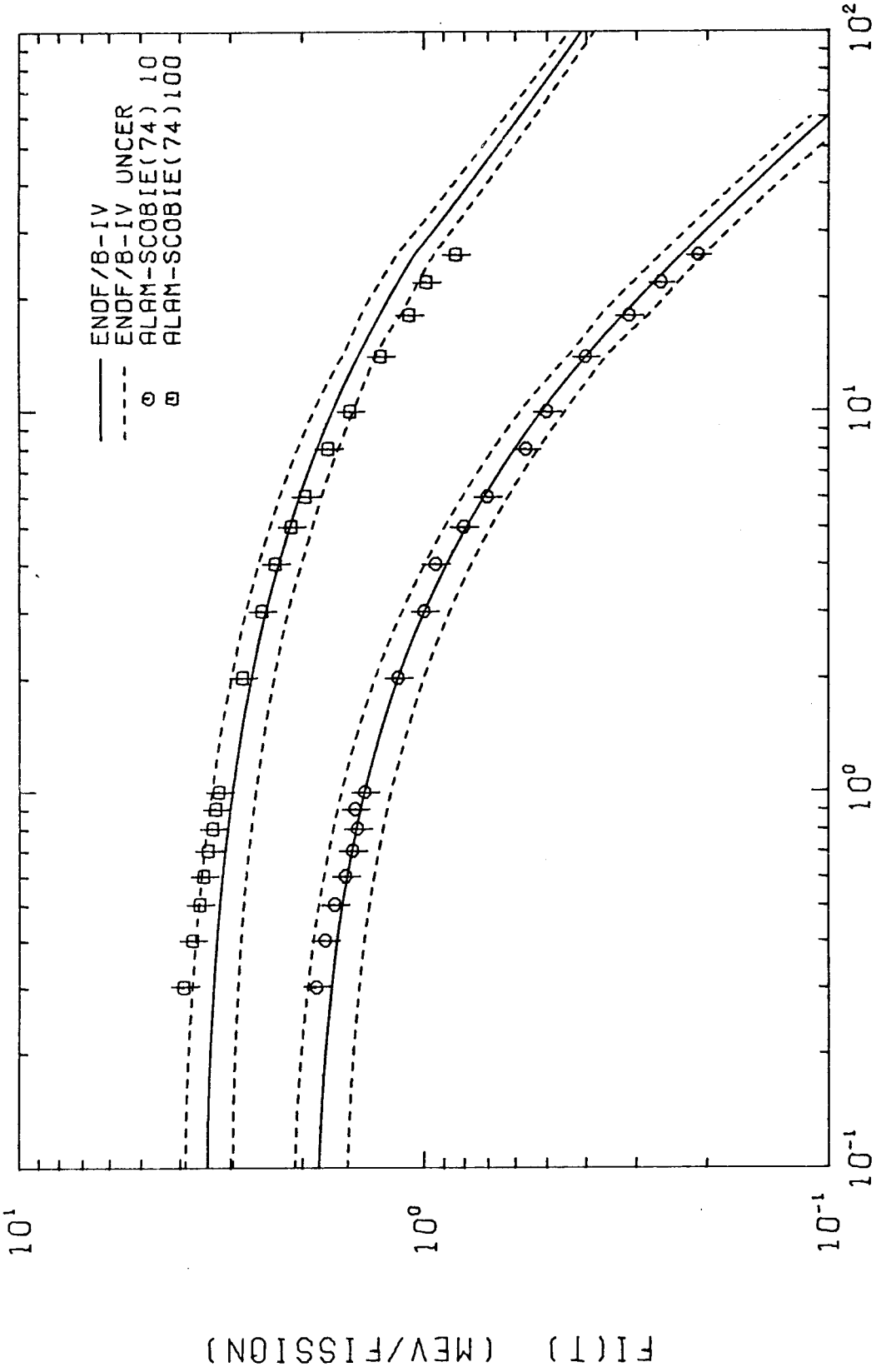
ENDF/B-IV
ENDF/B-IV UNCER
ALAM-SCOBIE(74) 10
ALAM-SCOBIE(74)100
BETA INTEGRAL AFTERHEAT U235T
10S AND 100S IRRADIATIONS
COOLING TIME T (SEC)
FI(T) (MEV/FISSION)
10^{1}
10^{0}
10^{-1}
10^{2}
10^{1}
10^{0}
10^{-1}

Figure 4.

3) Total Decay Power-Calorimetry-Fontenay-aux-Roses (1973)[10]

Samples of U235 were irradiated for periods of 100,1000 and 5000s , transferred to a calorimeter and observed for periods up to 70,000s (19.4h). The results of the measurements are given in the Lott et al. paper[10] in a table with the heading "Residual β and γ Power in Watts per fission second". Comparisons of the measurements with the ENDF/B-IV calculations are given in Table II, where it is assumed that units should be Watts-second per fission and are converted to MeV/fission by multiplying by 0.6242×10^{13}.

Detailed graphical comparisons of the Lott et al. data with calculations using ENDF/B-IV and indicated corrections to ENDF/B-IV are given in Figures 5-9. In Figure 5 the solid ENDF/B-IV and dashed ENDF/B-V UXZ* curves are shown to give good agreement with the measured points, where the 5% error bars assigned by the experimenters are plotted. The previously described uncertainty analysis has been applied for the Lott et al. exposures and the results are given in Figure 6. Again experiment and calculation are consistent with the uncertainty limits (the $\pm$5% experimental uncertainties are about the size of symbols plotted as shown in Figure 6). Typical results for the three irradiation periods compared to the ENDF/B-IV and ENDF/B-V UXZ calculations with uncertainty bands are given with greater detail in Figures 7-9.

---

* ENDF/B-V UXZ designates three changes to the ENDF/B-IV decay data. They are 1) Y96 halflife change to 9.3s (see Reference 30), 2) Te129M, Sb130M, Sb133, Cs138M, La140 and La142 $\bar{E}_\gamma$ change and Pm152M $\bar{E}_\beta$ change (see Reference 31 Table V), 3) Zr98 branching correction discussed in ORNL section.

Table II. Total Integral Afterheat Following Thermal Neutron Fission of U235 Comparing Lott et al. (Meas) with ENDF/B-IV (Calc)

Irradiation time	100 seconds			1000 seconds			5000 seconds			
Cooling time (s)	MeV/fission		(Calc-Meas)/Meas x 100	MeV/fission		(Calc-Meas)/Meas x 100	MeV/fission		(Calc-Meas)/Meas x 100	Cooling time (h)
	Meas	Calc		Meas	Calc		Meas	Calc		
70	0.982	1.121	14.1							
100	0.755	0.838	11.0							
150	0.539	0.577	7.1							
200	0.411	0.433	5.4	1.692	1.746	3.2				
300	0.275	0.285	3.6	1.385	1.389	0.3	2.579	2.679	3.9	
500	0.170	0.170	--	1.031	1.029	-0.2	2.158	2.211	2.4	
700	0.124	0.124	--	0.835	0.835	--	1.862	1.927	3.5	
1000	0.090	0.0894	-0.7	0.655	0.660	0.7	1.552	1.635	-5.3	
1500	0.0622	0.0618	-0.6	0.473	0.489	3.4	1.220	1.313	7.6	0.42
2000	0.0471	0.0467	-0.8	0.362	0.383	5.8	1.004	1.093	8.9	0.56
3000	0.0293	0.0301	2.7	0.237	0.258	8.9	0.735	0.807	9.8	0.83
5000				0.132	0.146	10.6	0.463	0.512	10.6	1.4
7000				0.0861	0.0968	12.4	0.331	0.363	9.7	1.9
10000				0.0546	0.0608	11.4	0.225	0.242	4.4	2.8
15000				0.0322	0.0346	7.5	0.140	0.146	4.3	4.2
20000				0.0214	0.0230	7.5	0.098	0.101	3.1	5.6
30000							0.0605	0.0614	1.5	8.3
50000							0.0334	0.0325	-2.7	13.9
70000							0.0201	0.0207	3.0	19.4

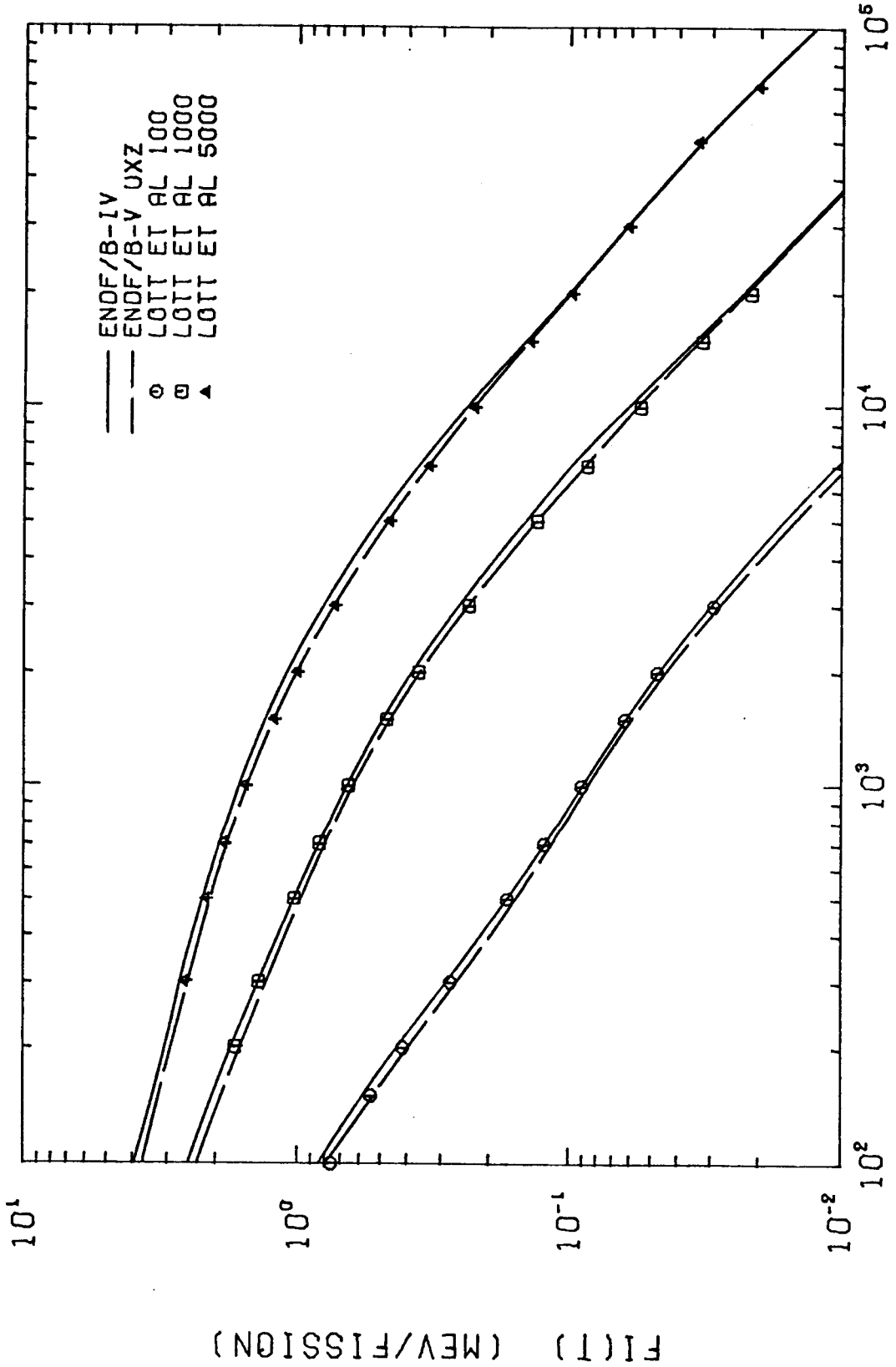
ENDF/B-IV
ENDF/B-V UXZ
LOTI ET AL 100
LOTI ET AL 1000
LOTI ET AL 5000
FI(T) (MEV/FISSION)
COOLING TIME (SEC)
TOTAL INTEGRAL AFTERHEAT U235T
100S 1000S AND 5000S IRRADIATIONS

Figure 5.

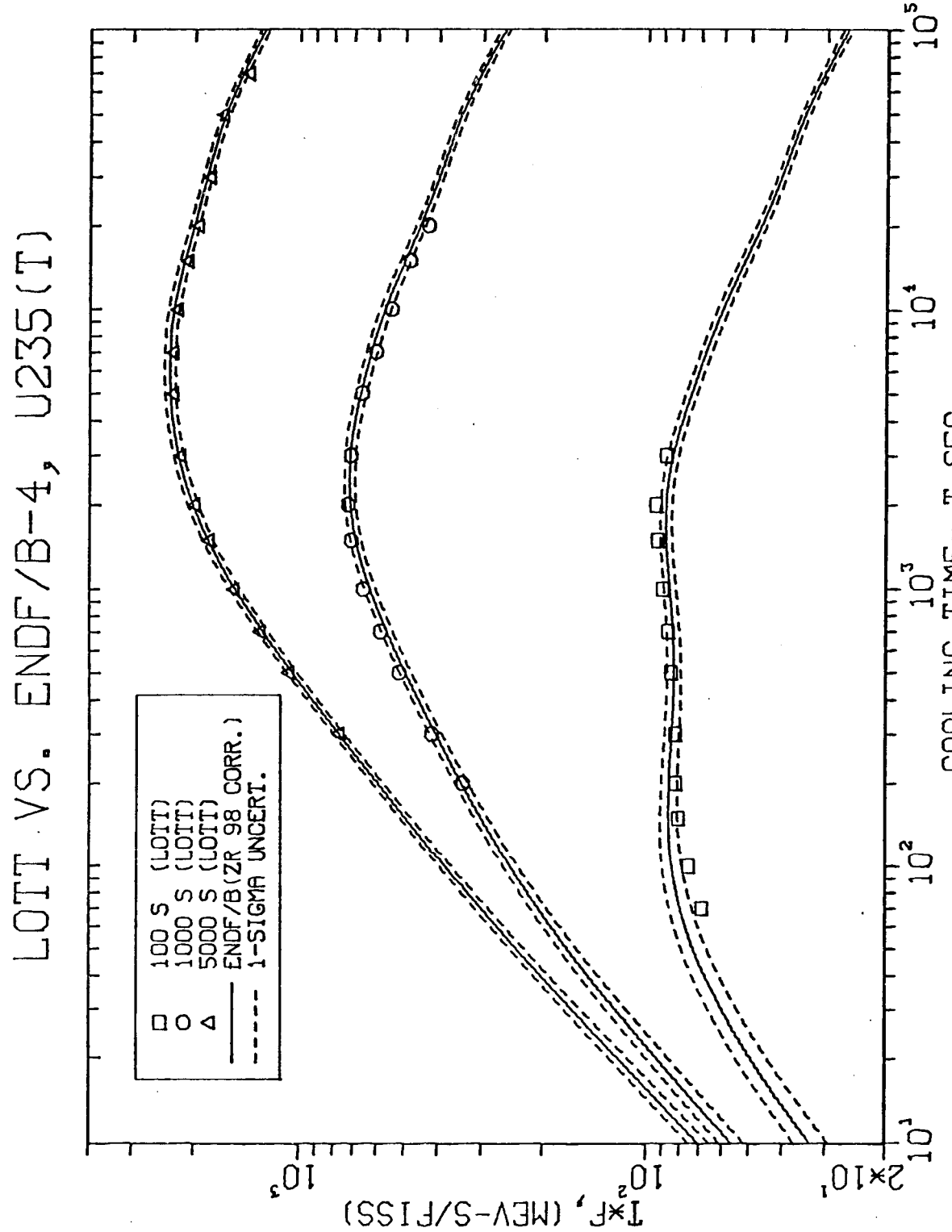
LOTT VS. ENDF/B-4, U235(T)
100 S (LOTT)
1000 S (LOTT)
5000 S (LOTT)
ENDF/B(ZR 98 CORR.)
1-SIGMA UNCERT.
T*F, (MEV-S/FISS)
COOLING TIME--T,SEC
2*10¹
10²
10³
10¹
10²
10³
10⁴
10⁵

Figure 6.

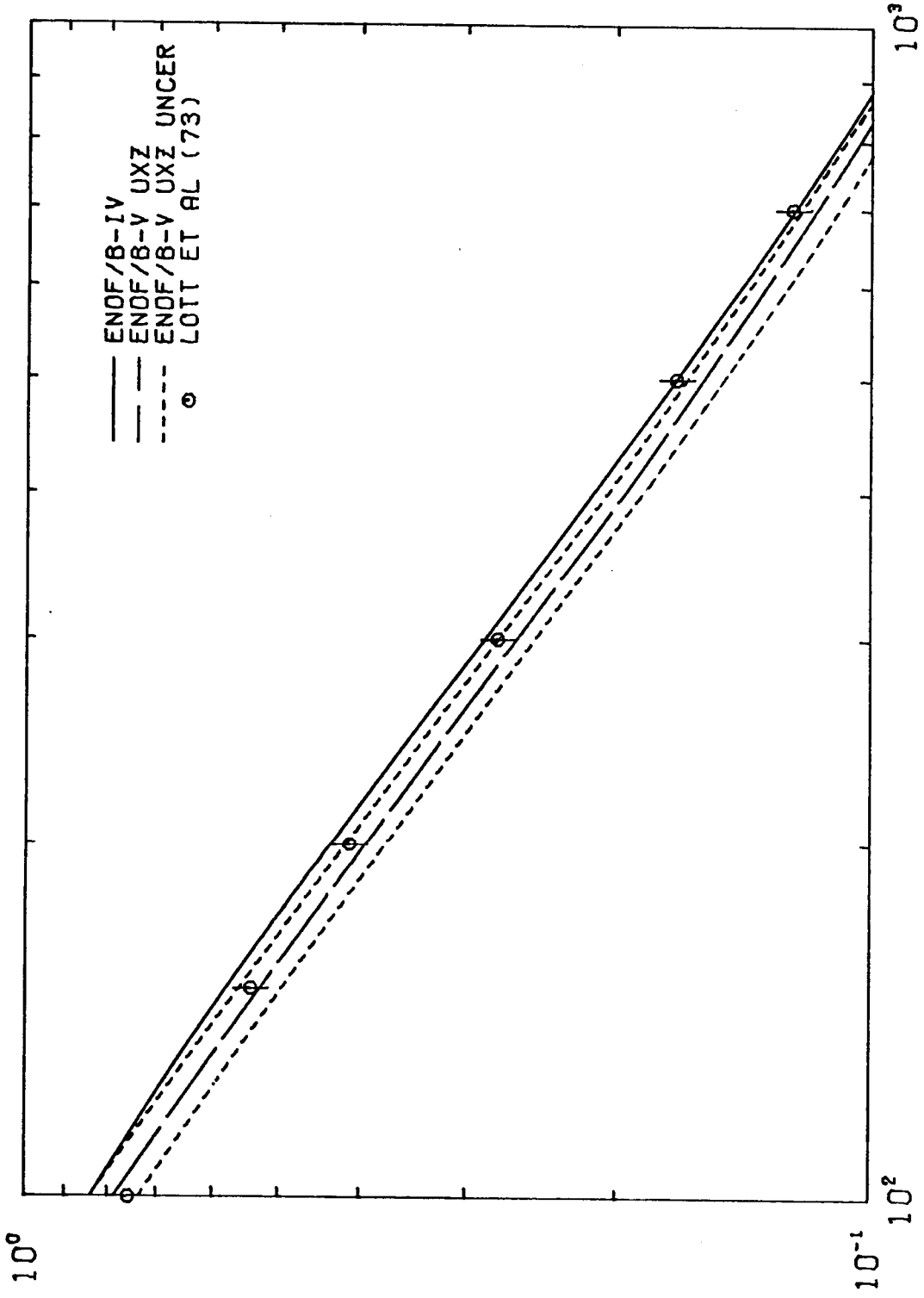
ENOF/B-IV
ENOF/B-V UXZ
ENOF/B-V UXZ UNCER
LOTT ET AL ('73)
10^0
10^{-1}
10^2
10^3
FI(T) (MEV/FISSION)
COOLING TIME T (SEC)
TOTAL INTEGRAL AFTERHEAT U235T
100S IRRADIATION

Figure 7.

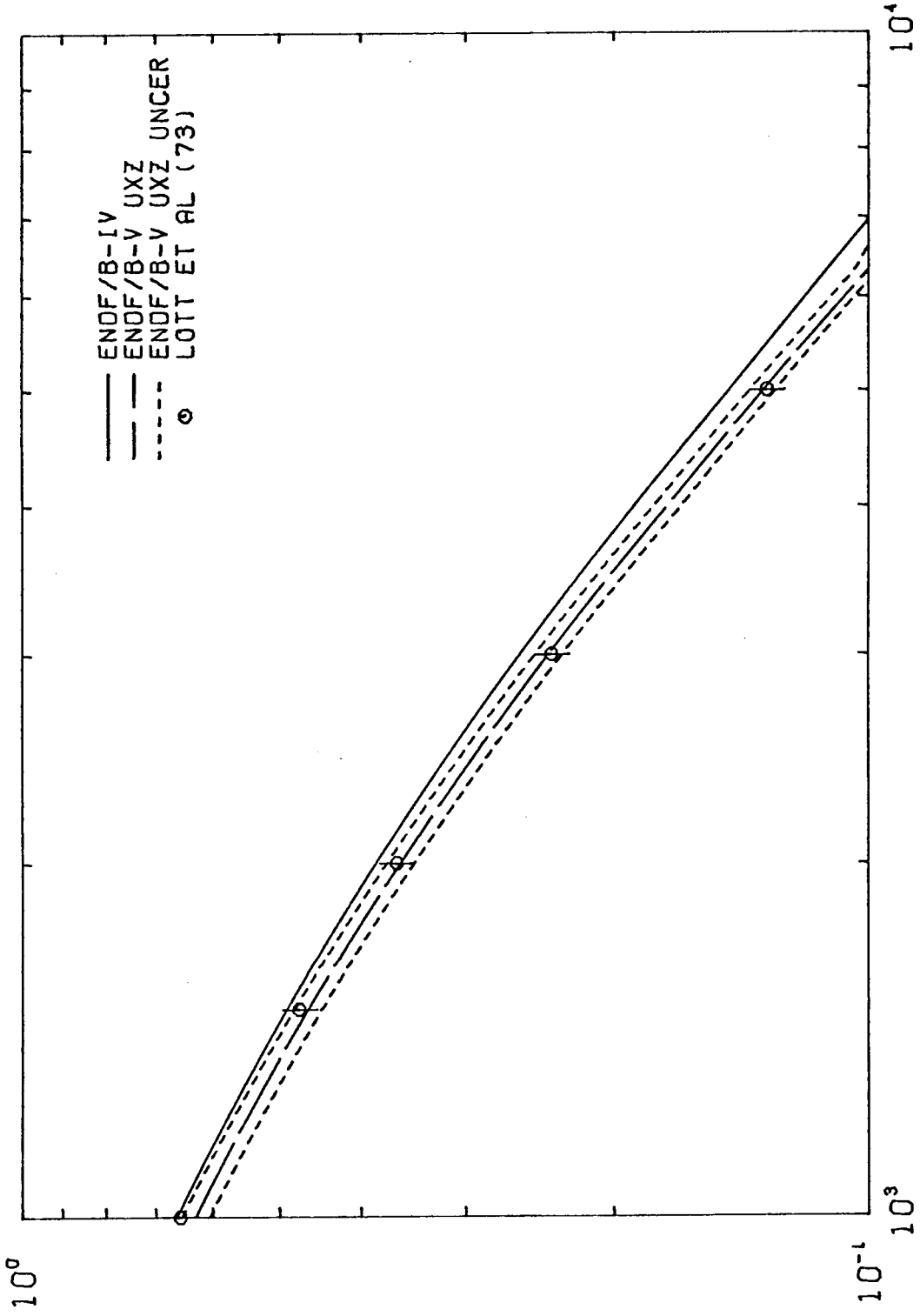
ENDF/B-IV
ENDF/B-V UXZ
ENDF/B-V UXZ UNCER
LOTT ET AL (73)
10^0
10^{-1}
10^3
10^4
FI(T) (MEV/FISSION)
COOLING TIME T (SEC)
TOTAL INTEGRAL AFTERHEAT U235T
1000S IRRADIATION

Figure 8.

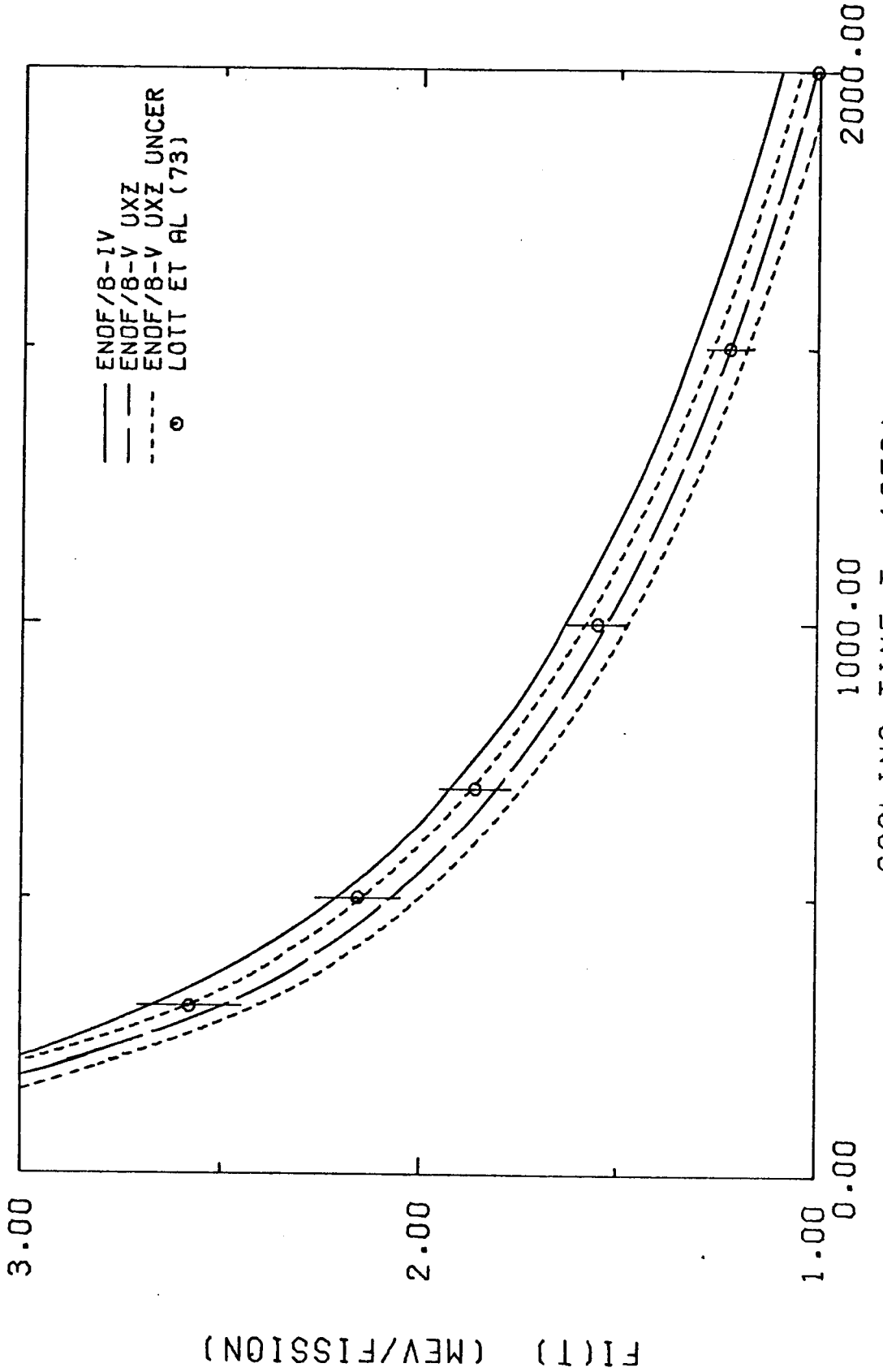
TOTAL INTEGRAL AFTERHEAT U235T
5000S IRRADIATION
ENDF/B-IV
ENDF/B-V UXZ
ENDF/B-V UXZ UNCER
LOTT ET AL ('73)
FI(T) (MEV/FISSION)
COOLING TIME T (SEC)
3.00
2.00
1.00
0.00
1000.00
2000.00

Figure 9.

4) Total Decay Power-Calorimetry - BAPL (1974)[11,12]

Samples of U235, U233, Pu239 and Th232 were irradiated to high burnups in the Materials Testing Reactor (MTR) and the Advanced Test Reactor (ATR) at Idaho National Engineering Laboratory. Following the final irradiation cycle, the samples were discharged from the ATR as expeditiously as possible and transferred to the canal of the Advanced Reactivity Measurement Facility where calorimetric measurements were carried out.

Calculations have been made using the FISSPROD-2 code with ENDF/B-IV input data to compare with these experimental results for U235 sample No. 25. The irradiation history is given in detail in the Gunst et al report[11] and comprised 3 cycles in MTR at fluxes ($n_{thermal}\bar{v}$) ranging up to 1.76×10^{14} n/cm^{2}s, and 1 cycle in ATR at fluxes mostly near 4.7×10^{14} n/cm^{2}s. There was a cooling period of 2.15 years before the ATR irradiation.

The FISSPROD-2 simulation follows flux changes in the ATR irradiation closely but reduces the three cycles in MTR to a single step irradiation. To see if the results depended at all on the flux and time of the assumed MTR irradiation two quite different sets were used. In the first the total irradiation time was used with an average flux, in the second the final flux in the MTR irradiation (which happened to be the highest) was used with a correspondingly shorter irradiation time. Since the two assumptions gave results that differed by less than 0.1% it was concluded that the simplified one-step MTR irradiation was adequate.

For the FISSPROD-2 calculations it was necessary to convert the listed group fluxes to a Westcott flux ($\phi_w = n_{total} v_o$) and epithermal index, r. The conversion is described in the discussion of the Westinghouse fission product absorption results that follows. The absorption cross sections for U235 for use with ϕ_w are 666.6 barns

(MTR) and 673.1 barns (ATR). The values, in combination with the irradiations listed below, give the observed depletion of U235.

	Δt	$\bar{\phi}_3$	$\bar{\phi}_w$	$r\sqrt{T/To}$	
	$- 10^5$ s	$- 10^{14}$	n/cm^{2}s -		
*	41.115	1.256	1.0924	0.06106	$\phi_w.\Delta t = 0.449 \times 10^{21}$ n/cm^2
	29.455	1.7536	1.5252	"	$\phi_w.\Delta t = 0.449 \times 10^{21}$ n/cm^2
	677.31	0	0		
	0.1728	0.0738	0.0683	0.120	
	0.0655	1.1908	1.1091	"	
	0.0349	2.5919	2.3996	"	
	0.0450	3.120	2.8885	"	
	0.1926	4.469	4.1373	"	
	3.2724	4.627	4.2823	"	
	2.4988	0	0		
	0.1404	0.0423	0.0391	0.119	
	0.0205	0.8367	0.7742	"	
	0.0684	1.9927	1.8436	"	$\Sigma\phi_w\Delta t = 0.487 \times 10^{21}$ n/cm^2
	0.0169	3.2887	3.0423	"	
	5.6329	4.7089	4.3537	"	
	0.0072	0	0		
	0.0330	3.8941	3.5993	0.118	
	0.0108	4.4637	4.1251	"	
	0.5796	4.7255	4.3665	"	
	0.00828	4.4845	4.1436	"	
	1.28268	4.7466	4.3853	"	
	0.12096	4.7381	4.3768	"	

* Alternative MTR irradiations

The measured heat from the sample was corrected by the authors for heat carried away by γ-rays (~ 50% of total γ-ray heat) and then the small contributions of heavy elements and capture products in structural materials were subtracted to obtain a value for the "measured" fission product heat. These were compared to the ANS standard[15] after correcting to the finite irradiation. In Table III the FISSPROD-2 calculations (ENDF/B-IV) are compared to the "measured" and ANS standard values listed in the Gunst et al. report. Figure 10 shows the good agreement between experiment and calculations for the above results.

Table III. Total Decay Power Following Thermal Neutron Fission Comparing Gunst et al. ("Measured") with ENDF/B-IV (Calc)

	Watts from sample		
Cooling time (h)	Calculated*	"Measured"	ANS Std.
14.55	61.40	65.1	63.8
14.97	60.53	64.4	62.9
15.45	59.59	63.0	61.8
15.90	58.73	61.9	60.9
34.49	39.46	41.49	39.99
35.49	38.88	41.15	39.36
81.77	25.28	25.83	25.30
83.34	25.03	24.72	25.04
201.5	15.08	15.73	15.12
202.2	15.04	15.36	15.09
296.3	11.45	11.24	11.51
297.6	11.41	11.20	11.48
1067	3.357	3.23	3.35
1068	3.354	3.35	3.35
2099	1.581	1.57	1.55
2436	1.354	1.16	1.32
2770	1.180	1.15	1.15
3108	1.039	1.10	1.01
4142	0.730	0.69	0.71
4551	0.641	0.64	0.64

* Using 0.6718 gms of U235 fissioned in the sample

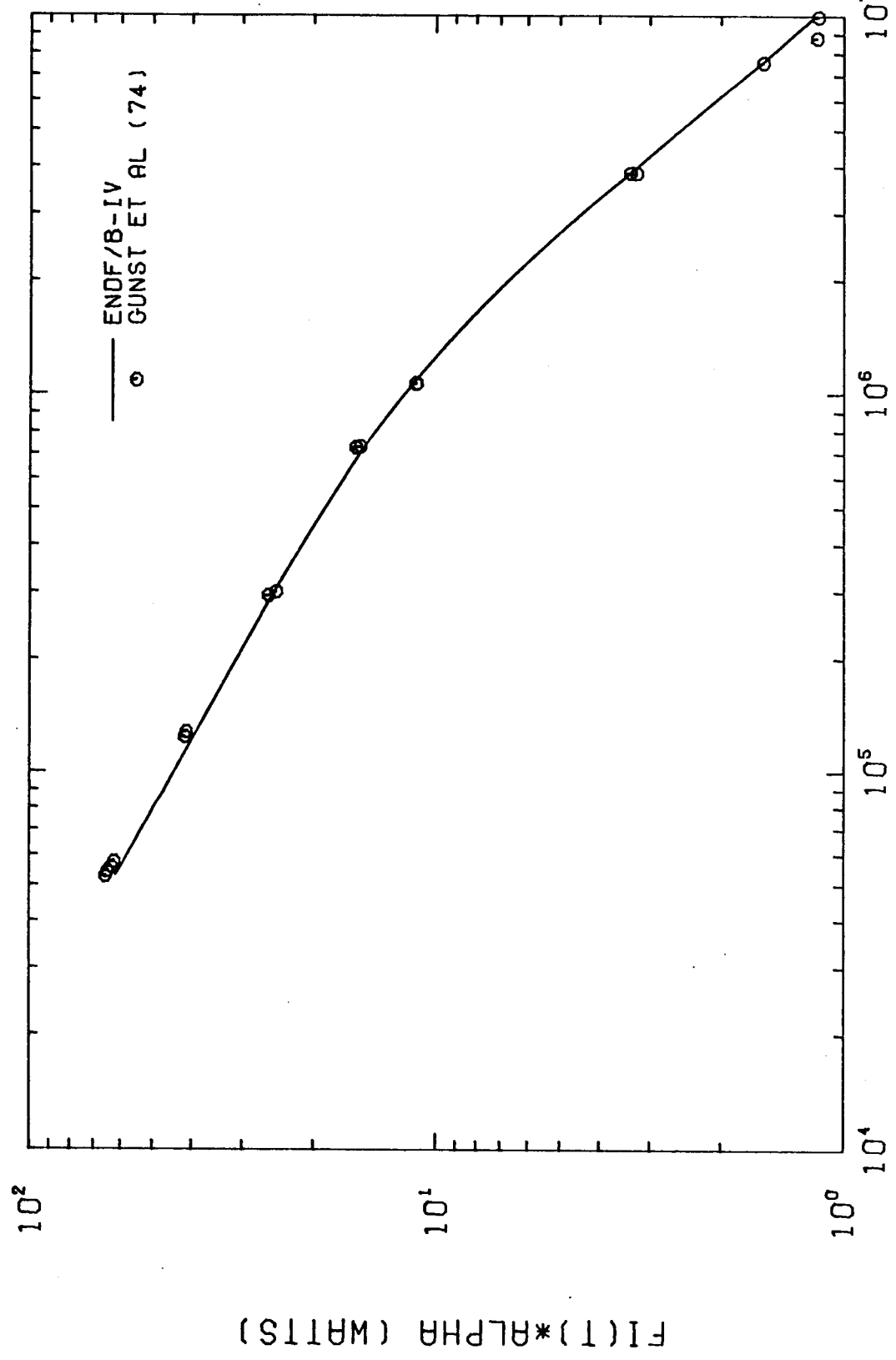
ENDF/B-IV
GUNST ET AL (74)
CALORIMETRIC RESULTS U235T
HIGH BURNUPS IN MTR AND ATR
COOLING TIME T (SEC)
FI(T)*ALPHA (WATTS)
10^0
10^1
10^2
10^4
10^5
10^6
10^7

Figure 10.

5) Experiments Reported Before 1973

Perry et al.[13] have reviewed previous (before 1973) integral measurements of decay heat following "burst" and long time exposure fission. These included both beta and gamma decay energy measurements. Perry et al. propose "after heat functions" based on these experiments for thermal-neutron fission of U235 for the cooling time interval of 1-5 x 10^5s. Figures 11-14 give the comparisons of the ENDF/B-IV decay heat curves to Perry et al.'s evaluations (10% uncertainty bars are shown) for the "infinite" exposure case. Also given in Figures 11 and 12 is the evaluation of Shure[16] which is the bases of the ANS 5.1 decay heat standard[15] and the Shure curve plus an uncertainty of 20% required by NRC regulations 10CRFR50.46 for ECCS analyses. The ENDF/B-IV curves are below the Shure curve for cooling times less than 200 seconds, which are most important for the analyses of major loss-of-coolant accidents. The 20% uncertainty of the ANS 5.1 standard appears to be conservative. Figures 13 and 14 show the result of splitting up the curves of Figure 11 into their β and γ energy components. The agreement with Perry et al.'s evaluation is not as good for the split as for the total.

Curves showing the comparison of the ENDF/B-IV calculations with the pre-1973 "burst" integral measurements are given in Reference 17.

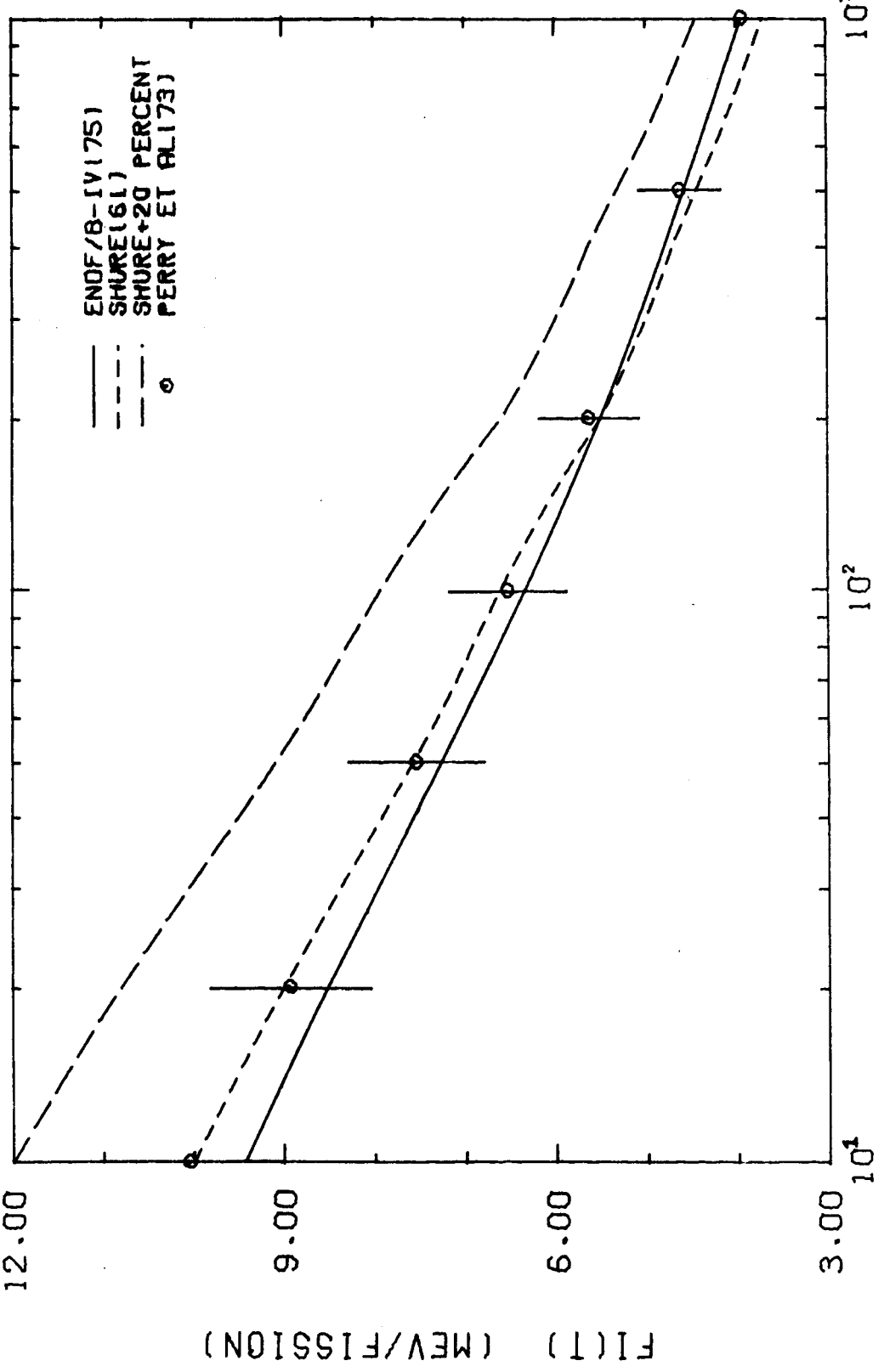

Figure 11. Total integral afterheat for U235 thermal, "infinite" exposure.

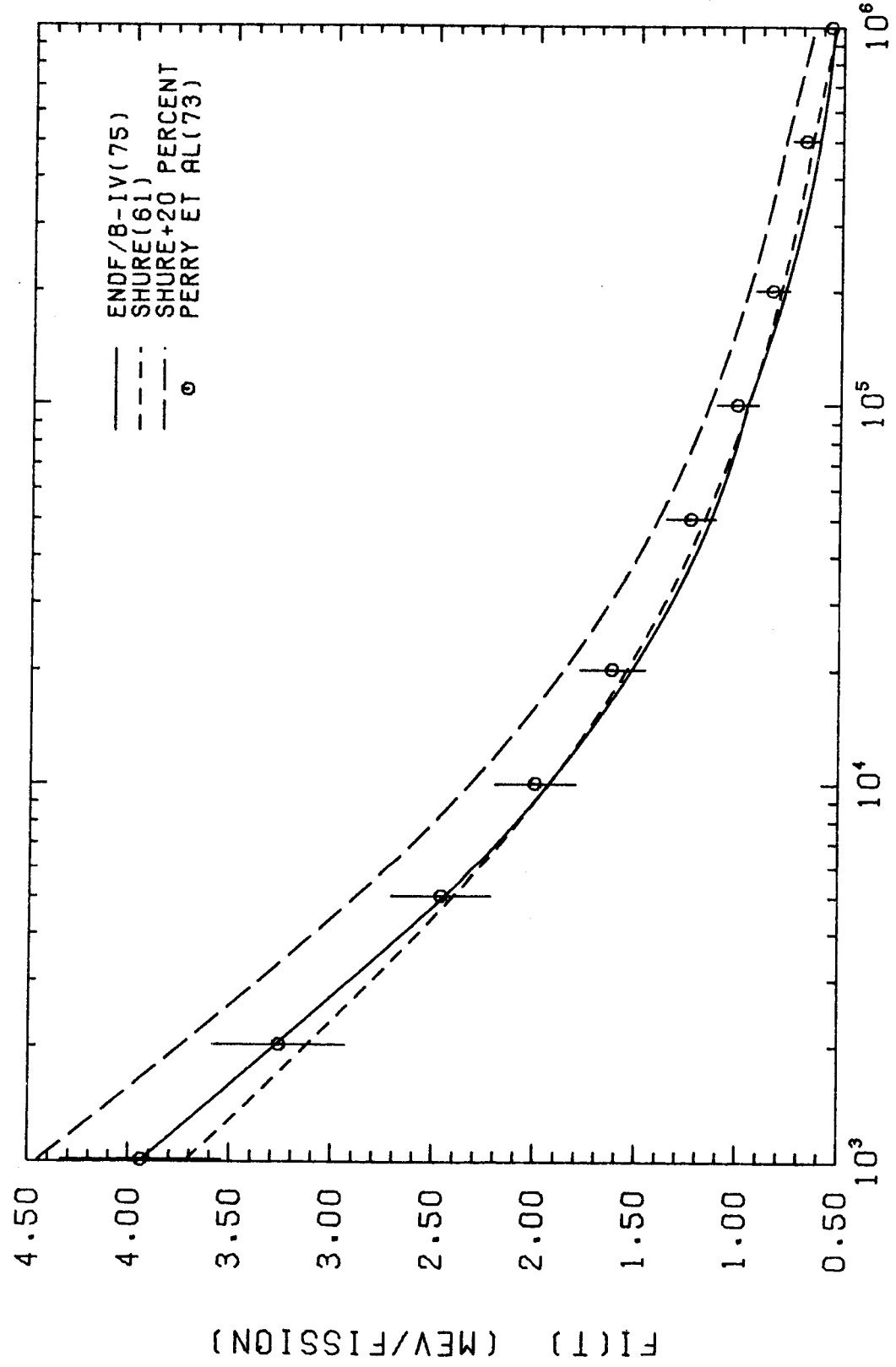

Figure 12. Total integral afterheat for U235 thermal, "infinite" exposure.

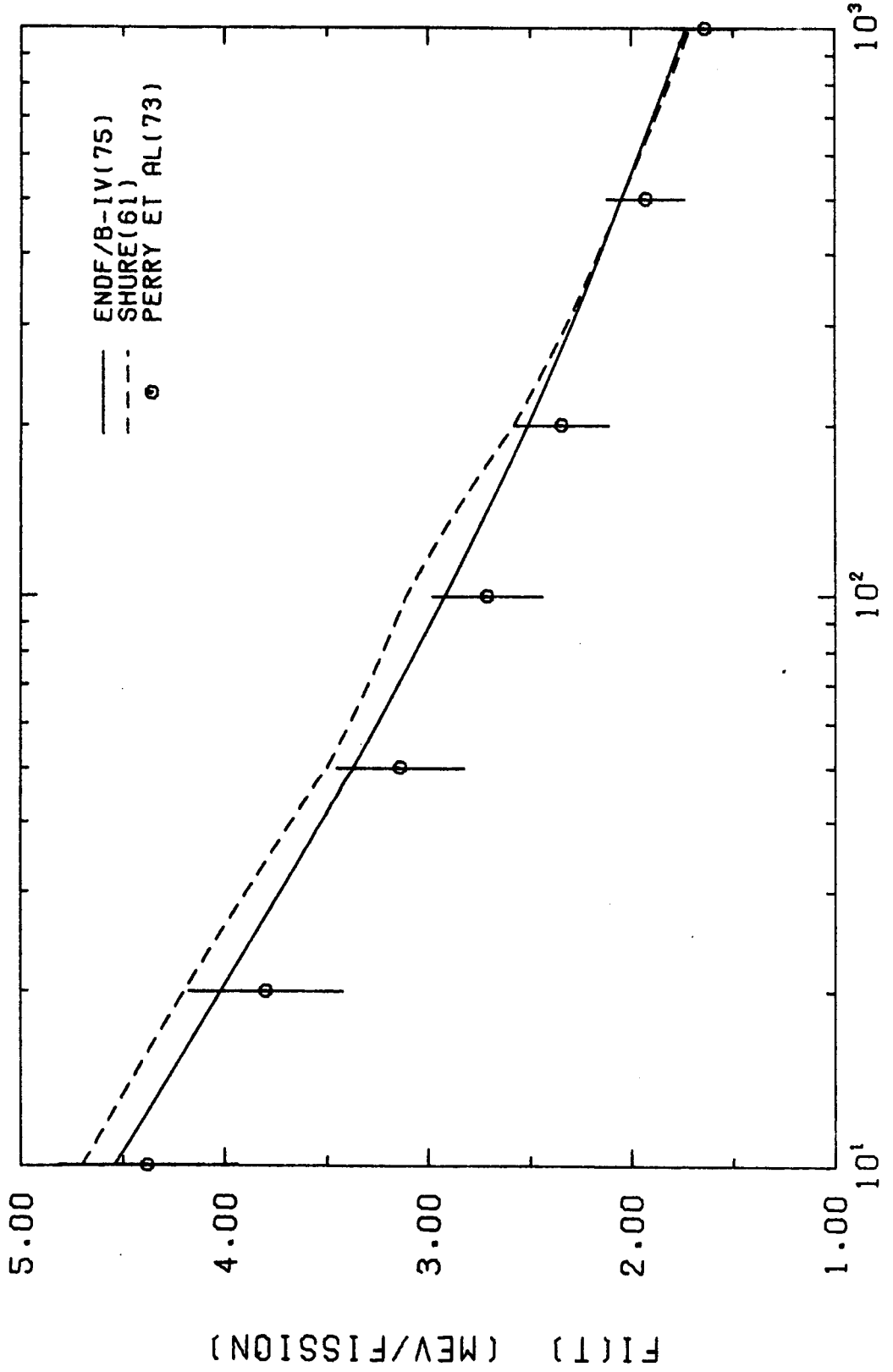

Figure 13. Beta integral afterheat for U235 thermal, "infinite" exposure.

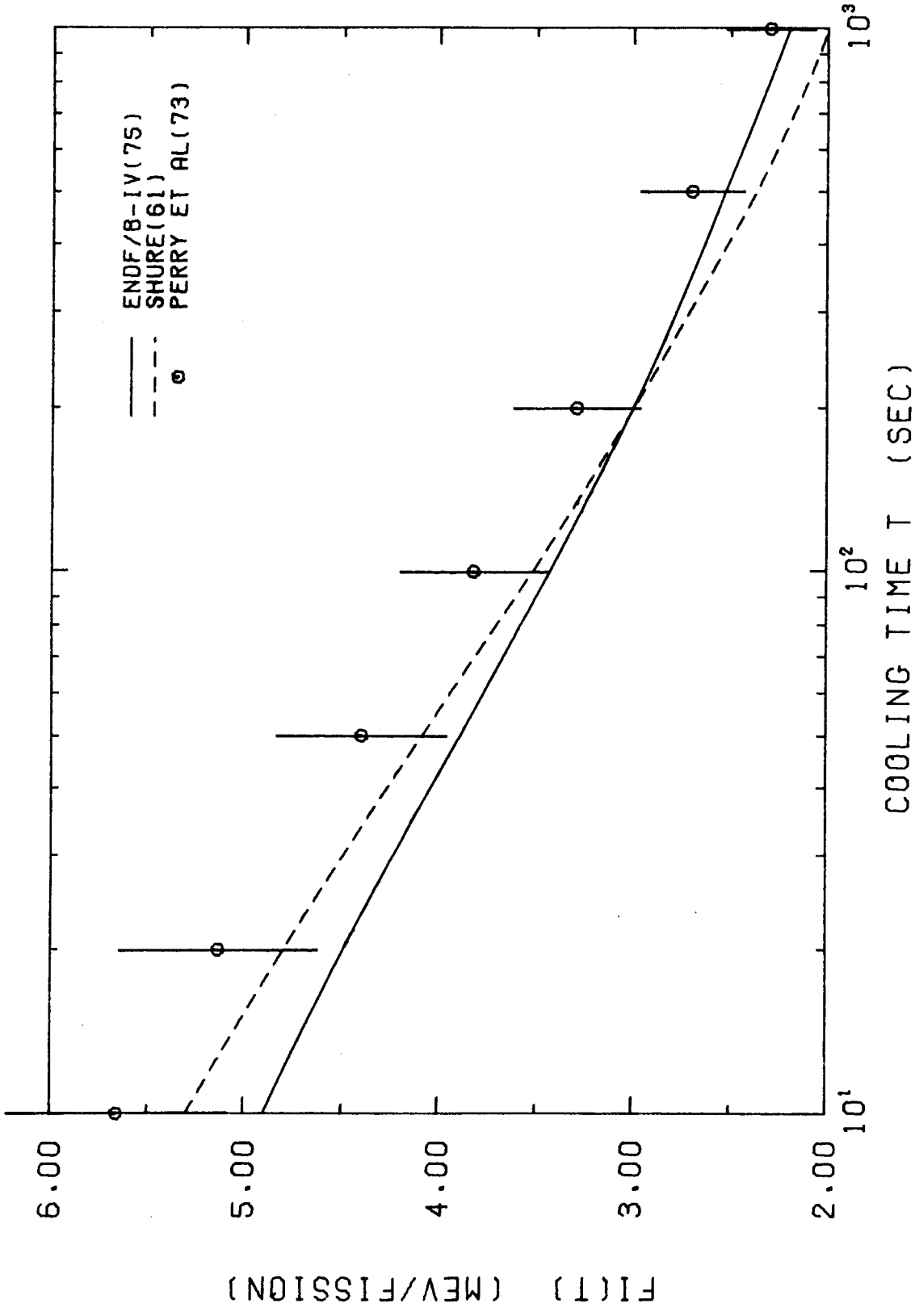

Figure 14. Gamma integral afterheat for U235 thermal, "infinite" exposure.

SPECTRA

Several beta and gamma spectra from FP decay experiments are currently in progress. Results by Dickens et al.[8] at ORNL are available for the gamma spectra, their beta results to be available at a later date. Figures 15-17 show gamma spectra plots for 3 of the 27 cooling time intervals described in the gamma power section. The "Present Data" symbols are the measured data points. The ENDF/B-IV FP files contains experimental "line data" (β end-point and γ energies and intensities) information for 180 nuclides[34] out of a total of 711 decaying nuclides. This set of data was used in the ORIGEN calculations shown as the solid curves in Figures 15-17.

Contributions from the 531 nuclides not having experimental "line data" decreases in importance as the cooling times increase. This is indicated in Figure 18, where the percent contribution to the total gamma heat from the 531 nuclides ($\bar{E}\gamma$, the average gamma energy per decay, is calculated theoretically) is shown to rapidly decrease with cooling times.* Using Figure 18, the three cases corresponding to Figures 15-17, for example, would have approximately 50%, 7% and 3% contributions, respectively, from the 531 "theoretical energy" nuclides, and hence 50%, 93% and 97% contribution from the 180 "experimental energy" nuclides. This is consistent with the results shown in Figures 15-17.

In Figure 15 (T_{cool}=10-30s) the ENDF/B-IV curve substantially underpredicts the measured data, whereas in Figures 16 and 17 (T_{cool}=750-1950s) it closely follows the data up to about 3 MeV.

Gamma spectra above the Be9 and H2 photoneutron threshold (1.67 MeV) have been calculated with CINDER-10 using the ENDF/B-IV data for various cooling times up to

---

* Contributions to the gamma spectra calculations were not included from the 531 "theoretical energy" nuclides, however, they are included in the gamma decay heat calculations presented in the previous section.

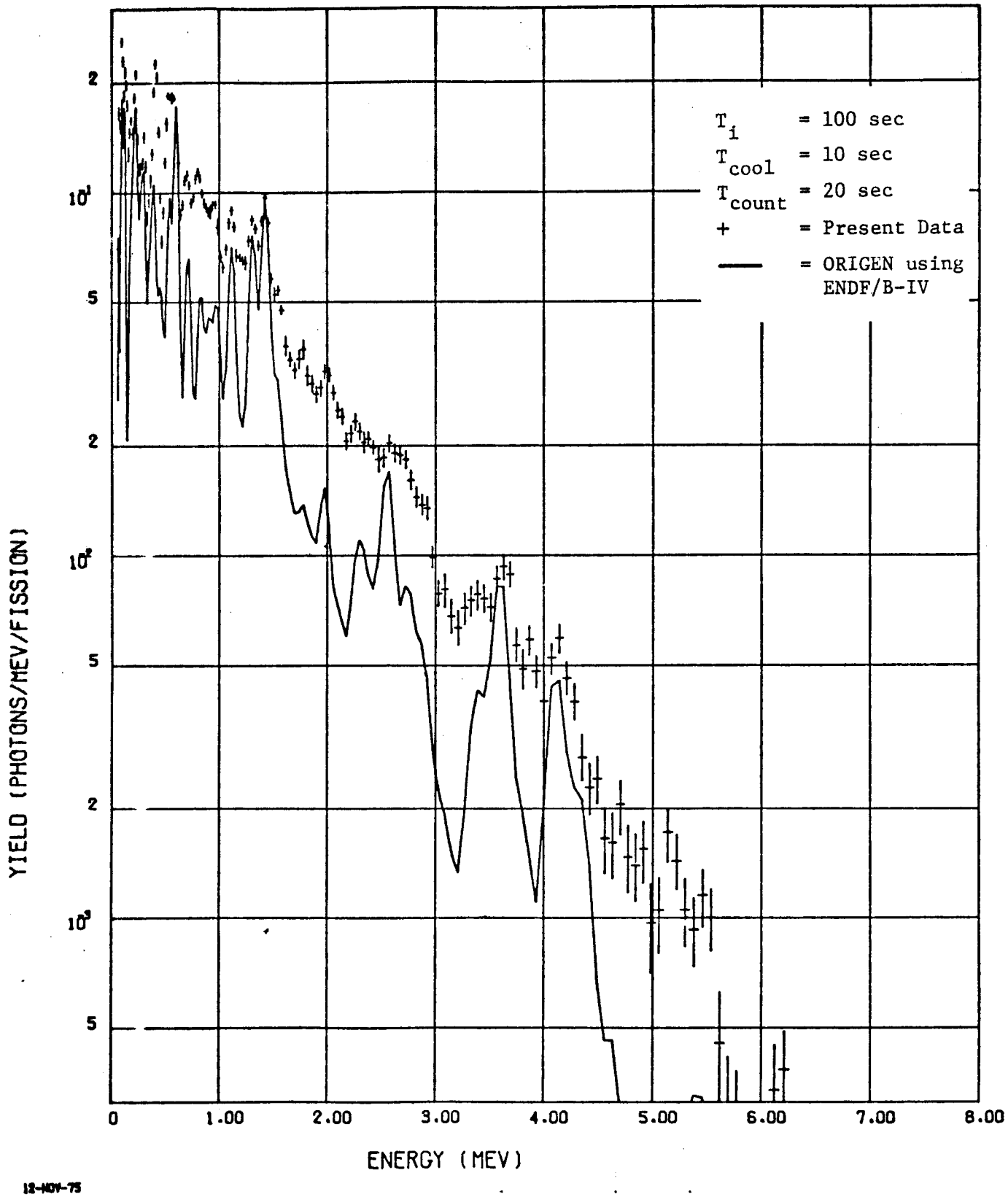
T_i = 100 sec
T_{cool} = 10 sec
T_{count} = 20 sec
+ = Present Data
—— = ORIGEN using ENDF/B-IV
YIELD (PHOTONS/MEV/FISSION)
ENERGY (MEV)
0
1.00
2.00
3.00
4.00
5.00
6.00
7.00
8.00
2
10^1
5
2
10^2
5
2
10^3
5
12-NOV-75

Figure 15.

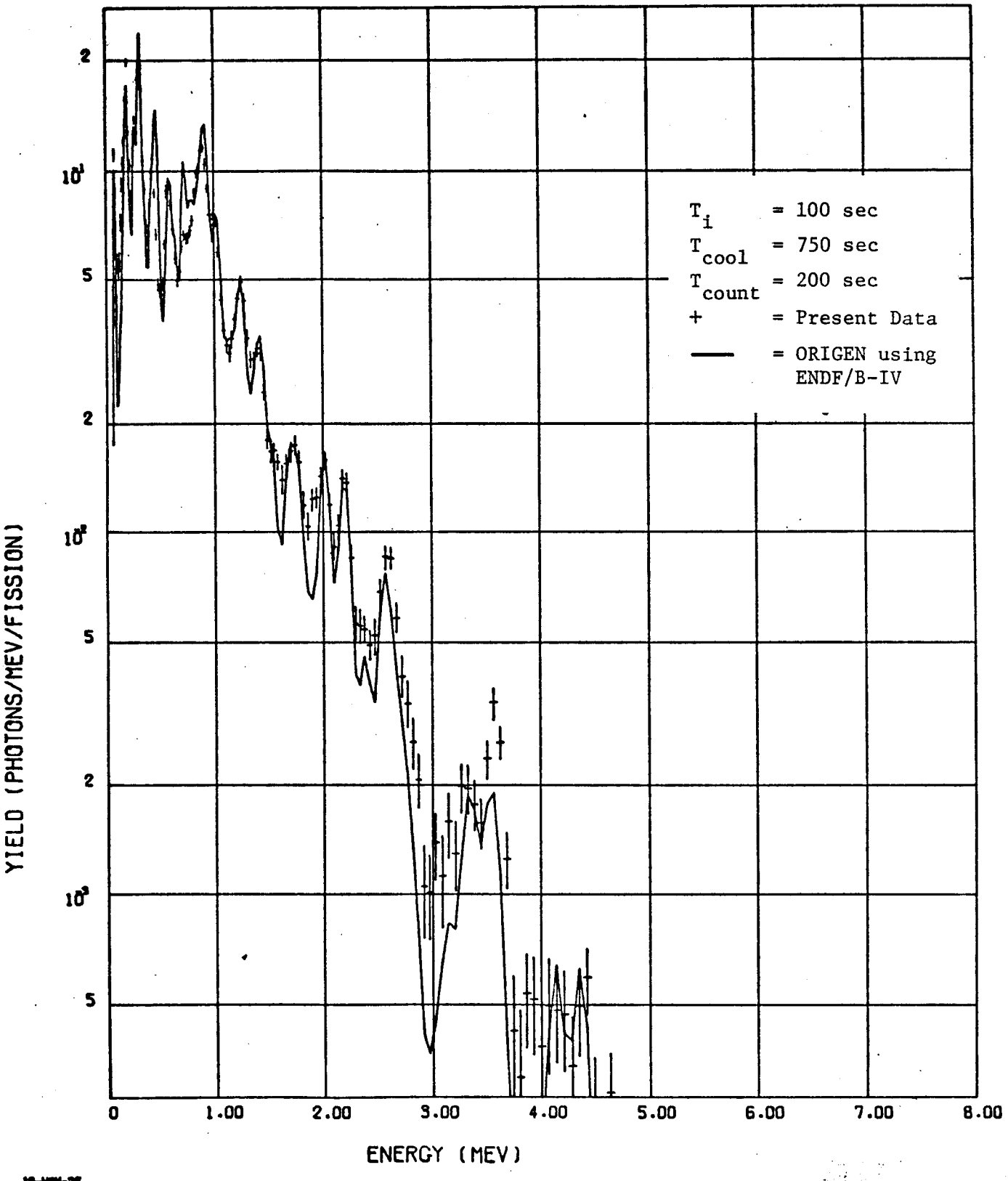
T_i = 100 sec
T_{cool} = 750 sec
T_{count} = 200 sec
+ = Present Data
— = ORIGEN using ENDF/B-IV
YIELD (PHOTONS/MEV/FISSION)
ENERGY (MEV)
0
1.00
2.00
3.00
4.00
5.00
6.00
7.00
8.00

Figure 16.

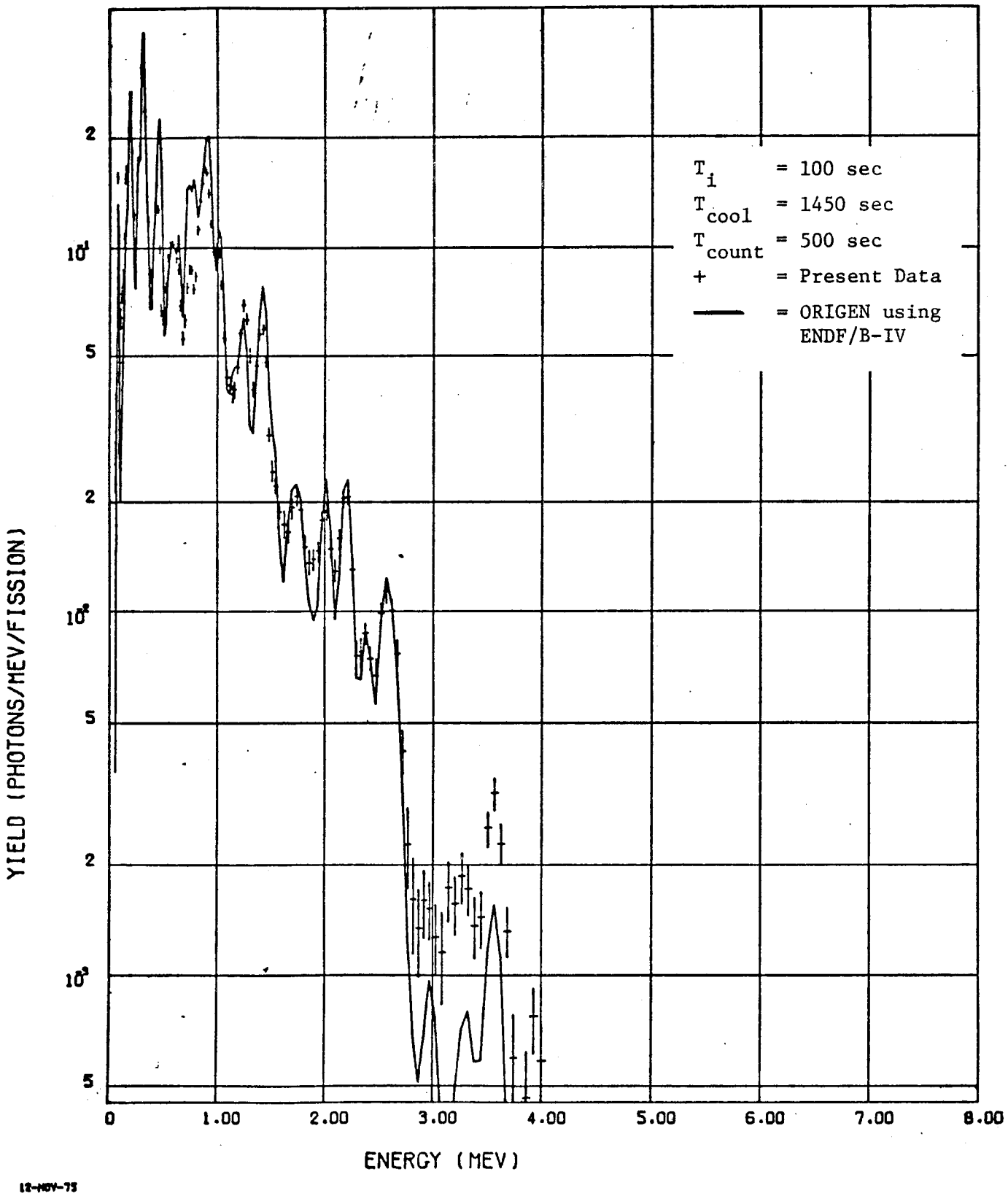
T_i = 100 sec
T_{cool} = 1450 sec
T_{count} = 500 sec
+ = Present Data
— = ORIGEN using ENDF/B-IV
YIELD (PHOTONS/MEV/FISSION)
ENERGY (MEV)
0
1.00
2.00
3.00
4.00
5.00
6.00
7.00
8.00
2
10^1
5
2
10^2
5
2
10^3
5
12-NOV-75

Figure 17.

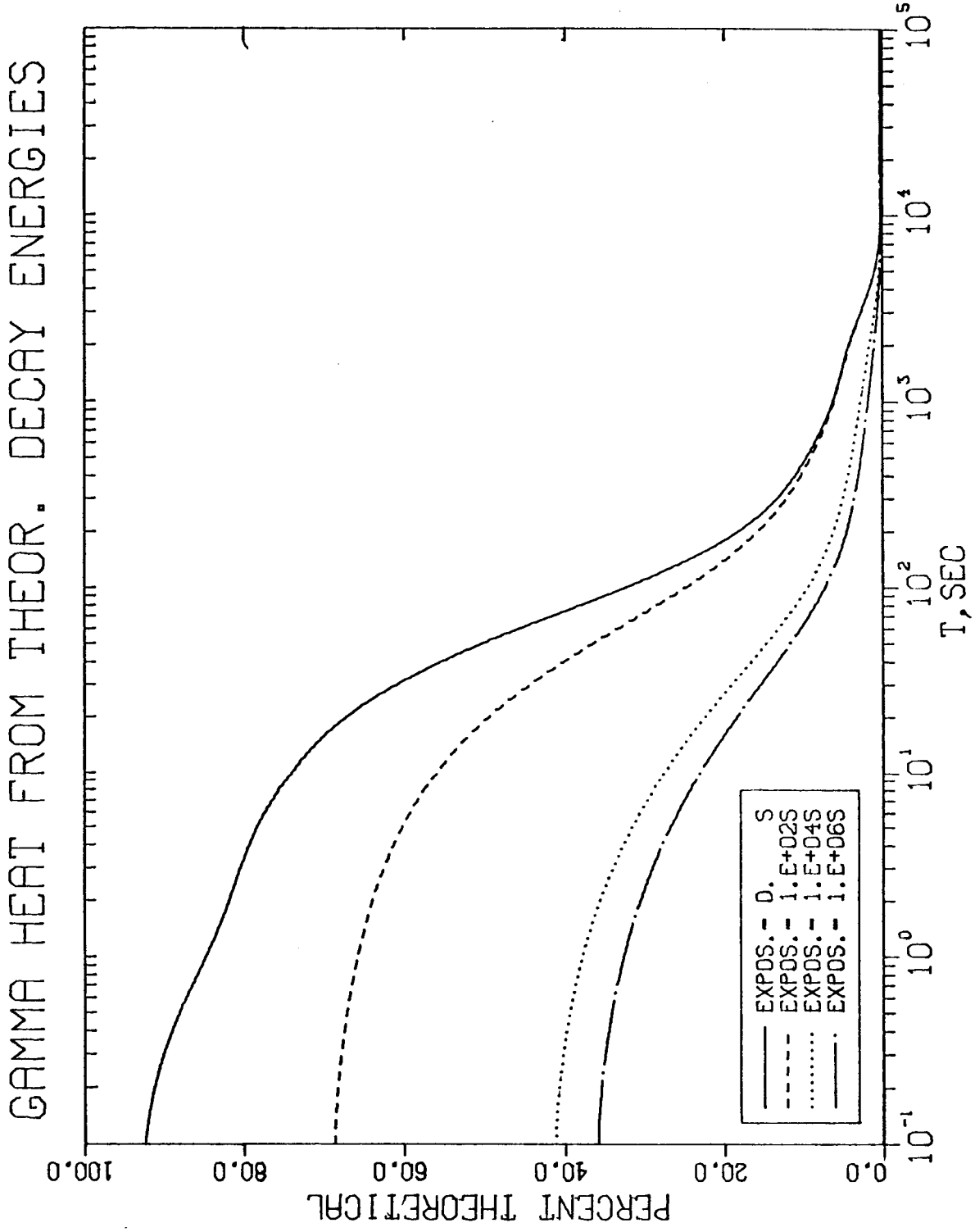
GAMMA HEAT FROM THEOR. DECAY ENERGIES
PERCENT THEORETICAL
0.0
20.0
40.0
60.0
80.0
100.0
T, SEC
10^{-1}
10^{0}
10^{1}
10^{2}
10^{3}
10^{4}
10^{5}
EXPOS.= 0. S
EXPOS.= 1.E+02S
EXPOS.= 1.E+04S
EXPOS.= 1.E+06S

Figure 18.

1000 hours.[18,19] Figure 19 shows the spectra from U235 thermal fission at a cooling time of 1 hour using 66 groups (50 keV bins). After a cooling time of ten hours, the spectra hardens with time and the total gamma emission rate remains nearly constant up to 200 hours.[35] This behavior is important to sourceless reactor startup.

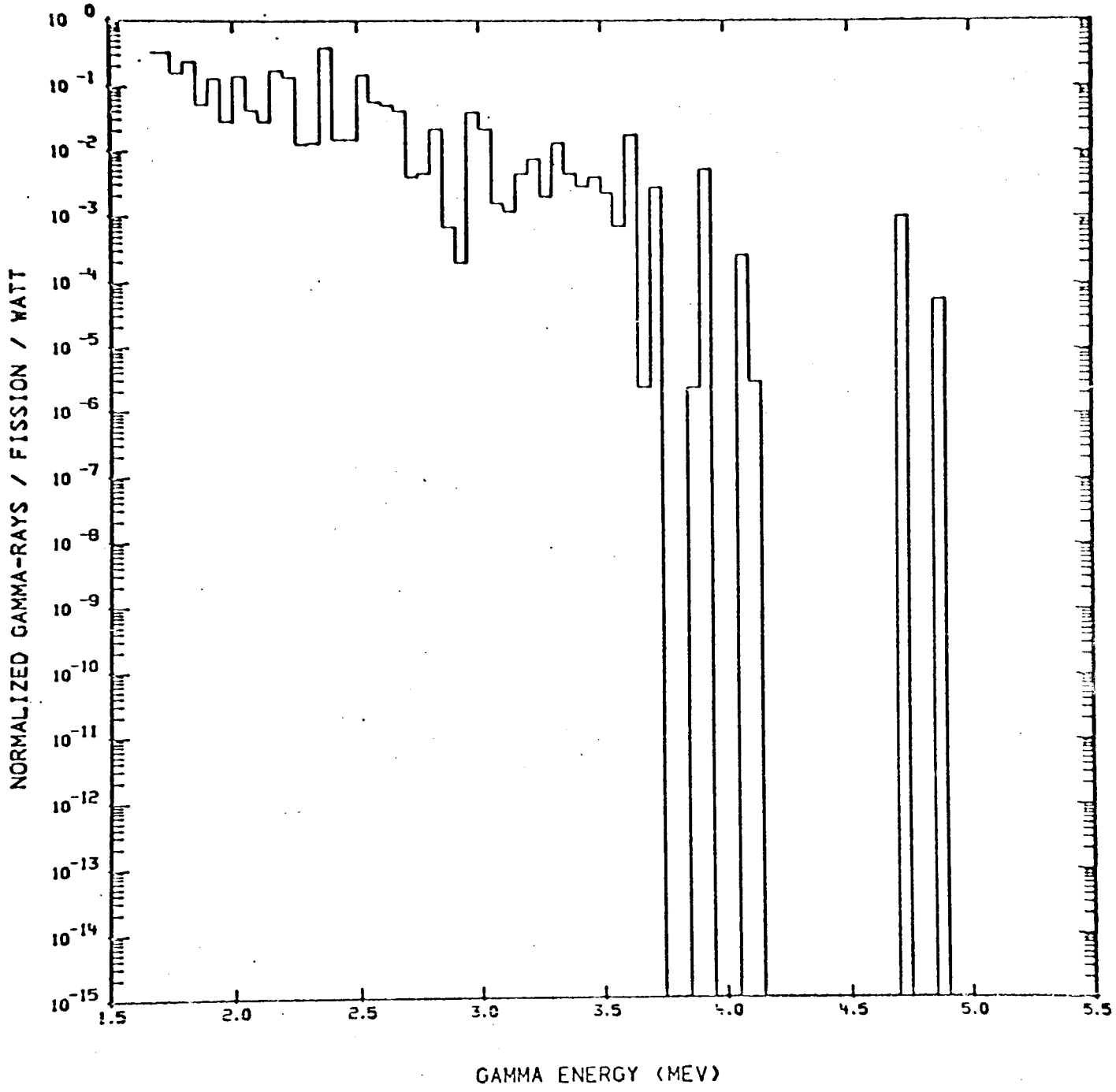

Figure 19. ^{235}U-thermal fission-product γ-ray spectrum at 1 hour following shutdown. The normalization constant is 9.5958×10^{-4}.

ABSORPTION

Absorption experiments which have been used as benchmarks are divided into results from fast and thermal reactor systems. The fast measurements were made at the Coupled Fast Reactivity Measurement Facility (CFRMF) by Harker et al.[20,21]. These measurements were direct capture on individual fission product nuclides. Reactivity measurements have also been made at CFRMF[22] and the STEK[23] facilities for individual important fission product nuclides and "lumped" fission products sets. At STEK, experiments were made in several fast assemblies (STEK-500,1000, 2000,3000,4000) for about 80 individual fission product nuclides and 4 "lumped" fission product sets. These reactivity results have not been compared to ENDF/B-IV calculations. However, they represent excellent possible future benchmarks.

For thermal systems Gunst et al.[24,25] have completed absorption measurements for samples of U233, natural uranium, U238 and natural thorium. Irradiations were made in high-flux facilities in different thermal neutron spectra and for different durations including exposure to more than 90% depletion in fissile material and more than 30,000 MWd/tonne in fertile material. Okazaki and Sokolowski[26] measured effective 2200 m/s cross sections on samples of U233, U235 and Pu239 irradiated at the Chalk River Laboratories. Finally, resonance integral measurements provide an integral test of individual fission product thermal and epithermal capture cross section energy dependences.

1) Fast Capture in CFRMF-ANC (1972, 1972)[20,21]

Direct capture measurement results for 30 important fission product isotopes are given in Table IV and compared with the ENDF/B-IV calculations. Most of the nuclides (23) have calculated versus measured differences greater than 10% which is the average quoted experimental uncertainty.

Table IV. Effective Cross Sections of FP Absorbers in CFRMF

Nuclide	Absorption Cross Sections (barns) Measurement*	Calculation**	Cal-Meas
Rb87	.0153±.0010	.0110	-.0043
Nb93	.189 ±.019	.121	-.068
Mo98	.062	.067	+.005
Tc99	.383 ±.063	.273	-.110
Ru102	.101 ±.007	.118	+.017
Ru104	.095 ±.005	.098	+.003
Rh103	.423	.415	-.008
Ag107	.468 ±.060	.414	-.054
Ag109	.563 ±.081	.292	-.271
Sb121	.315	.302	-.013
Sb123	.167	.163	-.004
I127	.308	.345	+.037
Xe132	.0401±.004	.0489	+.0088
Xe134	.0152±.0016	.0240	+.0088
Cs133	.333	.294	-.039
La139	.0207	.0243	+.0036
Ce140	.001	.0147	+.0137
Ce142	.020	.0248	+.0048
Pr141	.0855	.101	+.016
Nd148	.114	.161	+.047
Nd150	.113	.143	+.030
Pm147	.844	.545	-.299
Sm152	.330	.293	-.037
Sm154	.131	.154	+.023
Eu151	2.590 ±.150	2.240	-.350
Eu153	1.510 ±.120	1.390	-.120
Gd158	.200	.182	-.018
Gd160	.104	.138	+.034
Tb159	.999	.847	-.152
Ho165	.657 ±.100	.932	+.275
Au197	.450	.411	-.039

* Assumes value for Au197 equals .45 barns. Most of the results were reported by Harker et al. at the Kiamesha Lake Conference.[20] The Eu151 and Eu153 results were reported at the March Washington Meeting.[21]

**The calculated absorption cross sections were obtained by weighting the microscopic ENDF/B-IV capture cross sections with a 620 group SAND-II CFRMF spectrum. No corrections were made for self-shielding effects, which are assumed to be small.

2) FP Poisoning in Neutron-Irradiated U233 - BAPL (1974)[24,25]

Reactivity worths were measured for samples of U233 as functions of time following irradiation in high-level neutron fluxes. The irradiations were carried out in the Materials Testing Reactor (MTR) and the Advanced Test Reactor (ATR) at the Idaho National Engineering Laboratory. The fluxes for each irradiation interval were measured by bare and cadmium-covered cobalt monitor wires and normalized by mass spectrometer measurements of total and isotopic uranium. The reactivity worths of the U233 samples were calculated based upon the time-dependent concentrations of all significant uranium isotopes and fission products in each sample, and compared with the measured reactivity worths.[25] The measurements were made in different locations of the Advanced Reactivity Measurement Facility (ARMF-I).

2.1) Pm149 Resonance Integral

The measured and calculated transient reactivity worths indicate that the epi 0.105eV* resonance integral of Pm149 (precursor of Sm149) is at least 20,000 barns.[24] Since the ENDF/B-IV cross section for Pm149 is only 1400 barns at 0.0253eV, the 20,000-barn resonance integral result implies substantial resonance structure. In ENDF/B-IV, the epithermal cross section is represented by a smooth 1/v curve which provides a resonance integral of 801 barns above 0.5 eV. The ENDF/B-IV value was obtained using the recommendation of Ribon, et al.[27]

Conversion of the 0.105 eV resonance integral to an 0.5 eV cut requires knowledge of the energy dependence of the cross section between these two energies. The ENDF/B-IV data provide a resonance integral contribution that is less than 1000 barns for the energy region between these two cut points. If this is subtracted from the measured result, the Pm149 resonance integral above 0.5 eV is at least 19,000 barns.

---

* The 0.105 eV cutoff was selected because it facilitates calculations for samples irradiated in spectra with different epithermal-to-thermal flux ratios.

2.2) Xe135 Transient

The Xe135 transient reactivity measurements indicate that the product of the Xe135 thermal neutron cross section and the cumulative yield through I135 (for U233 fission) as given in ENDF/B-IV should be increased by about 7.5 percent.[25]

2.3) "Lumped" Fission Product Absorption Cross Sections

Calculations with the FISSPROD-2 code were made for one sample, No. 44, to test the ENDF/B-IV data. All irradiations considered were in MTR. It was first established that a single step irradiation gives an accurate estimate of fission product absorption by comparison over the first irradiation cycle with a computer run using the detailed flux changes listed in the Gunst et al. report.[24] The single step flux was equal to the average over the last few days of the cycle and the single step time interval was chosen to give the true integrated flux. The two results agreed to a small fraction of one percent. To obtain out-of-reactor time it was assumed that a full MTR cycle was 3 weeks.

MTR irradiation data is recorded as 2 $n\bar{v}$ flux groups, ϕ_2 and ϕ_3, with energies above and below 0.105 eV, while FISSPROD-2 uses the Westcott convention with a total flux $\phi_w = n_{total} v_{2200}$ and an epithermal index. The necessary conversion is done by equating reaction rates, i.e.

$$\phi_3\phi_3 + \sigma_2\phi_2 = \hat{\sigma}\phi_w = \sigma_{2200}\ (g + rs)\phi_w \tilde{} \sigma_{2200}\ (1 + r\sqrt{T/T_o}(2I\sqrt{\pi})) \qquad (1)$$

where $\hat{\sigma}$ is Westcott's effective cross section, r is the epithermal index, I is the reduced resonance integral,

T_o = 293.4°K and T = 343.2°K (for MTR). Using the definition of σ_2 and σ_3 given on p. 68 of the report[24]

$$\phi_w = \phi_3\ (0.81941 + 0.08991\ \sigma_2/\phi_3) \qquad (2)$$

$$r\sqrt{T/T_o} = 0.08153\ (\phi_2/\phi_3)\ (0.81941 + 0.08991\ \phi_2/\phi_3)^{-1} \quad (3)$$

Results are listed as an effective cross section, σ_{eff}, defined as

$$\sigma_{eff}(0.81941\ \phi_3) = \sigma_3\phi_3 + \sigma_2\phi_2 \quad (4)$$

and a resonance integral, RI, with lower limit 0.105 eV. Thus

$$\sigma_{eff} = \hat{\sigma}\ (1 + 0.10973\ \phi_2/\phi_3) \quad (5)$$

and

$$RI(.105) = I + 0.98\ \phi_{2200} \quad (6)$$

The approximate representation of $\hat{\sigma}$ in Equation (1) is used in FISSPROD-2. For cross sections such as that of Xe135 that cannot be so treated a value of $\hat{\sigma}$ is calculated for the particular spectrum and in the program $\sigma_{2200} = \hat{\sigma}$, I = 0. Values of $\hat{\sigma}$ and the parameters on which they are based are given in Table V. Note that for Xe135 the capture cross section is used, not the total cross section.

Values of σ_{2200} are taken from ENDF/B-IV while g and s values are from Westcott (AECL-1101) and, for Xe135, Sumner (AEEW-R116).

Table V. Effective Cross Section Parameters

Nuclide	σ_{2200} (kb)	g (343.2°K)	s	$\hat{\sigma}$ (kb) $\phi_2/\phi_3 = 0.6$	$\hat{\sigma}$ (kb) $\phi_2/\phi_3 = 0.536$
Cd113	19.877	2.42	-2.18	45.870	46.109
Xe135	2636	1.1925	-1.0	3007.7	3022.2
Sm149	41.19	2.187	-2.152	85.518	86.004
Sm151	15.01	0.693	-0.345	10.135	10.164

The MTR spectrum changed slowly over the total irradiation period with a more rapid change following the 17th cycle. The first value of $\hat{\sigma}$ in Table V ($\phi_2/\phi_3 = 0.6$) was used for cycles 1-17 while the second ($\phi_2/\phi_3 = 0.536$) was used for the remainder. It is probable that deviations from the assumed neutron temperature of 343.2°K will produce larger variations than this over the course of the irradiation.

Results of the calculation are compared with measured values in Table VI. The "measured" effective cross sections listed here were not measured, but are reconstituted for the MTR spectrom from σ_2 and σ_3 components extracted from measurements of effective cross sections in different parts of the test reactor ARMF-1. The measured values of σ_{2200} and RI(.105) in Table VI are derived from σ_2 and σ_3 and were taken from the report.[24]

Provided the neutron spectrum in MTR is similar to the spectra where the ARMF-1 measurements were made, the comparison of calculated and "measured" effective cross sections should be a more valid test of ENDF/B-IV data than the comparison of σ_{2200} and RI(.105).

Table VI. U233 "Lumped" Fission Product Absorption Cross Sections in ARMF-1 from Irradiations in MTR and ATR

Cycle No.	Cooling Hrs.	ϕ_2/ϕ_3	Calculated* (C) and Measured† (M) Cross Sections (barns/fission) σ_{2200} M	σ_{2200} C	rs x σ_{2200} C	RI(0.105 eV) M	RI(0.105 eV) C	σeffective M	σeffective C
2	190	0.6077	146.0	126.5	9.05	194.7	265.4	159.3	144.6
3	262	0.6290	20.6	100.0	9.68	185.2	247.5	126.5	117.3
4	37	0.5928	193.3	178.7	9.37	248.3	321.1	210.3	200.3
	252		80.4	87.5	9.74	317.1	237.4	102.1	103.5
7	235	0.6144	66.0	66.6	9.70	237.7	216.0	82.3	81.4
8	41	0.6259	88.9	90.4	9.64	264.9	237.9	107.1	106.9
	428		61.6	63.4	9.87	241.6	215.1	78.3	78.3
10	215	0.5945	56.8	57.4	9.60	234.2	205.7	72.9	71.4
12	44	0.5800	63.9	65.5	9.25	240.3	209.5	80.2	79.5
	389		49.7	53.9	9.40	237.3	200.5	65.9	67.3
14	227	0.5938	45.7	49.9	9.15	226.6	193.0	61.1	62.8
17	39	0.5846	50.3	53.0	8.80	228.3	191.2	65.7	65.8
	433		40.0	45.2	8.88	226.4	184.8	55.3	57.5
21	40	0.5120	46.5	49.4	8.21	213.1	181.9	60.5	60.8
	385		38.8	42.9	8.26	216.3	176.4	53.0	54.0
22	322	0.560	34.9	41.0	8.12	235.6	172.5	50.3	52.1
23	275	0.582	36.3	40.1	7.97	195.0	169.6	49.0	51.2
24	34	0.545	41.8	45.4	7.83	212.2	172.7	55.6	56.4
	495		35.1	38.9	7.86	209.5	166.9	48.7	49.5
25	35	0.550	41.5	43.3	7.69	196.5	168.7	54.2	54.1
	444		34.6	37.7	7.72	190.6	163.6	47.0	48.1
	3079		33.0	37.5	7.70	204.5	163.2	46.3	48.1

*FISSPROD-2 using ENDF/B-IV

†Gunst et al.

3) Effective 2200 m/s Cross Sections - CRNL (1970)[26]

Samples of U233, U235 and Pu239 were selected (from a group irradiated at Chalk River) for pile oscillator measurements in the thermal column of the heavy water moderated reactor RO at Studsvik, Sweden. At the measurement position the neutron spectrum is essentially Maxwellian with T = 28°C. The irradiations for these samples had been completed 8 years before the measurements.

The reactor history was not published but have since been obtained from the reactor records. In the computer simulation the main part of the irradiation was treated as a single irradiation of 357 days followed by a 1 day shutdown and then a further 14 days irradiation at a lower flux (down 2%).

Effective cross sections for Sm149 and Sm151 in the RO spectrum were 69.225 kb and 13.56 kb respectively. Table VII gives the "lumped" (gross fission product) 2200 m/s cross sections for two separate irradiations. The FISSPROD-2 calculated values using ENDF/B-IV data are generally higher by about 10% compared to the measured results.

4) Resonance Integrals

Tabulations of measured and evaluated resonance integrals have been made in the past by several authors. Table VIII compares the ENDF/B-IV values with those of Mughabghab and Garber (BNL-325)[28], Clayton[29] and Ribon and Krebs[27] for 33 major FP absorbers in thermal reactors. Most of the ENDF/B-IV resonance integrals are essentially equal to the BNL-325 evaluations.

Table VII. 2200 m/s "Lumped" Fission Product Absorption Cross Sections in R0 at Studsvik from Irradiations at Chalk River

Fissile Nuclide	Sample No.	Irradiation (n/kb)	σ_{2200} (barns/fission) Measurement	Calculation (ENDF/B-IV)	Calc/Meas
U233	A3B	2.147	41.9±2.5	45.83	1.09
U233	A3F	2.642	38.5±1.8	44.13	1.15
U235	A5B	1.888	48.7±2.2	54.00	1.11
U235	A5F	2.240	46.5±1.6	52.33	1.13
Pu239*	A9A	2.330	62.3±3.3	69.17	1.11
Pu239*	A9D	1.915	71.1±3.8	70.60	0.99

*The Pu241 contributions for these samples are 11.2% for A9A and 8.8% for A9D.

Table VIII. Resonance Integrals of Major FP Absorbers in Thermal Reactors

Nuclide	Resonance Integrals (barns)			
	ENDF/B-IV*	BNL-325(73)	Clayton(72)	Ribon and Krebs(74)
Xe135	7645.	7634.	7262.	7000.
Sm149	3200.	3183.	3705.	3300.
Pm147	2283.	2300.±350.	2178.	2200.
Xe131	879.	870.	790.	850.
Cs133	381.	415.±15.	460.	400.
Nd143	205.	140.	65.	100.
Sm151	3357.	3300.±700.	2200.	3000.
Rh103	1050.	1100.±50.	1014.	1050.
Tc99	354.	340.±20.	198.	300.
Nd145	226.	240.±35.	271.	280.
Sm152	3008.	3000.±200.	3240.	3000.
Pm148M	3608.	3600.	31990.	30000.
Mo95	113.	105.±7.	106.	105.
Eu153	1590.	1635.±200.	1279.	1500.
Kr83	192.	230.	217.	230.
Rh105	15850.	15800.±1500.	16990.	15000.
Sm150	320.	310.±15.	257.	260.
Pm148	40010.	40000.	44000.	40000.
Cs135	61.6	62.	62.	60.
Ru101	95.2	85.	80.	80.
Eu155	1856.	-	1200.	2000.
La139	13.0	12.2±.6	15.6	14.
Pr141	19.4	14.1±.2	17.5	18.
Eu154	2700.	-	1240.	1500.
Pr143	190.	190.±25.	190.	170.
Xe133	356.	-	53.	300.
Cd113	405.	-	366.	400.
Nd146	3.3	3.2±.5	2.4	3.
Cs134	213.	-	90.	200.
Mo97	16.1	13.±3.	15.	15.
Sm147	748.	714.±50.	566.	600.
Zr93	28.2	33.±15.	26.	10.
Pm149	801.	-	930.	800.

*ECUT=.5 ev, T=0°k

DELAYED AND PROMPT NEUTRON YIELDS

Delayed and prompt neutron yield measurements are an integral test of the direct fission yields and the delayed neutron branching probabilities (Pn). The ENDF/B-IV files contain, with the fissionable nuclides, evaluations of the delayed and prompt neutron yields. Table IX gives the calculated ENDF/B-IV results versus the evaluated yields, the latter expected to be the more accurate. The delayed neutron calculations were made summing the contributions from the 57 nuclide precursors on the ENDF/B-IV FP files, where most of the Pn values were taken from Tomlinson.[32] Also given in Table IX are calculations from a preliminary ENDF/B-V yield set which was reviewed at the CSEWG FP and Decay Data Subcommittee Yield Group meeting held at Los Alamos September 23, 1975. This set, denoted ENDF/B-5A, has factored in the recent fast yield measurements of Maeck et al.[33] The prompt yields in Table IX show good agreement between the "calculated" and "evaluated" results, especially for the thermal $\bar{\nu}_p$. The delayed neutron differences are large, especially for U238(F), reflecting the sensitivity of $\bar{\nu}_d$ to the specific precursor direct yield estimates.

Table IX. Delayed and Prompt Neutron Comparisons*

FISSION NUCLIDE	$\bar{\nu}_d$/100 Fissions			$\bar{\nu}_p$		
	Calculation			Calculation		
	ENDF/B-IV	ENDF/B-5A	ENDF/B-IV Evaluation	ENDF/B-IV	ENDF/B-5A	ENDF/B-IV Evaluation
$^{235}U(T)$	1.604	1.547	1.67 ± 0.07	2.41	2.38	2.40
$^{235}U(F)$	1.483	1.735	1.67 ± 0.07	2.38	2.42	2.53-2.65
$^{235}U(HE)$	1.095	1.034	0.90 ± 0.1	3.63	4.17	4.38-4.51
$^{238}U(F)$	2.934	3.013	4.60 ± 0.25	2.70	3.06	2.43-2.58
$^{238}U(HE)$	1.963	1.972	2.60 ± 0.2	4.02	4.44	4.43-4.58
$^{239}Pu(T)$	0.520	0.610	0.645 ± 0.04	2.92	2.92	2.87
$^{239}Pu(F)$	0.508	0.589	0.645 ± 0.04	2.77	2.82	3.01-3.15
$^{241}Pu(T)$	1.047	1.232	1.57 ± 0.15	3.00	2.99	2.92
$^{233}U(T)$	0.821	0.777	0.740 ± 0.04	2.47	2.45	2.49
$^{232}Th(F)$	3.933	4.833	5.27 ± 0.4	2.39	2.45	1.99-2.11

*Calculated values use ENDF/B yields and branching fractions.

Uncertainties on $\bar{\nu}_d$ are taken from a review by S. A. Cox (ANL/NDM-5, April 1974). The evaluated $\bar{\nu}_p$ values apply at 0.0253 eV for thermal (T) fission; 1.0 and 2.0 MeV for fast (F) fission, and 14 and 15 MeV for high energy (HE) fission.

D. Conclusions and Recommendations

Benchmark testing of the ENDF/B-IV fission product data files for the four areas of decay heat, spectra, absorption and neutron yields given in this report has been quite extensive and except for absorption is the first comprehensive reporting of integral testing on the ENDF/B FP file.* The results of this testing are quite encouraging, especially as to giving confidence in calculating decay heat using the summation method when applied to the LOCA analyses for thermal reactors. However, due to the large mass of data to be tested and the numerous applications for which fission product data is needed, there continues to be several integral experiments in progress or completed and not thoroughly reviewed in this report that should be good candidates for benchmark testing. These include: reactivity measurement at the CFRMF and STEK facilities, calorimetric experiments at LASL and Berkeley laboratories, beta and gamma spectra measurements at IRT, LASL and ORNL.

The testing results indicated areas of data improvement for several particular FP nuclides. These include, Kr83, Rb87, Zr98, Tc99, Xe134, Xe135, Ca133, Ce140, Pr141, Nd143, Nd148, Pm147 and Pm149. In addition, all four areas of benchmark testing showed some cases of need for general data improvement in the overall "lump" FP effects. Both thermal absorption measurements, for example, give significantly lower values for σ_{2200} than the ENDF/B-IV calculations. The fast fission yields give poor agreement with delayed neutron measurements.

For ENDF/B-V data updates it is recommended that the specific information from the subsections of this report be incorporated. To this should be added results from recent microscopic cross section, decay data, fission yield and β-strength function

---

* ENDF/B-IV is the first issuance of ENDF/B to have a "complete" set of FP decay information.

measurements. Finally, the papers from the IAEA Panl on Fission Product Nuclear Data[36] should be carefully reviewed.

References

1. T. R. England et al., "CINDER-7: An Interim Report for Users," LA-5885-MS, February 1975.

2. W. H. Walker et al., "FISSPROD-2: An Improved Fission Product Accumulation Program," AECL-5105, August 1975.

3. M. J. Bell, "ORIGEN - The ORNL Isotope Generation and Depletion Code," ORNL-4628 (1973).

4. D. R. Marr, "A User's Manual for Computer Code RIBD-II, A Fission Product Inventory Code," HEDL-TME 75-26, January 1975.

5. F. Schmittroth, Nucl. Sci. and Eng., 59 (1976) 117.

6. C. W. Kee et al., Trans. Am. Nucl. Soc., 19 (1974) 398.

7. R. E. Schenter et al., "ETOX, A Code to Calculate Group Constants for Nuclear Reactor Calculations, BNWL-1002, May 1969.

8. J. K. Dickens et al., "Fission Product Beta and Gamma Energy Release Quarterly Progress Report for July-September 1975," ORNL-TM-5156, November 1975.

9. B. Alam and J. Scobie, Ann. of Nucl. Sci. and Eng., 1 (1974) 537.

10. M. Lott et al., J. Nucl. Energy, 27 (1973) 597.

11. S. B. Gunst et al., "Decay Heating Measurements and Calculations for Irradiated ^{235}U, ^{233}U, ^{239}Pu, and ^{232}Th," WAPD-TM-1183, July 1974.

12. S. B. Gunst et al., Nucl. Sci. and Eng. 56 (1975) 241.

13. A. M. Perry et al., "Fission-Product Afterheat," ORNL-TM-4197, October 1973.

14. T. D. MacMahon et al., J. Nucl. Energy, 24, 493 (1970).

15. "Proposed ANS Standard Decay Energy Release Rates Following Shutdown of Uranium-Fueled Thermal Reactors," Draft Standard ANS 5.1, October 1971, revised October 1973.

16. K. Shure, "Fission-Product Decay Energy," Bettis Technical Review, WAPD-BT-24, December 1961.

17. R. E. Schenter, F. Schmittroth, "Radioactive Decay Heat Analysis," Proceedings of the Conference on Neutron Cross Sections and Technology, Washington, D.C., March 1975.

18. M. G. Stamatelatos and T. R. England, "Fission Product Gamma-Ray and Photoneutron Spectra," Conference of Nuclear Cross Sections and Technology, Washington, D.C., March 3-7, 1975.

19. R. E. Schenter and T. R. England, Trans. Am. Nucl. Soc., 21 (1975) 517.

20. Y. D. Harker and E. H. Turk, "The Use of CFRMF Integral Data in Cross-Section Evaluations," Kiamesha Lake Conference, CONF-720901 Book 2, p. 613 (September 1972).

21. R. A. Anderl et al., "Integral Capture Cross-Section Measurements in CFRMF for LMFBR Control Materials," Conference of Nuclear Cross Sections and Technology, Washington, D.C., March 3-7, 1975.

22. J. W. Rogers et al., "Comparison of Measured and Calculated Reactivities in CFRMF," Conference of Nuclear Cross Sections and Technology, Washington, D.C., March 3-7, 1975.

23. H. Gruppelaar et al., "Evaluation, Uncertainty Estimation and Adjustment of Capture Cross Sections for Fission Product Nuclei," Conference of Nuclear Cross Sections and Technology, Washington, D.C., March 3-7, 1975.

24. S. B. Gunst et al., "Measurements and Calculations of Heavy Isotopes in Irradiated Fuels and of ^{233}U Fission-Product Poisoning," WAPD-TM-1182 (July 1974).

25. S. B. Gunst et al., Nucl. Sci. and Eng. 58 (1975) 387.

26. A. Okazaki and E. K. Sokolowski, "Nuclear Data for Reactors I," IAEA-CN-26/58, Helsinki Symposium, 1 (1970) 703.

27. P. Ribon and J. Krebs, Bologna Panel Report (April 1974).

28. S. F. Mughabghab and D. I. Garber, "Neutron Cross Sections Volume 1, Resonance Parameters," BNL-325 (June 1973).

29. E. Clayton, AAEC/TM 619 (September 1972).

30. G. Sadler et al., Nucl. Phys. A252 (1975) 365.

31. T. R. England and R. E. Schenter, "ENDF/B-IV Fission-Product Files: Summary of Major Nuclide Data", LA-6116-MS, ENDF-223, October 1975.

32. L. Tomlinson, Atomic and Nuclear Data Tables 12 (1973) 179.

33. W. J. Maeck, Ed., "Fast Reactor Fission Yields for U233, U235, U238, and Pu239 and Recommendations for the Determination of Burnup on FBR Mixed Oxide Fuels: An Interim Project report," Idaho Chemical Programs report ICP-1050-I, January 1975.

34. C. W. Reich and R. G. Helmer, "Radioactive-Nuclide Decay Data in Science and Technology," Conference of Nuclear Cross Sections and Technology, Washington, D. C., March 3-7, 1975.

35. M. G. Stamatelatos and T. R. England, Trans. Am. Nucl. Soc. 21 (1975) 508.

36. "Fission Product Nuclear Data (FPND)", Proceedings of an IAEA panel held in Bologna, November 1973, IAEA-169 (1974).